DEUTSCHES ELEKTRONEN – SYNCHROTRON

DESY 91-030
April 1991

The Hyperbola Billiard: A Model for the Semiclassical Quantization of Chaotic Systems

M. Sieber

II. Institut für Theoretische Physik, Universität Hamburg

ISSN 0418-9833

NOTKESTRASSE 85 · D-2000 HAMBURG 52

To be sure that your preprints are promptly included in the
HIGH ENERGY PHYSICS INDEX,
send them to the following (if possible by air mail):

DESY
Bibliothek
Notkestrasse 85
D–2000 Hamburg 52
Germany

DESY 91-030
April 1991

ISSN 0418 - 9833

The Hyperbola Billiard: A Model for the Semiclassical Quantization of Chaotic Systems [1]

by

Martin Sieber

II.Institut für Theoretische Physik , Universität Hamburg
Luruper Chaussee 149 , 2000 Hamburg 50
Federal Republic of Germany

[1]Supported by Deutsche Forschungsgemeinschaft under Contract No. DFG-Ste 241/4-1,4-2,4-3

Abstract

Classical and quantum mechanical properties of a chaotic billiard system are studied with special emphasis on a detailed numerical investigation of the periodic-orbit theory of Gutzwiller. This theory gives semiclassical approximations to the quantum mechanical energies of a classically chaotic system by means of a sum over all periodic orbits of the system. Parts of the derivation of the periodic-orbit theory are reviewed. The convergence properties of the periodic-orbit sum are discussed and smoothing techniques are introduced, which allow the determination of the energies by absolutely convergent sums.

A code is introduced for the periodic orbits of the hyperbola billiard, a chaotic system which is bounded by the x-axis, the y-axis and the hyperbola $y = 1/x$. An extremum principle for the periodic orbits is proved, which allows a very fast and accurate determination of the periodic orbits. More than 500 000 periodic orbits are determined, out of which the 13 098 shortest orbits are complete. The distributions of lengths and Lyapunov exponents of the orbits are studied. The statistical distribution of lengths is shown to be in good agreement with a Poisson distribution, if not very long-range correlations are considered.

The quantum mechanical energies of the hyperbola billiard are determined by a boundary element method. A correction to the asymptotic approximation for the spectral staircase $N(E)$, which counts the number of energy eigenvalues of the Schrödinger equation below a given energy E, is determined numerically. The energy statistics is investigated, and it is shown to agree with the predictions of random matrix theory for the Gaussian orthogonal ensemble only for very short-range statistics. Long-range correlations are studied by means of the spectral rigidity $\Delta_3(L)$ and the number variance $\Sigma^2(L)$, which saturate at relatively small values of the parameter L.

The properties of the periodic-orbit theory are investigated by an evaluation of the unsmoothed Gutzwiller trace formula and various versions of smoothed trace formulae. The advantage of different smoothing methods are discussed and compared. The effect of the semiclassical approximation is demonstrated by a smoothing, which leads to a truncation of the periodic-orbit sum. An alternative approximation for the energies in terms of a dynamical zeta function is investigated and shown to yield comparable results as the previous trace formulae. Finally, an approximation to this zeta function in analogy to the Riemann-Siegel formula for the Riemann zeta function is studied.

Contents

I Introduction

Classical mechanics is still an active field despite its long history reaching back several hundred years. This is mainly due to new developments in the second half of this century, which brought a change in the way classical systems are viewed. These developments are connected with the term "chaos", which has become very popular also in areas outside of physics.

About hundred years ago Poincaré discovered that the solutions of the classical equations of motion are for most systems utterly complicated [1]. He also developed methods for the examination of qualitative properties of dynamical systems. A deeper understanding of the main features of classical systems, however, was achieved only during the last few decades. This progress on the one hand is due to the advancement of basic mathematical theorems for dynamical systems. On the other hand the development of fast and powerful computers made extensive numerical investigations of classical systems possible, which led to new insight in the general structure of dynamical systems.

Here we restrict to Hamiltonian systems, that is to systems, for which the energy is conserved. According to the present understanding, classical systems are classified in a range between two extreme cases. One is that of integrable systems. These systems have the property that there exist as many independent constants of motion as degrees of freedom. Let this number be f. The f constants of motion have to satisfy certain conditions, from which follows that the classical motion is restricted to f-dimensional tori in phase space [2]. The equations of motion can be integrated, and the motion is characterized as being regular and predictable. Standard examples for integrable systems are the multidimensional harmonic oscillator, the Kepler problem or the heavy symmetrical top.

On the other end of the scale are systems, which show a very irregular behaviour. If the motion is considered stroboscopically after finite, sufficiently large time intervals, the positions in phase space seem to jump in a very unpredictable way. There is a hierarchy of properties, which describe an increasing degree of randomness: ergodicity, mixing, K-system, B-system. These terms are explained for example in [3]. The weakest property is ergodicity. Ergodic systems are characterized by the fact, that almost all trajectories explore the $(2f\text{-}1)$-dimensional constant-energy surface in phase space uniformly. Among systems for which ergodicity could be proved are the Sinai billiard [4] and the stadium billiard of Bunimovich [5]. For the term chaos no mathematically exact definition exists. However, chaos is connected with a property that is stronger than ergodicity. The common definition is, that chaotic systems are characterized by an exponential divergence of trajectories with neighbouring initial conditions. The above two billiard systems are chaotic. A standard example for a chaotic system is the motion on a smooth compact Riemannian surface with constant negative curvature. It was already studied by the mathematician Hadamard at the end of the last century [6].

Most systems, however, are neither completely chaotic nor completely integrable. Instead they exhibit a mixed behaviour. The phase space is divided into parts, where the motion is restricted to invariant tori, and parts, where a typical trajectory fills out regions of dimensionality $2f$-1. The exact way by which integrable systems change into mixed systems, if they are subject to a small generic perturbation, is described by the KAM-theorem, which is named after the three mathematicians Kolmogorov [7], Arnold [8] and Moser [9].

The above classification scheme for classical systems cannot be easily carried over to quantum mechanical systems. Although quantum mechanics is the more general theory,

which contains the classical mechanics as limiting case for which Planck's constant is equal to zero, quantum mechanical functions are typically not analytic in $\hbar$ as $\hbar \to 0$. For that reason the transition from quantum mechanics to classical mechanics is not straightforward, and the quantum dynamics has qualitatively different properties than the classical dynamics. So it appears to be that quantum systems do not exhibit chaotic behaviour as classical systems do. More precisely, the practical predictability of the time evolution of expectation values of observable operators is not limited in the way it is for classical trajectories. An intuitive argument for this is obtained from the uncertainty principle. In classical systems the extreme sensitivity on the initial conditions prevents an accurate computation of a classical trajectory for a long time t. Due to the exponential divergence of neighbouring trajectories the computation of a trajectory with some given accuracy for a time t requires the knowledge of the initial conditions to a number of digits, which is proportional to t. This soon exceeds the capacity of any computer. The limits in the predictability of classical systems thus are also a consequence of the fact, that differences in the initial conditions of neighbouring trajectories can be arbitrarily small. In quantum mechanics, however, structures in phase space over areas which are of the order of Planck's constant can hardly be of significance for the quantum evolution because of the uncertainty relation. This phenomenon is the reason for what is called the quantum suppression of classical chaos. On the other hand there has to be a correspondence between the classical mechanics and the quantum mechanics in the semiclassical limit, that is as $\hbar$ tends to zero. If the underlying classical motion is chaotic, this has to be reflected by the quantum mechanical time evolution in some way. The answer is that quantum mechanics can mimic chaotic behaviour, but only for a finite time. That is, the quantum mechanical time evolution can be characterized as being unstable, but this instability does not persist as $t \to \infty$. On the other hand the persistency of instability is a characteristic property of chaotic systems. In this way the absence of chaos in the quantum dynamics can be seen to be a consequence of the fact, that the two limits $\hbar \to 0$ and $t \to \infty$ in general do not commute [10].

Since there seems to be no chaotic quantum evolution, stress is layed upon the question: what specific properties do quantum mechanical systems have (in the semiclassical limit), whose classical counterpart is chaotic? The study of this question is named quantum chaology [11]. Progress in answering this question was achieved by the consideration of the energy statistics of quantum mechanical systems. Extensive numerical and experimental investigations showed, that in the semiclassical limit the energy statistics has universal properties, which are different, if the corresponding classical system is chaotic or not [12]. In this way the nature of the underlying classical motion is reflected by the energy statistics of the quantum system.

For a deeper understanding of the correspondence between classical and quantum mechanical properties in the semiclassical regime analytical methods are necessary. A powerful semiclassical approximation technique is the Einstein-Brillouin-Keller (EBK) quantization method, which is a generalization of the WKB method to multidimensional systems. But this method can be applied to integrable systems only, since its application is based on the assumption that phase space is divided into invariant tori [13]. An extension of this method can be applied to weakly perturbed integrable systems. In case of chaotic systems on the other hand there also is a theory, which semiclassically relates the quantum mechanical energy spectrum to purely classical quantities. This is the periodic-orbit theory of Gutzwiller [14]. In its original formulation it approximates the trace of the Green function $g(E) = \sum_n (E - E_n)^{-1}$,

a function, which has poles at the energy eigenvalues E_n of the Schrödinger equation. This function is semiclassically expressed by a sum over all periodic orbits of the associated classical system. Since the so-called trace formula, which establishes this relation, allows the semiclassical determination of the quantum mechanical energies, this theory can be considered as a substitute for the EBK quantization rules. The relation between quantum mechanics and classical mechanics is, however, much more complicated than in the integrable case. There is a sum over an infinite number of periodic orbits. Each orbit contributes a term to the sum, which oscillates as a function of the energy E. With an increasing classical action of the periodic orbits the terms oscillate faster, so that the fine structure of the energy spectrum is determined by the very long orbits. An approximation to the periodic-orbit sum by a truncation of the sum often is sufficient for a determination of a lower part of the energy spectrum. By including more and more periodic orbits in the sum the energy resolution can be improved. Yet chaotic systems have the specific property that the number of periodic orbits increases exponentially with period T. This soon sets a limit to the energy resolution, which can be achieved in practice. Furthermore, the periodic-orbit sum is at best conditionally convergent. In case that the sum is divergent the method has to be modified by an appropriate smoothing of the original trace formula. This technique allows the determination of the energies by absolutely convergent periodic-orbit sums. A further question is, how good the semiclassical approximations for the energies are. Due to the complex structure of the trace formula it is very difficult to give any estimation of this accuracy.

Despite of the problems, that are connected with the trace formula, there has been a great interest in the periodic-orbit theory in recent years. It is one of the few analytical tools for the examination of the quantum mechanics of classically chaotic systems in the semiclassical regime. The universality of certain energy statistics could be explained with the use of the trace formula [15]. A new development for the semiclassical quantization of non-integrable systems is a method which was proposed by Bogomolny recently [16]. By this method a quantization condition is obtained from the quantum version of a classical Poincaré mapping.

The present work contains a detailed examination of the classical and quantum mechanical properties of a chaotic system with special emphasis on an investigation of the properties of the periodic-orbit theory. The considered system is the so-called hyperbola billiard, a two-dimensional plane billiard system, which is bounded by the x-axis, the y-axis and the hyperbola $y = 1/x$. This system has properties, which allow a very fast and very accurate determination of the periodic orbits. In addition, all periodic orbits can be classified by a simple code. For that reason very detailed examinations of certain properties of the periodic orbits and the trace formula can be carried out, which for most chaotic systems would not be possible. The hyperbola billiard has a geometrical symmetry, which is the invariance under reflection on the line $y = x$. Most of the numerical investigations were carried out for a desymmetrized version of the hyperbola billiard, which is obtained by introducing an additional boundary along the line $y = x$. The consideration of the desymmetrized hyperbola billiard allows a separate application of the periodic-orbit theory to the energy eigenvalues of even and odd wavefunctions, respectively, of the full hyperbola billiard. In detail the content of this paper is the following:

In chapter II parts of the derivation of Gutzwiller's periodic-orbit theory are given. A special formula for systems with discrete symmetries is derived, and an alternative formulation in terms of a dynamical zeta function is given. The convergence properties of the trace formula are discussed, and it is shown for chaotic billiard systems how absolutely convergent smoothed

trace formulae can be obtained in a mathematically exact way.

Chapter III contains an examination of the properties of the classical trajectories of the hyperbola billiard. Codes for the orbits of the full and the desymmetrized hyperbola billiard are given. Equations for the number of code words with a certain symmetry are presented. The distributions of the lengths and Lyapunov exponents of all periodic orbits of the desymmetrized hyperbola billiard with a constant code length N are examined for $N \leq 14$. Furthermore, the 13 098 shortest periodic orbits are determined completely and statistical properties of their length distribution are investigated.

In chapter IV the method for the determination of the energies is described. The two partial energy spectra of even and odd wavefunctions of the hyperbola billiard are considered separately. The first 294 even and 284 odd energies of the hyperbola billiard are determined, and the results are compared to the mean spectral staircase $\bar{N}(E)$, for which an analytical approximation exists. A correction to this analytical formula is determined numerically for both subspaces of the energy spectrum. The statistical properties of the two partial energy spectra are investigated numerically, and the results for the spectral rigidity and the number variance are compared with the predictions of Berry's semiclassical theory.

Chapter V contains a detailed numerical investigation of properties of the periodic-orbit theory. First the unsmoothed trace formula for the energy density is evaluated and its convergence properties are examined. Next the advantage of certain methods of smoothing the trace formula are discussed for the Breit-Wigner and the Gaussian smoothing. The effect of the semiclassical approximation is demonstrated by the $\sin^3$-smoothing for which the periodic-orbit sum is finite. The possibility of a determination of the lengths of the periodic orbits by means of the energy spectrum is shown by a consideration of the trace of the cosine-modulated heat kernel. The representation of the dynamical zeta function by a sum over all possible combinations of periodic orbits is evaluated and its convergence properties are investigated. Finally a formula for this zeta function is examined, which was suggested in analogy with the Riemann-Siegel formula for the Riemann zeta function by Berry and Keating.

In chapter VI the results of this paper are summarized.

II The Periodic-Orbit Theory

The periodic-orbit theory was developed in a series of papers by Gutzwiller [17]. The derivation starts from the Feynman path integral expression for the propagator $K(\vec{q}'', t'', \vec{q}', t')$ of the Schrödinger equation. Semiclassical approximation techniques, like the stationary phase approximation for integrals, based on the assumption that occuring classical actions are large in comparison with $\hbar$, are used in order to arrive at a semiclassical expression for the (regularized) trace $g(E)$ of the Green function of the Schrödinger equation. This trace is a function of energy E, which has poles at the energy eigenvalues of the Schrödinger equation. In case that all periodic orbits of the corresponding classical system are isolated, $g(E)$ is expressed as a sum over all periodic orbits. The periodic-orbit theory therefore relates quantum mechanical energies to classical orbits and can serve as a semiclassical quantization method for chaotic systems.

The Gutzwiller trace formula, however, has to be handled with care. It contains a sum over an infinite number of orbits, which in general is not convergent on the real energy axis. For the discussion of the convergence properties of the trace formula, $g(E)$ is considered as a function of complex values of the energy E. The periodic-orbit theory gives an approximation to this function by a periodic-orbit sum, which is convergent in parts of the complex energy plane only. In general, the region of convergence is too far away from the real energy axis in order to discriminate single energies. A solution to this problem consists in a smoothing of the original trace formula with the effect, that the sum over periodic orbits of the smoothed trace formula is absolutely convergent for real values of the energy E. If the smoothing is done in a proper way, the smoothing parameter can be chosen to be arbitrarily small, so that the smoothing sets no limit for the accuracy of the determination of the semiclassical energies.

This chapter contains parts of the derivation of the Gutzwiller trace formula. Special periodic-orbit sum rules for systems with discrete symmetries are derived, and a periodic-orbit representation of a dynamical zeta function is given. The convergence properties of the periodic-orbit sum are discussed, and methods of smoothing the trace formula are introduced.

II.1 The Green Function $G(\vec{q}'', \vec{q}', E)$

Consider a conservative system of f degrees of freedom, whose Hamiltonian is given by

$$H(\vec{q}, \vec{p}) = \frac{\vec{p}^2}{2m} + V(\vec{q}) \ . \tag{1}$$

It is assumed that this system has a purely discrete quantum mechanical energy spectrum. The Green function of this system is defined by the inhomogeneous equation

$$[E + i\varepsilon - \hat{H}(\vec{q}'', \vec{p}'')]\, G(\vec{q}'', \vec{q}', E) = \delta(\vec{q}'' - \vec{q}') \ , \tag{2}$$

where the ε indicates that the outgoing Green function is considered, which is the solution of eq. (2) in the limit $\varepsilon \to 0$. $G(\vec{q}'', \vec{q}', E)$ can be expressed in terms of the eigenfunctions and eigenvalues of the Hamiltonian operator

$$G(\vec{q}'', \vec{q}', E) = \sum_n \frac{\psi_n(\vec{q}'')\psi_n^*(\vec{q}')}{E + i\varepsilon - E_n} \ , \tag{3}$$

with functions $\psi_n(\vec{q})$, which form a complete orthonormal set of solutions of the Schrödinger equation

$$\hat{H}(\vec{q},\vec{p})\,\psi_n(\vec{q}) = E_n\,\psi_n(\vec{q}) \ . \tag{4}$$

In terms of the propagator $K(\vec{q}'',t'',\vec{q}',t')$, which is defined by the scalar product

$$K(\vec{q}'',t'',\vec{q}',t') = <\vec{q}'',t''|\vec{q}',t'> \ \Theta(t''-t') \tag{5}$$

in the Heisenberg representation, $G(\vec{q}'',\vec{q}',E)$ is expressed as

$$G(\vec{q}'',\vec{q}',E) = \frac{1}{i\hbar}\int_0^\infty \mathrm{d}t\ K(\vec{q}'',t,\vec{q}',0)\ \exp\{\frac{i(E+i\varepsilon)t}{\hbar}\} \ . \tag{6}$$

$\Theta(t)$ denotes the step-function

$$\Theta(t) = \begin{cases} 1 & t \geq 0 \\ 0 & t < 0 \ . \end{cases} \tag{7}$$

A semiclassical approximation for the Green function is obtained by first deriving an asymptotic expression for the propagator in the limit $\hbar \to 0$, and then evaluating the integral in eq.(6). The propagator $K(\vec{q}'',t'',\vec{q}',t')$ can be expressed as a Feynman path integral. In the limit that the actions of the classical paths connecting $\vec{q}'$ and $\vec{q}''$ in time $(t''-t')$ are large in comparison with $\hbar$, the main contributions to this path integral come from paths, which are close to classical trajectories from $\vec{q}'$ to $\vec{q}''$. Those contributions can be calculated approximately by expanding the potential energy $V(\vec{q})$ around the classical trajectory up to second order and neglecting higher order terms. In this approximation the integral over paths can be evaluated [18,19]. The result is an expression already given by Van Vleck in 1928 [20]. Special care has to be taken, if along the classical trajectory from $\vec{q}'$ to $\vec{q}''$ there are points $\vec{q}$, which are conjugate to $\vec{q}'$, i.e. points for which the semiclassical approximation for $K(\vec{q},t,\vec{q}',t')$ is infinite. Van Vlecks expression is unambiguously valid only up to the first conjugate point. To go beyond conjugate points, results of Morse theory [21] can be used with the result, that appropriate phase factors have to be chosen, if a conjugate point is passed. The final result is an expression for the propagator as a sum over all classical trajectories from $\vec{q}'$ to $\vec{q}''$. This expression is inserted into eq.(6) and the integral is evaluated using a stationary phase approximation. All these steps are explained in detail for example in [22]. Here only the final result is stated, which is

$$G(\vec{q}'',\vec{q}',E) \approx \sum_{\substack{classical\\ trajectories}} \frac{1}{i\hbar(2\pi i\hbar)^{(f-1)/2}}\sqrt{|D|}\,\exp\{\frac{i}{\hbar}S(\vec{q}'',\vec{q}',E) - i\frac{\pi}{2}\mu\} \ . \tag{8}$$

The sum runs over all classical trajectories which go from $\vec{q}'$ to $\vec{q}''$ with energy E.

$$S(\vec{q}'',\vec{q}',E) = \int_{\vec{q}'}^{\vec{q}''} \vec{p}\ \mathrm{d}\vec{q} \tag{9}$$

is the classical action along these trajectories. Its derivatives satisfy

$$\frac{\partial S}{\partial \vec{q}''} = \vec{p}'' \ , \quad \frac{\partial S}{\partial \vec{q}'} = -\vec{p}' \ , \quad \frac{\partial S}{\partial E} = t \ , \tag{10}$$

where $\vec{p}'$ and $\vec{p}''$ are the momenta at points $\vec{q}'$ and $\vec{q}''$, respectively, and t is the time that is needed to go from $\vec{q}'$ to $\vec{q}''$ with energy E along the considered trajectory. D is the determinant of an $(f+1)\times(f+1)$ matrix and is given by

$$D = (-1)^{f+1}\begin{vmatrix} \partial^2 S/(\partial\vec{q}'\partial\vec{q}'') & \partial^2 S/(\partial E\partial\vec{q}'') \\ \partial^2 S/(\partial\vec{q}'\partial E) & \partial^2 S/(\partial E^2) \end{vmatrix} \ . \tag{11}$$

With the use of equations (10) D can be interpreted as a Jacobian

$$D = -\det\left(\frac{\partial x_i}{\partial y_j}\right) \quad i,j = 1,\ldots,f+1 \ , \tag{12}$$

where

$$x_i = \begin{cases} p_i' & i = 1,\ldots,f \\ t & i = f+1 \end{cases} \quad \text{and} \quad y_j = \begin{cases} q_j'' & j = 1,\ldots,f \\ E & j = f+1 \end{cases} \ . \tag{13}$$

The determinant in eq.(12) is determined by expressing $\vec{p}'$ and t as functions of $\vec{q}''$, $\vec{q}'$ and E with the use of equations (10), and then holding $\vec{q}'$ fixed. At points $\vec{q}''$ at which the matrix $(A_{ij}) = (\partial y_i/\partial x_j)$ is singular, the semiclassical approximation for $G(\vec{q}'',\vec{q}',E)$ is infinite. Those points are called constant-energy conjugate points of $\vec{q}'$. The phase μ counts the number of conjugate points of $\vec{q}'$ along the classical trajectory from $\vec{q}'$ to $\vec{q}''$. If at one point the rank of the matrix $(A_{ij}) = (\partial y_i/\partial x_j)$ is reduced by more than one, then this point is considered as a multiple conjugate point. The number μ is increased by one for every reduction in the rank of the matrix $(\partial y_i/\partial x_j)$ by one.

In case that billiard type systems are considered, μ contains additional contributions from reflections on the billiard boundary in order to satisfy the boundary conditions. Let us consider the case that there are parts of the boundary, on which the wavefunctions have to satisfy Dirichlet boundary conditions, and parts, on which they have to satisfy Neumann boundary conditions. Then for every reflection of the classical trajectory on those parts of the boundary, on which the wavefunctions vanish, μ is increased by two. Reflections on parts of the boundary, on which the normal derivative of the wavefunctions vanishes, do not change μ.

The cases in which the determinant D is infinite can be made more explicit by expressing D in a different form. For that reason a special coordinate system is introduced in the vicinity of a particular trajectory, whose contribution to the semiclassical Green function is considered. The first coordinate q_1 is chosen to vary along the trajectory, the remaining $(f-1)$ coordinates are perpendicular to it. In this coordinate system the determinant D can be shown to have the following form [22]

$$D = \frac{1}{\dot{q}_1'\dot{q}_1''}\det{}'\left(-\frac{\partial^2 S}{\partial q_i'\partial q_j''}\right) = \frac{1}{\dot{q}_1'\dot{q}_1''}\det{}'\left(\frac{\partial p_i'}{\partial q_j''}\right) \quad , i,j = 2,\ldots,f \ , \tag{14}$$

where the prime at the determinant indicates that i and j do not take on the value 1. $\dot{q}_1'$ and $\dot{q}_1''$ are the velocities at the starting point and end point, respectively. Now a family of trajectories is considered, which start at point $\vec{q}'$ with energy E and momentum in a volume element $\mathrm{d}p_2'\ldots\mathrm{d}p_f'$ around $\vec{p}' \neq 0$. Their endpoints, which are characterized by having all the same first coordinate q_1'', lie in the neighbourhood $\mathrm{d}\Omega''$ of $\vec{q}''$. The determinant D, which is equal to the Jacobian $\mathrm{d}^{f-1}p'/\mathrm{d}\Omega''$ times $1/(\dot{q}_1'\dot{q}_1'')$, can be infinite for two reasons. First it is infinite, if $\dot{q}_1''$ is equal to zero, and second, if the dimension of the volume element $\mathrm{d}\Omega''$ is

smaller than $f-1$. This is the case, if there are different trajectories, which start at point $\vec{q}'$ with the same energy E, but with infinitesimally different momentum $\vec{p}'$, and which have the same endpoint $\vec{q}''$.

The approximation eq.(8) is quite general. The one-dimensional WKB approximation can be obtained from it. In higher dimensions the Poisson summation formula can be used in order to obtain the EBK approximation for integrable systems, as has been shown on particular examples [22]. In case of the rectangular billiard, for example, eq. (8) has the right poles and the right residua, so that the semiclassical approximation differs from the exact Green function only by an entire function. Eq. (8) was used by Bogomolny as starting point for the derivation of a semiclassical theory for the wavefunctions of chaotic systems [23], which is the theoretical basis for the explanation of the scars of periodic orbits, that were discovered by Heller [24]. In case of the motion on a smooth compact Riemannian surface with constant negative curvature, the theory for the wavefunctions is even exact rather than a semiclassical approximation, as was shown by Aurich and Steiner [25]. A general theory, which contains Bogomolny's theory as a special case, was developed by Berry, who derived a semiclassical approximation for the Wigner function, starting from the semiclassical approximation to the propagator $K(\vec{q}'',t'',\vec{q}',t')$ [26].

We end this section by considering the approximation for the contribution of a trajectory to the Green function $G(\vec{q}'',\vec{q}',E)$ in the opposite limiting case $S(\vec{q}'',\vec{q}',E) \to 0$, so that the action of the classical trajectory from $\vec{q}'$ to $\vec{q}''$ is small in comparison with $\hbar$. Naturally a term in eq. (8) in general does not describe correctly this contribution, though it happens that it does if f is odd. In the limit $S(\vec{q}'',\vec{q}',E) \to 0$ the contribution of a trajectory to the semiclassical Green function reduces to the free-particle Green function

$$G_{free}(\vec{q}'',\vec{q}',E) = \frac{m}{2i\hbar^2}\left(\frac{1}{2\pi\hbar}\frac{\sqrt{2mE}}{|\vec{q}''-\vec{q}'|}\right)^{f/2-1} H^{(1)}_{f/2-1}\left(\frac{\sqrt{2mE}}{\hbar}|\vec{q}''-\vec{q}'|\right) , \qquad (15)$$

where the energy E has to be replaced by $E - V((\vec{q}'+\vec{q}'')/2)$ and $H^{(1)}_i$ denotes a Hankel function of the first kind [27].

II.2 The Trace Formula

The Green function $G(\vec{q}'',\vec{q}',E)$ contains all information about a quantum mechanical system, but in general the evaluation of eq.(8) is too complicated, since one has to sum over all trajectories from $\vec{q}'$ to $\vec{q}''$, whose number is in general infinite. Such a sum has to be evaluated for every pair of points $\vec{q}'$ and $\vec{q}''$. In case that one is interested only in the quantum mechanical energies, it is easier to concentrate only on the trace of the Green function, which has poles at the energies E_n, but contains no information on the wavefunctions:

$$g(E) = \int \mathrm{d}^f q\, G(\vec{q}'',\vec{q}',E)\Big|_{\vec{q}''=\vec{q}'=\vec{q}} = \lim_{\epsilon\to 0}\sum_n \frac{1}{E+i\epsilon-E_n} . \qquad (16)$$

In general this trace does not exist, since the sum over energies is divergent, but it can be regularized in a proper way, which is discussed below. A semiclassical approximation for $g(E)$ is obtained by inserting eq.(8) into eq.(16) and evaluating the integral for $\hbar \to 0$.

In the limit $\vec{q}'' \to \vec{q}'$ two kinds of trajectories have to be considered. First there are the direct trajectories from $\vec{q}'$ to $\vec{q}''$, whose length goes to zero if $\vec{q}'' \to \vec{q}'$. Their contribution to

the trace of the semiclassical $g(E)$ is denoted by $g_{(0)}(E)$. Second there are trajectories which close if $\vec{q}'' \to \vec{q}'$ and whose length does not go to zero. They give an oscillatory contribution to $g(E)$, which is denoted by $g_{osc}(E)$.

$$g(E) \approx g_{(0)}(E) + g_{osc}(E) . \qquad (17)$$

From now on we restrict ourselves to the two-dimensional case $f=2$.

The term $g_{(0)}(E)$ is considered first. Contributions of trajectories, whose length goes to zero if $\vec{q}'' \to \vec{q}'$, are described by the free Green function eq.(15) with the replacement $E \to E - V((\vec{q}'+\vec{q}'')/2)$. This Green function diverges in the limit $\vec{q}'' \to \vec{q}'$, and for that reason the term $g_{(0)}(E)$ is infinite. Different regularization techniques can be applied in order to obtain a finite result. For example, one can consider the level density $d(E)$ instead of $g(E)$.

$$d(E) = \sum_n \delta(E-E_n) = -\frac{1}{\pi}\lim_{\epsilon\to 0}\mathrm{Im}\sum_n \frac{1}{E+i\epsilon-E_n} = -\frac{1}{\pi}\mathrm{Im}\, g(E) . \qquad (18)$$

Then the limit $\vec{q}'' \to \vec{q}'$ can be carried out, and with the limiting form for the Hankel function with small argument

$$H^{(1)}_0(z) \to \frac{2i}{\pi}(\log\frac{z}{2}+\gamma)+1 \quad if \quad z\to 0 , \qquad (19)$$

one then obtains

$$d_{(0)}(E) = \frac{mA}{2\pi\hbar^2} , \qquad (20)$$

where A is the classically accessible coordinate space at energy E. The fact that eq. (20) does not depend explicitly on the potential $V(\vec{q})$ is a special property of two-dimensional systems. Eq. (20) is the Thomas-Fermi approximation for the level density. In case of billiard systems it is equal to Weyl's law.

If the classically accessible coordinate space is the same for different energies (as is the case for billiard systems, for example), one can choose a reference energy E' and consider the function $G(\vec{q}'',\vec{q}',E) - G(\vec{q}'',\vec{q}',E')$ instead of $G(\vec{q}'',\vec{q}',E)$. In this case the result is

$$g_{(0)}(E) - g_{(0)}(E') = \frac{mA}{2\pi\hbar^2}\ln(\frac{E}{E'}) . \qquad (21)$$

Next we turn to the term $g_{osc}(E)$. Consider one particular closed trajectory, which starts at $\vec{q}' = \vec{q}$ and ends at $\vec{q}'' = \vec{q}$. If $\vec{q}$ is slightly changed, then in general there is a neighbouring closed trajectory, which is obtained by a continuous deformation of the original trajectory. For conditions on which this assumption holds see [28]. The integral in eq. (16) has to be evaluated over these continuous families of closed orbits. Again it is assumed that $S(\vec{q},\vec{q},E) \gg \hbar$ for the considered closed orbits. Then the integrand is a rapidly varying function of $\vec{q}$, and contributions from neighbouring trajectories usually cancel away. Significant contributions come only from $\vec{q}$-values in the neighbourhood of closed trajectories for which the exponent $S(\vec{q},\vec{q},E)$ is stationary

$$\left(\frac{\partial S(\vec{q}'',\vec{q}',E)}{\partial \vec{q}''} + \frac{\partial S(\vec{q}'',\vec{q}',E)}{\partial \vec{q}'}\right)\Big|_{\vec{q}''=\vec{q}'=\vec{q}} = \vec{p}''-\vec{p}' = 0 . \qquad (22)$$

This means that the largest contribution to the integral comes from closed orbits that are close to periodic trajectories, which satisfy $\vec{q}'' = \vec{q}' = \vec{q}$ and $\vec{p}'' = \vec{p}'$. Now a distinction has

to be made between integrable and chaotic systems. In integrable systems one has families of periodic orbits and the integral has to be extended over these families of trajectories. In chaotic systems one has isolated periodic orbits and possibly families of neutral periodic orbits as in the stadium billiard and the Sinai billiard. We restrict ourselves to systems which have isolated and unstable periodic orbits only. Then only coordinate values close to periodic orbits contribute to the integral eq.(16). Again a local coordinate system is introduced in the vicinity of a periodic orbit with the first coordinate along the periodic orbit. The action $S(\vec{q},\vec{q},E)$ does not change along the orbit. Perpendicular to the orbit the action is stationary. The q_2-integration is considered first. Since only small q_2-values contribute to the integral, the exponent is expanded in the variable q_2 up to second order and higher order terms are neglected. The determinant factor varies very slowly in comparison with the rapidly oscillating exponential function, and it is therefore assumed to be constant with respect to the q_2-integration. This approximation is called stationary phase approximation. Taking into account eq.(22) the expansion gives

$$S(\vec{q},\vec{q},E) = \left[S(\vec{q}'',\vec{q}',E) + \frac{1}{2}\left(\frac{\partial^2 S}{\partial q_2' \partial q_2'} + 2\frac{\partial^2 S}{\partial q_2' \partial q_2''} + \frac{\partial^2 S}{\partial q_2'' \partial q_2''}\right) q_2^2\right]_{\vec{q}''=\vec{q}'} \quad , \tag{23}$$

where $\vec{q}'' = \vec{q}''$ has the same q_1-coordinate as $\vec{q}$ and is the coordinate vector of the nearby periodic orbit. The integral over q_2 is a Fresnel integral, which results in

$$g_{osc}(E) = \sum_{\substack{\text{periodic}\\ \text{orbits}}} \frac{1}{i\hbar}\int \mathrm{d}q_1 \frac{1}{|\dot{q}_1|}\sqrt{\left|\frac{-\partial^2 S/(\partial q_2' \partial q_2'')}{\kappa}\right|}\exp\left\{\frac{i}{\hbar}S(\vec{q}'',\vec{q}',E) - \frac{i\pi}{2}\nu\right\}\Bigg|_{\vec{q}''=\vec{q}'} \quad , \tag{24}$$

where

$$\kappa = \frac{\partial^2 S}{\partial q_2' \partial q_2'} + 2\frac{\partial^2 S}{\partial q_2' \partial q_2''} + \frac{\partial^2 S}{\partial q_2'' \partial q_2''} \tag{25}$$

and

$$\nu = \begin{cases} \mu & , \kappa > 0 \\ \mu + 1 & , \kappa < 0 \end{cases} . \tag{26}$$

This result can be expressed more clearly in terms of the monodromy matrix M, which contains information about the stability properties of an orbit. Consider a particular trajectory which starts at $\vec{q}'$ with momentum $\vec{p}'$ and ends at $\vec{q}''$ with momentum $\vec{p}''$. If the initial coordinates in phase space are changed infinitesimally by $\mathrm{d}q_2'$ and $\mathrm{d}p_2'$, then the final coordinates in phase space, which are determined by having the same q_1-coordinate, change infinitesimally by $\mathrm{d}q_2''$ and $\mathrm{d}p_2''$. The monodromy matrix is defined by

$$\begin{pmatrix} \mathrm{d}q_2'' \\ \mathrm{d}p_2'' \end{pmatrix} = M \begin{pmatrix} \mathrm{d}q_2' \\ \mathrm{d}p_2' \end{pmatrix} \quad . \tag{27}$$

From equations (10) one has

$$\begin{aligned} \mathrm{d}p_2' &= -\frac{\partial^2 S}{\partial q_2' \partial q_2'}\mathrm{d}q_2' - \frac{\partial^2 S}{\partial q_2' \partial q_2''}\mathrm{d}q_2'' \\ \mathrm{d}p_2'' &= +\frac{\partial^2 S}{\partial q_2'' \partial q_2'}\mathrm{d}q_2' + \frac{\partial^2 S}{\partial q_2'' \partial q_2''}\mathrm{d}q_2'' \quad , \end{aligned} \tag{28}$$

so that an explicit expression for M is given by

$$M = \begin{pmatrix} \frac{\partial^2 S}{\partial q_2' \partial q_2''} \end{pmatrix}^{-1} \begin{pmatrix} -\partial^2 S/(\partial q_2' \partial q_2') & -1 \\ |\partial^2 S/(\partial q_2' \partial q_2'')\,\partial^2 S/(\partial q_2' \partial q_2'') & -\partial^2 S/(\partial q_2'' \partial q_2'') \\ -\partial^2 S/(\partial q_2' \partial q_2')\,\partial^2 S/(\partial q_2'' \partial q_2'')] & \end{pmatrix} \quad . \tag{29}$$

M has the property that its determinant is equal to one. If $|\mathrm{Tr}M| > 2$, then the periodic orbit is unstable and M has eigenvalues $\lambda_{1,2} = \exp(\pm u)$ or $\lambda_{1,2} = -\exp(\pm u)$, where $u > 0$ is the stability exponent. The line in (q_2, p_2)-space along the direction of the eigenvector of M with eigenvalue $\lambda = \exp(u)$ or $\lambda = -\exp(u)$ is called the unstable manifold, the line along the direction of the second eigenvector is called the stable manifold. If $|\mathrm{Tr}M| < 2$, then the periodic orbit is stable and M has eigenvalues $\lambda_{1,2} = \exp(\pm iv)$, where v is the angle of stability.

From eq. (24),(25) and (29) it follows that

$$\kappa = -\frac{1}{M_{12}}(2 - \mathrm{Tr}M) \tag{30}$$

and

$$g_{osc}(E) = \sum_{p.o.} \frac{1}{i\hbar}\int \mathrm{d}q_1 \frac{1}{|\dot{q}_1|}\frac{1}{\sqrt{|2 - \mathrm{Tr}M|}}\exp\{\frac{i}{\hbar}S(\vec{q}'',\vec{q}',E) - \frac{i\pi}{2}\nu\}\Bigg|_{\vec{q}''=\vec{q}'} \quad . \tag{31}$$

In order to perform the q_1-integration several points have to be taken into consideration. The action $S(\vec{q}'',\vec{q}',E)$ for the periodic orbit does not depend on q_1, and neither does the trace of the matrix M. This is the case, because if one chooses a different starting coordinate $\bar{q}_1$ then

$$M_{\bar{q}_1} = M^{-1}_{\bar{q}_1 \to q_1} M_{q_1} M_{\bar{q}_1 \to q_1} \quad , \tag{32}$$

where $M_{\bar{q}_1 \to q_1}$ is the monodromy matrix of the part of the periodic orbit from $\bar{q}_1$ to q_1. The number μ of conjugate points along the periodic orbit can change with q_1. A careful examination of the differential equation, that a deviation δq_2 of the periodic orbit satisfies as a function of time t, shows that μ can change at most between two values, which differ by 1. A detailed description is given in [28]. It further can be shown, that μ has the smaller one of the two values if $\kappa < 0$, and the larger value if $\kappa > 0$. For this reason the quantity ν is constant along the periodic orbit and can be interpreted as the maximum number of conjugate points of the periodic orbit. For a further interpretation we restrict ourselves on unstable periodic orbits, which are not reflected on a hard wall. The points at which μ changes are points, which are conjugate to itself, so-called self-conjugate points. They have the property, that if one starts with $\mathrm{d}q_2' = 0$ and $\mathrm{d}p_2' \neq 0$, then after a traversal of the periodic orbit one has $\mathrm{d}q_2'' = 0$. This is the case if and only if one of the eigenvectors of the monodromy-matrix is in the p_2-direction. If one now moves along the periodic orbit, the stable and unstable manifolds of the monodromy matrix for the periodic trajectory rotate in (q_2, p_2)-space around the origin, and it can be shown that the infinitesimal vector $(\mathrm{d}q_2, \mathrm{d}p_2)$ rotates together with the manifold on which it was at the starting point. Every point, at which the vector $(\mathrm{d}q_2, \mathrm{d}p_2)$ is orthogonal to the q_2-direction, is a conjugate point of the starting point. Since ν is equal to the number of conjugate points of the considered self-conjugate point, including the point itself, it follows that ν can also interpreted as $1/\pi$ times the total angle that either the unstable or the stable manifold rotates around the origin during one traversal of the periodic orbit. It follows that

the total number of self-conjugate points is equal to 2ν, since one can start along the unstable or the stable manifold.

We now come back to eq.(31) and perform the q_1-integration. This is done easily and the result is

$$g_{osc}(E) = \frac{1}{i\hbar} \sum_{p.o.} \frac{T_0}{\sqrt{|2 - \mathrm{Tr}M|}} \exp\{\frac{i}{\hbar} S(E) - \frac{i\pi}{2}\nu\} \ . \tag{33}$$

Here $S(E)$ is the short-hand notation for the action along the classical orbit. The summation extends over all periodic orbits of the classical system, including periodic orbits which are multiple repetitions of shorter periodic orbits. The q_1-integration is an integration in coordinate-space. It extends only up to the first returning to the starting point $(\vec{q}', \vec{p}')$ in phase space, i.e. the integration runs along the underlying primitive periodic orbit. T_0 is the period of this primitive periodic orbit. If the periodic orbit is self-retracing, i.e. it is invariant under time reversal, then the q_1-integration runs only along one half of the underlying primitive periodic orbit. But in this case every orbit counts twice, since there are two starting conditions for the momentum $\vec{p}'$ at every point of the orbit, which yield the same periodic orbit. For this reason again the form in eq.(33) is obtained.

It is convenient to split the sum over all periodic orbits into a double sum over all primitive periodic orbits and their multiple traversals. If k is the number of repetitions of the primitive orbit, then $S^{(k)}(E) = kS^{(1)}(E)$, $M^{(k)} = [M^{(1)}]^k$ and $\nu^{(k)} = k\nu^{(1)}$. One obtains

$$g_{osc}(E) = \frac{1}{i\hbar} \sum_{\gamma} \sum_{k=1}^{\infty} \frac{T_\gamma \exp(ikS_\gamma(E)/\hbar - i\pi k\nu_\gamma/2)}{\exp(ku_\gamma/2) - \sigma_\gamma^k \exp(-ku_\gamma/2)} \ . \tag{34}$$

Here γ labels all primitive periodic orbits, and $\mathrm{Tr}M_\gamma$ is expressed in terms of the stability exponent u_γ and the sign σ_γ of the trace of M_γ.

Eq.(34) is the final result of this section. It was derived in a series of papers by Gutzwiller [17]. Together with the background term $g_{(0)}(E)$ it gives the trace formula for the trace of the Green function. A corresponding expression for the level density $d(E)$ follows immediately from eq.(18). In two papers Balian and Bloch too derived contributions, that periodic orbits give to the semiclassical level density [29]. A corresponding formula for integrable systems was derived by Berry and Tabor [30,31].

There are several review articles, which either deal directly with the periodic-orbit theory, or treat it in connection with the quantum mechanics of classically chaotic systems. Among these articles are [22,10,32,33,34], see also [14].

In the derivation of the trace formula it is very difficult to keep control over the errors and to make any statements about the accuracy of the semiclassical approximation. For this reason it is very remarkable, that there exist strongly chaotic systems, for which the trace formula is exact rather than asymptotic. These systems describe the motion of particles on smooth compact Riemannian surfaces with constant negative curvature. In this case the trace formula is identical to the Selberg trace formula. A review is given by Balazs and Voros [35]. The Selberg trace formula has been studied intensively by mathematicians for many years. Mathematical tools have been developed in this connection, which are useful for the examination of the properties of the trace formula of Gutzwiller. Besides, the fact that the periodic-orbit theory is exact for some systems, suggests that it also gives useful approximations for other chaotic systems. Detailed numerical studies of the Selberg trace formula have been published in [36]. Further numerical examinations of smooth compact

Riemannian surfaces with constant negative curvature concern the classical periodic orbits [37], the quantum mechanical energy spectrum [38,39] and the wavefunctions [25].

The trace formula is one of the few analytical tools for the examination of the quantum mechanical energy spectrum of classically chaotic systems. For that reason there is a great interest in the trace formula despite its complicated structure and the fact, that it contains a sum over an infinite number of periodic orbits, which at best is conditionally convergent.

The trace formula was applied to the anisotropic Kepler model by Gutzwiller. He was able to obtain approximations for the first 22 energies [40,14]. In case of the H-atom in a strong magnetic field there are several papers which establish a relation between classical orbits and the quantum mechanical absorption or energy spectrum [41,42,43]. A generalization of the trace formula to the quasi-energy spectral density of a class of area-preserving maps was given by Tabor [44]. In case of the cat map the relation between the quasi-energy spectrum and the classical fixed points of the map is even exact [45]. Starting from the KKR-method of solid-state physics, Berry obtained a variant of eq.(34) for the Sinai billiard with additional contributions from families of neutral periodic orbits, whose monodromy matrix has eigenvalues $\lambda_{1,2} = 1$ [46]. Keating and Berry showed for the example of the (integrable) motion on the torus that singularities of partial sums of the trace formula not necessarily correspond to energy eigenvalues [47].

Despite the strong interest in the trace formula, up to now only little is known about the properties of the periodic-orbit theory as approximative theory. An analytical examination would require the knowledge about fine details of the asymptotic properties of the long periodic orbits, which is not available. A numerical examination of the accuracy of the trace formula on the other hand is difficult, since an accurate and complete determination of a sufficient number of the shortest periodic orbits is necessary, which is very difficult for most chaotic systems.

II.3 Discrete Symmetries

In this section the treatment of systems with discrete symmetries such as the invariance under reflection on a straight line is discussed. Discrete Symmetries can be used in order to restrict the periodic-orbit approximations to subspaces of the energy spectrum, which are defined by having a fixed eigenvalue of the symmetry operator. Such restrictions allow a much more effective application of the periodic-orbit theory. Part of the following discussion is given in [22]. The contribution of periodic orbits which run along the axis of symmetry is new. The derivation is carried out for one special symmetry, which is the invariance under reflection on the line $y = x$, since this is the symmetry of the system, which is considered in the following chapters. For other discrete symmetries the derivation can be done analogously.

The reflection on the line $y = x$ is represented by the operator R:

$$R(x, y) := (y, x) \ . \tag{35}$$

Let us consider a system, whose potential is invariant under the reflection on the line $y = x$:

$$V(x, y) = V(y, x) \ . \tag{36}$$

It then is possible to choose a basis of eigenfunctions of the Hamiltonian, which are either even or odd under reflection on the line $y = x$:

$$U_R\psi_n(x, y) := \psi_n(R(x, y)) = \psi_n(y, x) = \pm\psi_n(x, y) \ . \tag{37}$$

The Green function of the system can be splitted into an even and an odd part

$$G(\vec{q}'',\vec{q}',E) = \sum_n \frac{\psi_n(\vec{q}'')\psi_n^*(\vec{q}')}{E-E_n} \tag{38}$$

$$= G^+(\vec{q}'',\vec{q}',E) + G^-(\vec{q}'',\vec{q}',E) \ . \tag{39}$$

$G^+(\vec{q}'',\vec{q}',E)$ and $G^-(\vec{q}'',\vec{q}',E)$ are even and odd, respectively, with respect to both arguments $\vec{q}''$ and $\vec{q}'$ under the unitary operation U_R. Both functions are represented by sums of the form of eq. (38), where the summation is restricted to even and odd wavefunctions, respectively. They can be expressed as

$$G^\pm(\vec{q}'',\vec{q}',E) = \frac{1}{2}[G(\vec{q}'',\vec{q}',E) \pm G(R\vec{q}'',\vec{q}',E)] \ , \tag{40}$$

and using eq. (40) a periodic-orbit representation for their trace can be obtained

$$g^\pm(E) = \int \mathrm{d}x \int \mathrm{d}y \, G^\pm((x,y),(x,y),E) \ . \tag{41}$$

We restrict ourselves to the derivation of the oscillatory part of $g^\pm(E)$. The following steps are carried out analogously to the derivation of the general trace formula eq. (34). The Green function $G(\vec{q}'',\vec{q}',E)$ is represented by the sum over classical trajectories in eq. (8). The main contributions to the integral in eq. (41) come from trajectories from (x,y) to (x,y), which are close to trajectories, for which the phase of their contribution to the sum over trajectories is stationary. For the first term on the right-hand side of eq. (40) this argument gives the usual condition for periodic orbits, and the integration then yields the previously obtained periodic-orbit sum eq. (34) with an additional factor 1/2. For the second term on the right-hand side of eq. (40) the stationary phase argument gives the condition

$$[\frac{\mathrm{d}}{\mathrm{d}x''}S((y'',x''),(x',y'),E) + \frac{\mathrm{d}}{\mathrm{d}x'}S((y'',x''),(x',y'),E)]_{(x'',y'')=(x',y')=(x,y)} = 0 \ , \tag{42}$$

and an analogous condition for the y-derivatives. Both conditions can be combined into

$$[(R\vec{\nabla}'')S(\vec{q}'',\vec{q}',E) + \vec{\nabla}'S(\vec{q}'',\vec{q}',E)]_{R\vec{q}''=\vec{q}'=\vec{q}} = 0 \ , \ \vec{q}=(x,y) \ , \tag{43}$$

which results in

$$R\vec{p}'' = \vec{p}' \ . \tag{44}$$

The stationary phase argument thus selects trajectories, that start at point $\vec{q}'$ with momentum $\vec{p}'$, and end at point $\vec{q}'' = R\vec{q}'$ with momentum $\vec{p}'' = R\vec{p}'$. Let the time of the trajectory from $\vec{q}'$ to $\vec{q}''$ be T. Because of the invariance of the system under the reflection R, a trajectory that starts at $\vec{q}''$ with momentum $\vec{p}''$ will after time T arrive at $R\vec{q}'' = \vec{q}'$ with momentum $R\vec{p}'' = \vec{p}'$. That means that $\vec{q}'$ and $\vec{p}'$ are also the initial conditions of a periodic orbit. This periodic orbit has the property that it is invariant under reflection on the line $y = x$. For that reason the trajectories, which are obtained by the stationary phase argument, can be given a direct interpretation. In doing so one has to consider two cases. If there are periodic orbits which run along the line $y = x$ only, then these orbits satisfy the conditions $\vec{q}'' = R\vec{q}'' = \vec{q}'$ and $\vec{p}'' = R\vec{p}'' = \vec{p}'$, which in this case are the conditions for the periodic orbit itself. In all other cases the conditions $\vec{q}'' = R\vec{q}'$ and $\vec{p}'' = R\vec{p}'$ mark

trajectories, which are halves of periodic orbits, which are invariant under reflection on the line $y = x$.

The integral in eq. (41) is done by stationary phase approximation. The main contributions to the integral come from trajectories, which run from a point $\vec{q}$ to its mirror point $R\vec{q}$, and which are close to a trajectory that additionally satisfies eq. (44). In the following this trajectory is called the central trajectory. The contributions of trajectories, which are close to the central trajectory, are approximated by expanding the phase of their contribution to the Green function up to second order. For that reason again a local coordinate system is introduced, whose first coordinate q_1 varies along the trajectory, and whose second coordinate q_2 is perpendicular to it. Let the starting point of the central trajectory be $\vec{q}'$ and its end point be $\vec{q}'' = R\vec{q}'$. Now consider a trajectory, which starts at $\vec{q} = \vec{q}' + \delta\vec{q}'$ and ends at $R\vec{q} = \vec{q}'' + \delta\vec{q}'' = R\vec{q}' + R\delta\vec{q}'$. If $\delta\vec{q}'$ has only a component in the q_1-direction then

$$S(R\vec{q},\vec{q},E) = S(\vec{q}'',\vec{q}',E) \ , \tag{45}$$

which follows from the symmetry of the system. For that reason it is assumed in the following that $\delta\vec{q}'$ has only a component in the q_2-direction. This component is denoted by q_2. The component of $\delta\vec{q}''$ in the q_2-direction then is equal to $(-q_2)$. In order to see this it is assumed that the coordinate q_1 increases monotonically with time, and that the positive axis of the coordinate q_2 is anticlockwise with respect to the positive q_1-axis. If $\delta\vec{q}'$ is clockwise with respect to $\vec{p}'$, then $R\delta\vec{q}' = \delta\vec{q}''$ is anticlockwise with respect to $R\vec{p}' = \vec{p}''$ and vice versa. From this it follows that the q_2-coordinate of $\delta\vec{q}''$ has the opposite sign of the q_2-coordinate of $\delta\vec{q}'$. The expansion of the action then gives

$$S(R\vec{q},\vec{q},E) = \left[S(\vec{q}'',\vec{q}',E) + \frac{1}{2}\left(\frac{\partial^2 S}{\partial q_2' \partial q_2'}q_2^2 + 2\frac{\partial^2 S}{\partial q_2' \partial q_2''}(-q_2)q_2 + \frac{\partial^2 S}{\partial q_2'' \partial q_2''}(-q_2)^2\right)\right]_{R\vec{q}''=\vec{q}'} \tag{46}$$

After the q_2-integration the contribution of one trajectory is given by

$$\pm\frac{1}{2}\frac{1}{i\hbar}\int \mathrm{d}q_1 \, \frac{1}{|\dot{q}_1|}\sqrt{\left|\frac{-\partial^2 S/(\partial q_2' \partial q_2'')}{\kappa}\right|}\exp\left\{\frac{i}{\hbar}S(\vec{q}'',\vec{q}',E) - \frac{i\pi}{2}\nu\right\}\Bigg|_{R\vec{q}''=\vec{q}'} \ , \tag{47}$$

where

$$\kappa = \frac{\partial^2 S}{\partial q_2' \partial q_2'} - 2\frac{\partial^2 S}{\partial q_2' \partial q_2''} + \frac{\partial^2 S}{\partial q_2'' \partial q_2''} \tag{48}$$

and

$$\nu = \begin{cases} \mu & , \kappa > 0 \\ \mu + 1 & , \kappa < 0 \ . \end{cases} \tag{49}$$

From eq. (29) it follows that

$$\kappa = -\frac{1}{M_{12}}(-2 - \mathrm{Tr}M) = -\frac{1}{(-M_{12})}(2 - \mathrm{Tr}(-M)) \ , \tag{50}$$

where M is the monodromy matrix of the trajectory from $\vec{q}'$ to $\vec{q}''$. In contrast to eq. (30), in eq. (50) all elements of the monodromy matrix enter with an additional minus sign. This result can be interpreted in a different way. For that purpose a desymmetrized system is introduced, which is defined by restricting the original system to the region $\{(x,y)|x > y\}$,

and introducing a hard wall along the line $y = x$. For every orbit in the full system a corresponding trajectory in the desymmetrized system is found, by reflecting that part of the trajectory, which runs in the region $\{(x,y)|x < y\}$, about the line $y = x$ into the region $\{(x,y)|x > y\}$. Every crossing of the line $y = x$ in the full system corresponds to a reflection on the line $y = x$ in the desymmetrized system. In the following discussion we first do not consider possible periodic orbits along the line $y = x$. Trajectories, which run from $\vec{q}'$ to its mirror point $\vec{q}'' = R\vec{q}'$ in the full system, correspond to periodic orbits in the desymmetrized system, which are reflected an odd number of times on the line $y = x$. The monodromy matrix of such a periodic orbit in the desymmetrized system differs from the monodromy matrix of the corresponding trajectory in the full system by an overall minus sign, whose origin is the odd number of reflections on the line $y = x$. Expressed in terms of the monodromy matrix of the periodic orbit in the desymmetrized system, the quantity κ has the previous form as in eq. (30). The q_1-integration is carried out in the full system along the symmetrical periodic orbit, which has the property, that the trajectory from $\vec{q}'$ to $\vec{q}''$ is one half of it. By this integration the period of the underlying primitive periodic orbit is obtained, which is twice the period of the corresponding primitive periodic orbit in the desymmetrized system. This factor two cancels the factor $1/2$ of the term (47). The total result, which is obtained from the second term in eq. (40), can be written as

$$\frac{1}{i\hbar}\sum_{\substack{p.o.\\ odd}}\frac{T_0\exp\{iS(E)/\hbar - i\pi\nu/2\}}{\sqrt{|2-\mathrm{Tr}M|}} \pm \frac{1}{2}\frac{1}{i\hbar}\sum_{\substack{p.o.\\ y=x}}\frac{T_0\exp\{iS(E)/\hbar - i\pi\nu/2\}}{\sqrt{|2+\mathrm{Tr}M|}} \quad . \tag{51}$$

The first term is the contribution of all periodic orbits of the desymmetrized system, which are reflected an odd number of times on the line $y = x$. All classical quantities are determined in the desymmetrized system, and the contributions of the periodic orbits have the same form as in eq. (33). The sign $\pm$ is included in the phase factor $\exp\{-i\pi\nu/2\}$. In the case of even wavefunctions, which satisfy Neumann boundary conditions on the line $y = x$, ν does not contain contributions from the reflections on the line $y = x$. In the case of odd wavefunctions, which satisfy Dirichlet boundary conditions on the line $y = x$, the odd number of reflections on the line $y = x$ contribute an odd multiple of 2 to the integer ν. The second term in (51) is the contribution of the orbits along the line $y = x$. In this case the factor $1/2$ does not cancel, since the length of such an orbit is the same in the full and the desymmetrized system. The monodromy matrix M in eq. (51) for these orbits is the monodromy matrix of the full system.

The result, which is obtained from the first term of eq. (40), is the usual sum over all periodic orbits of the full system, weighted with a factor $1/2$. This also can be reinterpreted in terms of the periodic orbits of the desymmetrized system. In doing so, one has to consider the contributions of three different kinds of periodic orbits separately. The periodic orbits along the line $y = x$ give the contribution

$$\frac{1}{2}\frac{1}{i\hbar}\sum_{\substack{p.o.\\ y=x}}\frac{T_0\exp\{iS(E)/\hbar - i\pi\nu/2\}}{\sqrt{|2-\mathrm{Tr}M|}} \quad . \tag{52}$$

A periodic orbit, which is symmetric with respect to the reflection on the line $y = x$, corresponds to a periodic orbit in the desymmetrized system, which is an even number of times repetition of a primitive periodic orbit. The underlying primitive periodic orbit is reflected an odd number of times on the line $y = x$, and twice its period is equal to the period of the

underlying primitive periodic orbit in the full system. This factor two cancels the factor $1/2$ coming from eq. (40).

A periodic orbit, which is not symmetric with respect to the reflection on the line $y = x$, corresponds to a periodic orbit in the desymmetrized system, whose underlying primitive periodic orbit is reflected an even number of times on the line $y = x$. In this case the period of the two underlying primitive periodic orbits in the full and the desymmetrized system are the same. But there are two periodic orbits in the full system, which are related by reflection on the line $y = x$, which correspond to the same orbit in the desymmetrized system, and this factor two cancels the factor $1/2$ coming from eq. (40).

Putting everything together, the final result is

$$\begin{aligned} g^{\pm}_{osc}(E) \;=\; & \frac{1}{i\hbar}\sum_{\substack{p.o.\\ even}}\frac{T_0\exp\{iS(E)/\hbar - i\pi\nu/2\}}{\sqrt{|2-\mathrm{Tr}M|}} + \frac{1}{i\hbar}\sum_{\substack{p.o.\\ odd}}\frac{T_0\exp\{iS(E)/\hbar - i\pi\nu/2\}}{\sqrt{|2-\mathrm{Tr}M|}} \\ & + \frac{1}{i\hbar}\sum_{\substack{p.o.\\ y=x}}\exp\{iS(E)/\hbar - i\pi\nu/2\}\,\frac{1}{2}\left(\frac{T_0}{\sqrt{|2-\mathrm{Tr}M|}} \pm \frac{T_0}{\sqrt{|2+\mathrm{Tr}M|}}\right) \quad . \end{aligned} \tag{53}$$

An analogous formula for bordered Riemann surfaces was derived by Bolte and Steiner [48]. The last term in eq. (53) can also be given an interpretation in terms of the quantities of the desymmetrized system. Its special form is the result of the fact, that for orbits along the line $y = x$ there is no unique monodromy matrix. For such an orbit two monodromy matrices M^+ and M^- have to be defined, which differ by an overall minus sign: $M^+ = M = -M^-$, where M is the monodromy matrix of the full system. The behaviour of trajectories, which are infinitesimally close to the periodic orbit and are reflected an even number of times on the line $y = x$ during one traversal, is described by M^+. In case of an odd number of reflections the monodromy matrix is equal to M^-.

The final result eq. (53) can be expressed in terms of the primitive periodic orbits

$$g^{\pm}_{osc}(E) = \frac{1}{i\hbar}\sum_{\gamma}\sum_{k=1}^{\infty}\frac{T_\gamma\exp(ikS_\gamma(E)/\hbar - i\pi k\nu_\gamma/2)}{\exp(ku_\gamma/2) - \sigma_\gamma^k\exp(-ku_\gamma/2)}a^{\pm}_{\gamma,k} \quad , \tag{54}$$

where

$$a^{+}_{\gamma,k} = \begin{cases} [1+\sigma_\gamma^k\exp(-ku_\gamma)]^{-1} & \text{for orbits along the line } y = x \\ 1 & \text{otherwise} \end{cases} \tag{55}$$

and

$$a^{-}_{\gamma,k} = \begin{cases} [1+\sigma_\gamma^k\exp(ku_\gamma)]^{-1} & \text{for orbits along the line } y = x \\ 1 & \text{otherwise} \quad , \end{cases} \tag{56}$$

and σ_γ is the sign of the trace of the matrix M^+ in case of orbits along the line $y = x$.

II.4 The Dynamical Zeta Function

Up to now the periodic-orbit approximation for the trace of the Green function $g(E)$ was considered, which has poles at the quantum mechanical energies. In this section an alternative formulation in terms of a dynamical zeta function is given, whose zeros approximate the quantum mechanical energies. This zeta function is defined in analogy to the Selberg zeta function for the motion on smooth compact Riemannian surfaces with constant negative curvature.

The result is given in a form, which can be applied also to the two partial spectra of a system, which is invariant under reflection on a straight line. Then the periodic-orbit sum is evaluated with the periodic orbits of the desymmetrized system. We again choose the axis of symmetry to be equal to the line $y = x$. The results of this section, however, can also be applied to systems with no symmetry, which possibly have periodic orbits, that run along a straight line segment of the boundary only.

In this section the derivation is given for orbits, that do not run along the boundary. The calculation for orbits along the boundary is carried out in appendix A, and the result is stated.

$$\begin{aligned} g(E) &\approx g_{(0)}(E) + \frac{1}{i\hbar}\sum_\gamma \sum_{k=1}^{\infty} \frac{T_\gamma \exp(ikS_\gamma(E)/\hbar - i\pi k\nu_\gamma/2)}{\exp(ku_\gamma/2) - \sigma_\gamma^k \exp(-ku_\gamma/2)} \\ &= g_{(0)}(E) + \frac{1}{i\hbar}\sum_\gamma \sum_{k=1}^{\infty} \frac{T_\gamma \exp(ikS_\gamma(E)/\hbar - i\pi k\nu_\gamma/2 - ku_\gamma/2)}{1 - \sigma_\gamma^k \exp(-ku_\gamma)} \\ &= g_{(0)}(E) + \frac{1}{i\hbar}\sum_\gamma \sum_{k=1}^{\infty}\sum_{n=0}^{\infty} T_\gamma \sigma_\gamma^{kn} \exp(\frac{i}{\hbar}kS_\gamma(E) - \frac{i\pi}{2}k\nu_\gamma - \frac{ku_\gamma}{2} - knu_\gamma) \\ &= g_{(0)}(E) + \frac{1}{i\hbar}\sum_\gamma \sum_{n=0}^{\infty} \frac{T_\gamma \sigma_\gamma^n \exp(iS_\gamma(E)/\hbar - i\pi\nu_\gamma/2 - u_\gamma/2 - nu_\gamma)}{1 - \sigma_\gamma^n \exp(iS_\gamma(E)/\hbar - i\pi\nu_\gamma/2 - u_\gamma/2 - nu_\gamma)} \\ &= g_{(0)}(E) + \sum_\gamma \sum_{n=0}^{\infty} \frac{\mathrm{d}}{\mathrm{d}E} \log[1 - \sigma_\gamma^n \exp(\frac{i}{\hbar}S_\gamma(E) - \frac{i\pi}{2}\nu_\gamma - \frac{u_\gamma}{2} - nu_\gamma)] \\ &= g_{(0)}(E) + \frac{\mathrm{d}}{\mathrm{d}E}\log Z(E) \ , \end{aligned} \tag{57}$$

where

$$Z(E) = \prod_\gamma \prod_{n=0}^{\infty} [1 - \sigma_\gamma^n \exp\{\frac{i}{\hbar}S_\gamma(E) - \frac{i\pi}{2}\nu_\gamma - u_\gamma(\frac{1}{2} + n)\}] \ . \tag{58}$$

The general result including contributions of possible orbits along the line $y = x$ for a desymmetrized system, whose corresponding full system is invariant under reflection on this line, is given by

$$Z(E) = \prod_\gamma \prod_{n=0}^{\infty} [1 - \sigma_\gamma^n b_{\gamma,n} \exp\{\frac{i}{\hbar}S_\gamma(E) - \frac{i\pi}{2}\nu_\gamma - u_\gamma(\frac{1}{2} + n)\}] \ , \tag{59}$$

where in the case of Neumann boundary conditions along the line $y = x$ one has

$$b_{\gamma,n} = \begin{cases} \sigma_\gamma^n \exp\{-nu_\gamma\} & \text{for orbits along the line } y = x \\ 1 & \text{otherwise} \ , \end{cases} \tag{60}$$

and in the case of Dirichlet boundary conditions

$$b_{\gamma,n} = \begin{cases} \sigma_\gamma^{(n+1)} \exp\{-(n+1)u_\gamma\} & \text{for orbits along the line } y = x \\ 1 & \text{otherwise} \ . \end{cases} \tag{61}$$

This can be interpreted in the following way. The zeta function of the full system is the product of the two zeta functions of the desymmetrized system: $Z(E) = Z^+(E) \cdot Z^-(E)$. In particular the contribution of an orbit along the line $y = x$ to $Z(E)$ consists of the product of the contributions of this orbit to $Z^+(E)$ and $Z^-(E)$. From equations (59), (60) and (61) it

follows that the contribution of this orbit to $Z^+(E)$ is identical to the product over all even n in the contribution of this orbit to $Z(E)$. The product over all odd n in the contribution to $Z(E)$ is identical to contribution of this orbit to $Z^-(E)$.

In deriving eq. (58) the convergence properties of the occuring sums and products have not been considered. A discussion of the problems that are connected with the product representation of the zeta function is given in [49].

There is an analogy between eq. (58) and the Euler product representation of the Riemann zeta function $\zeta(z)$. According to the famous Riemann hypothesis all complex zeros of $\zeta(z)$ have real part 1/2. On the assumption that this hypothesis is true, there are suggestions to interpret the imaginary parts of the complex zeros of $\zeta(z)$ as the eigenvalues of a hermitian operator, which has a classical limit that describes a chaotic system [50].

The product eq. (58) is the starting point for the cycle-expansion of Cvitanović for systems, in which an effective code for the periodic orbits is available. By this method the product eq. (58) is expanded and subsequently the terms are sorted according to certain properties of the code of the periodic orbits [51,52,53].

The product representation of the zeta function is transformed into a series by using the Euler identity [54]

$$\prod_{n=0}^{\infty}(1 - yx^n) = \sum_{m=0}^{\infty} \frac{(-1)^m y^m x^{m(m-1)/2}}{\prod_{j=1}^m (1 - x^j)} \ , \tag{62}$$

where $\prod_{j=1}^{m=0}(1 - x^j)$ is defined to be equal to one. The contribution of an ordinary orbit to the product representation of the zeta function then is transformed in the following way

$$\begin{aligned} &\prod_{n=0}^{\infty}[1 - \sigma_\gamma^n \exp\{\frac{i}{\hbar}S_\gamma(E) - \frac{i\pi}{2}\nu_\gamma - u_\gamma(\frac{1}{2} + n)\}] \\ &= \sum_{m=0}^{\infty} \frac{(-1)^m \sigma_\gamma^{m(m-1)/2} \exp\{imS_\gamma(E)/\hbar - i\pi m\nu_\gamma/2 - mu_\gamma/2 - m(m-1)u_\gamma/2\}}{\prod_{j=1}^m [1 - \sigma_\gamma^j \exp(-ju_\gamma)]} \\ &= \sum_{m=0}^{\infty} \frac{(-1)^m \sigma_\gamma^{m(m-1)/2} \exp\{imS_\gamma(E)/\hbar - i\pi m\nu_\gamma/2 - u_\gamma m(m-1)/4\}}{\prod_{j=1}^m [\exp(ju_\gamma/2) - \sigma_\gamma^j \exp(-ju_\gamma/2)]} \ . \end{aligned} \tag{63}$$

The total result is given by

$$\begin{aligned} Z(E) = \prod_\gamma \Bigg[&\sum_{m=0}^{\infty} (-1)^m \sigma_\gamma^{m(m-1)/2} \exp\{\frac{i}{\hbar}mS_\gamma(E) - \frac{i\pi}{2}m\nu_\gamma - u_\gamma \frac{m(m-1)}{4}\} \\ &\times \prod_{j=1}^m \frac{c_{\gamma,j}}{\exp(ju_\gamma/2) - \sigma_\gamma^j \exp(-ju_\gamma/2)} \Bigg] \ , \end{aligned} \tag{64}$$

where in the case of Neumann boundary conditions along the line $y = x$ one has

$$c_{\gamma,j} = \begin{cases} \sigma_\gamma \exp(u_\gamma)[1 + \sigma_\gamma^j \exp(ju_\gamma)]^{-1} & \text{for orbits along the line } y = x \\ 1 & \text{otherwise} \ , \end{cases} \tag{65}$$

and in the case of Dirichlet boundary conditions

$$c_{\gamma,j} = \begin{cases} [1 + \sigma_\gamma^j \exp(ju_\gamma)]^{-1} & \text{for orbits along the line } y = x \\ 1 & \text{otherwise} \ . \end{cases} \tag{66}$$

A representation of the zeta function by a series is obtained by expanding the product over primitive periodic orbits in eq. (64). The result is a series of the form

$$Z(E) = 1 + \sum_{n=1}^{\infty} A_n \exp\{\frac{i}{\hbar} S_n(E)\} \ , \tag{67}$$

where the sum extends over all possible combinations of primitive periodic orbits. More precisely, the quantities $S_n(E)$ denote all possible linear combinations of the actions of all primitive periodic orbits

$$S_n(E) = \sum_{i=1}^{k} m_i S_{\gamma_i}(E) \ , \tag{68}$$

where $k \geq 1$, all m_i are arbitrary positive integers, and all γ_i are different. These linear combinations of periodic orbits are called pseudo-orbits, and the quantities $S_n(E)$ denote their actions. The amplitudes A_n are defined as

$$A_n = \prod_{i=1}^{k} \frac{(-1)^{m_i} \sigma_{\gamma_i}^{m_i(m_i-1)/2} \exp\{-i\pi m_i \nu_{\gamma_i}/2 - u_{\gamma_i} m_i(m_i-1)/4\}}{\prod_{j=1}^{m_i} |(\exp(j u_{\gamma_i}/2) - \sigma_{\gamma_i}^{j} \exp(-j u_{\gamma_i}/2)| c_{\gamma_i,j}^{-1}} \ . \tag{69}$$

An approximation for eq. (67) by a sum over a finite number of pseudo-orbits in analogy with the Riemann-Siegel formula for the Riemann zeta function was suggested by Berry and Keating [55]. It is discussed in more detail in section V.8.

II.5 The Convergence Properties of the Trace Formula

Gutzwiller's semiclassical approximation for $g_{osc}(E)$ eq. (34) has the general form of a sum over an energy-dependent oscillating term multiplied by an amplitude factor. The convergence of the periodic-orbit sum strongly depends on the phase-factors ν_γ. In the general case there is not sufficient information about asymptotic properties of long periodic orbits available, in order to estimate, whether the periodic-orbit sum converges for real values of the energy E or not. The sum is, however, not absolutely convergent for real values of E. This is a consequence of the specific property of chaotic systems, that the number of periodic orbits proliferates exponentially with period T. In the limit $T \to \infty$ the number of periodic orbits, which have a period between T and $T + \mathrm{d}T$, is given by

$$\mathrm{d}\mathcal{N} \to \frac{\exp(hT)}{T} \mathrm{d}T \quad , T \to \infty \ , \tag{70}$$

where h is the topological entropy. For an estimation, if the periodic-orbit sum converges absolutely, also the asymptotic properties of the stability exponents u_γ are needed. From the property, that very long orbits of bounded chaotic systems explore the surface of constant energy in phase space uniformly, it is estimated that [10]

$$< \exp(\frac{u_\gamma}{2}) > \ \to \ < \exp(\frac{hT}{2}) > \quad , T \to \infty \ , \tag{71}$$

where the average is taken over all periodic orbits with a period in the interval between T and $T + \mathrm{d}T$. The sum of amplitudes in the interval $[T, T + \mathrm{d}T]$ thus increases like $\exp(hT/2)$ as $T \to \infty$, and thus the periodic-orbit sum is not absolutely convergent.

A solution to the problem of a divergent periodic-orbit sum is the smoothing of the original trace formula. By this smoothing the function $g(E)$, which has poles at the energies E_n, is replaced by a function, which has peaks of finite height and width at the energies E_n. The width of the peaks has to be sufficiently smaller than the mean level spacing, in order to allow the discrimination of individual energies. In the following the convergence properties of the periodic-orbit sum are examined in more detail, and it is shown, how the smoothing can be done in a mathematically exact way. Further it is discussed, what kind of smoothing leads to absolutely convergent periodic-orbit sums.

For simplicity from now on we restrict ourselves to plane billiard systems. The classical motion of a particle in a billiard system consists of the free motion within the billiard area and elastic reflections on the boundary. The corresponding quantum mechanical problem is described by the free Schrödinger equation with Dirichlet boundary conditions on the billiard boundary. In the following only systems are considered, which have unstable periodic orbits only. A sufficient condition for this is, that the boundary consists of concave and straight pieces only, with the additional condition, that every classical trajectory is reflected from a concave part of the boundary at least once.

The classical action is given by $S_\gamma = p\, l_\gamma$ and the period is $T_\gamma = (m/p) l_\gamma$, where l_γ is the length of the orbit γ and $p = \sqrt{2mE}$ is the momentum of the moving particle with mass m. The stability exponents $u_\gamma > 0$ can be expressed by geometrical quantities and are energy-independent. They can be determined according to the method of appendix B. In order to obtain a convergent periodic-orbit sum, the momentum p is considered to be complex with a positive imaginary part. In the double sum over periodic orbits this leads to an exponential damping of the contributions of orbits with large length l_γ. In case of the energy density the introduction of a finite positive imaginary part for the energy $E \to E + i\Gamma/2$ corresponds to a substitution of the δ-functions by Breit-Wigner curves

$$\delta(E - E_n) \implies -\frac{1}{\pi} \mathrm{Im} \frac{1}{E + i\frac{\Gamma}{2} - E_n} = \frac{1}{\pi} \frac{\frac{\Gamma}{2}}{(E - E_n)^2 + (\frac{\Gamma}{2})^2} \ . \tag{72}$$

For an estimation of the values of momentum p, for which the periodic-orbit sum for the oscillatory part of $g(E)$ is absolutely convergent, the sum over the absolute values of the terms in the series over periodic orbits is considered. From now on the more general form eq. (54) for the trace of the Green function is used.

$$\begin{aligned}
\sum_\gamma \sum_{k=1}^{\infty} \left| \frac{m l_\gamma}{\hbar p} \frac{\exp\{ikpl_\gamma/\hbar\}\, \chi_\gamma^k\, a_{\gamma,k}}{\sqrt{|2 - \mathrm{Tr} M_\gamma^k|}} \right| &= \sum_\gamma \sum_{k=1}^{\infty} \frac{m l_\gamma}{\hbar |p|} \frac{\exp\{-\mathrm{Im}\, p\, k l_\gamma/\hbar\}\, |a_{\gamma,k}|}{\exp\{k u_\gamma/2\} - \sigma_\gamma^k \exp\{-k u_\gamma/2\}} \\
&< \frac{c_1}{|p|} \sum_\gamma \sum_{k=1}^{\infty} l_\gamma \exp\{-k(\frac{\mathrm{Im}\, p}{\hbar} l_\gamma + \frac{u_\gamma}{2})\} \\
&= \frac{c_1}{|p|} \sum_\gamma \frac{l_\gamma \exp\{-\mathrm{Im}\, p\, l_\gamma/\hbar - u_\gamma/2\}}{1 - \exp\{-\mathrm{Im}\, p\, l_\gamma/\hbar - u_\gamma/2\}} \\
&< \frac{c_2}{|p|} \sum_\gamma l_\gamma \exp\{-\mathrm{Im}\, p\, l_\gamma/\hbar - u_\gamma/2\} \ ,
\end{aligned} \tag{73}$$

where $a_{\gamma,k}$ is equal to $a_{\gamma,k}^+$ or $a_{\gamma,k}^-$ in equations (55) and (56), respectively, depending on the choice of the boundary conditions. $\chi_\gamma = \exp\{-i\pi\nu_\gamma/2\}$ denotes the phase factors of the individual terms. For the above estimation it is assumed that $u_\gamma \geq u_{min} > 0$ and

$l_\gamma \geq l_{min} > 0$ for all γ. c_1 and c_2 are two constants, whose value is not important for the present consideration. From eq. (70) follows, that in the limit $l \to \infty$ the number of periodic orbits, which have a length l_γ in the interval $[l, l + \mathrm{d}l]$, is given by

$$\mathrm{d}\mathcal{N} \to \frac{\exp(\tau l)}{l}\,\mathrm{d}l \quad , \; l \to \infty \; , \tag{74}$$

where $\tau = hm/p$. For the stability exponents it is assumed that

$$\exp\{-\frac{u_\gamma}{2}\} = O(\exp\{-\frac{\bar{\lambda} l_\gamma}{2}\}) \; , \; l_\gamma \to \infty \; , \; \bar{\lambda} \geq 0 \; , \tag{75}$$

which is weaker than eq. (71). On these conditions the sum in eq. (73) is convergent, if the integral

$$\int_{l_0}^{\infty} \mathrm{d}l \, \exp\{\tau l\} \exp\{-\frac{\mathrm{Im}\, p}{\hbar} l - \frac{\bar{\lambda}}{2} l\} \tag{76}$$

converges. This leads to the condition

$$\frac{\mathrm{Im}\, p}{\hbar} \; > \; \tau - \frac{\bar{\lambda}}{2} \; =: \; \frac{\sigma}{\hbar} \tag{77}$$

for the imaginary part of p. Similar considerations for systems with a homogeneous potential have been carried out by Eckhardt and Aurell [56]. Eq. (77) is a condition on the minimum width Γ_{min} of the Breit-Wigner curves in eq. (72) of the smoothed level density, $\Gamma > \Gamma_{min} := 4\sigma \mathrm{Re}\, p$. For billiards with finite area A the mean level spacing is asymptotically constant. When Γ_{min} as a function of $\mathrm{Re}\, p$ becomes larger than the mean level spacing, it is impossible to resolve different peaks. Therefore it is desirable to have a different kind of smoothing, which leads to convergent sums, but with no condition on the minimum width of the peaks.

This can be achieved by carrying out the smoothing with suitable functions $h(p)$. In order to derive the corresponding *generalized periodic-orbit sum rules* one considers a regularization of the trace $g(E)$ of the Green function. For billiards with finite area A the sum $\sum_n (E - E_n)^{-1}$ is infinite, since the eigenvalues E_n obey asymptotically $E_n = O(n)$, $n \to \infty$. However, the trace of the combination $(E - \hat{H})^{-1} - (E' - \hat{H})^{-1}$ is finite. Its semiclassical representation is obtained by using equations (21) and (54)

$$\begin{aligned} &\sum_n \left(\frac{2m}{p^2 - p_n^2} - \frac{2m}{p'^2 - p_n^2} \right) \\ &\approx \frac{mA}{\pi\hbar^2} \ln \frac{p}{p'} - \frac{i}{\hbar} \sum_\gamma \sum_{k=1}^{\infty} \frac{m l_\gamma \chi_\gamma^k a_{\gamma,k}}{\sqrt{|2 - \mathrm{Tr} M_\gamma^k|}} \left(\frac{\exp\{ipkl_\gamma/\hbar\}}{p} - \frac{\exp\{ip'kl_\gamma/\hbar\}}{p'} \right) \; , \end{aligned} \tag{78}$$

where $p_n = \sqrt{2mE_n}$ and A is the area of the billiard. Here all sums are absolutely convergent, if $\mathrm{Im}\, p > \sigma$ and $\mathrm{Im}\, p' > \sigma$.

All derivations up to this point have been carried out on the assumption, that the values of energy E have a positive imaginary part. The corresponding formula for energies E with negative imaginary part is obtained by using the relation

$$G(\vec{q}\,'', \vec{q}\,', E^*) = [G(\vec{q}\,'', \vec{q}\,', E)]^* \; . \tag{79}$$

A careful examination of the limiting process $\vec{q}\,'' \to \vec{q}\,'$ then shows, that formula (78) is also valid for the trace of the ingoing Green function ($\mathrm{Im} E < 0$), if the momentum p satisfies the

conditions $p^2 = 2mE$ and $\mathrm{Im}\, p > 0$. This means that eq. (78) is valid for *all* values of p with $\mathrm{Im}\, p > \sigma$.

Now eq. (78) is multiplied on both sides by $ip\,h(p)(2\pi m)^{-1}$ and integrated over p from $(i\sigma_o - \infty)$ to $(i\sigma_o + \infty)$, where $\sigma_o = \sigma + \varepsilon$ for some $\varepsilon > 0$, and σ is defined in eq. (77). The function $h(p)$ has to satisfy the following three conditions:

a) $h(p)$ is an even function of p

b) $h(p)$ is analytic in the strip $|\mathrm{Im}\, p| \leq \sigma + \varepsilon$

c) $|h(p)| \leq a|p|^{-2-\delta}$ for some $\delta > 0$, $a > 0$, $|p| \to \infty$.

The significance of these conditions will become clear in the following. The integration over the left-hand side of eq. (78) yields

$$\begin{aligned} &\sum_n \frac{i}{\pi} \int_{i\sigma_o - \infty}^{i\sigma_o + \infty} \mathrm{d}p\, h(p)\, p \left(\frac{1}{p^2 - p_n^2} - \frac{1}{p'^2 - p_n^2} \right) \\ &= \sum_n \frac{i}{2\pi} \left[\int_{i\sigma_o - \infty}^{i\sigma_o + \infty} \mathrm{d}p\, h(p)\, p \left(\frac{1}{p^2 - p_n^2} - \frac{1}{p'^2 - p_n^2} \right) + \int_{-i\sigma_o + \infty}^{-i\sigma_o - \infty} \mathrm{d}p\, h(p)\, p \left(\frac{1}{p^2 - p_n^2} - \frac{1}{p'^2 - p_n^2} \right) \right] \\ &= \sum_n h(p_n) \; . \end{aligned} \tag{80}$$

Here the evenness of $h(p)$ was used and the residue theorem was applied. Condition c) ensures the convergence of the last sum.

The integral over the first term on the right-hand side of eq. (78) can be evaluated by shifting the contour of integration to the real axis. The result is

$$\frac{iA}{2\pi^2\hbar^2} \left[\int_{-\infty}^{0} \mathrm{d}p\, p\, h(p) (\ln \frac{|p|}{p'} + i\pi) + \int_0^{\infty} \mathrm{d}p\, p\, h(p) \ln \frac{|p|}{p'} \right] = \int_0^{\infty} \mathrm{d}p\, p\, h(p) \frac{A}{2\pi\hbar^2} \; , \tag{81}$$

where again the evenness of $h(p)$ was used.

The integral over the last term in eq. (78) yields

$$\begin{aligned} &\sum_\gamma \sum_{k=1}^{\infty} \frac{l_\gamma \chi_\gamma^k a_{\gamma,k}}{2\pi\hbar \sqrt{|2 - \mathrm{Tr} M_\gamma^k|}} \int_{i\sigma_o - \infty}^{i\sigma_o + \infty} \mathrm{d}p\, p\, h(p) \left(\frac{\exp\{ipkl_\gamma/\hbar\}}{p} - \frac{\exp\{ip'kl_\gamma/\hbar\}}{p'} \right) \\ &= \sum_\gamma \sum_{k=1}^{\infty} \frac{l_\gamma \chi_\gamma^k a_{\gamma,k}}{2\pi\hbar \sqrt{|2 - \mathrm{Tr} M_\gamma^k|}} \int_{-\infty}^{\infty} \mathrm{d}p\, p\, h(p) \left(\frac{\exp\{ipkl_\gamma/\hbar\}}{p} - \frac{\exp\{ip'kl_\gamma/\hbar\}}{p'} \right) \\ &= \sum_\gamma \sum_{k=1}^{\infty} \frac{l_\gamma \chi_\gamma^k a_{\gamma,k}}{\hbar \sqrt{|2 - \mathrm{Tr} M_\gamma^k|}} g(\frac{kl_\gamma}{\hbar}) \; , \end{aligned} \tag{82}$$

where

$$g(x) = \frac{1}{\pi} \int_0^{\infty} \mathrm{d}p\, h(p) \cos(px) \; . \tag{83}$$

Here the contour of integration could be shifted to the real axis, since condition b) implies, that $g(x)$ drops faster than $\exp(-\sigma x)$ as $x \to \infty$. The total result is

$$\sum_n h(p_n) \approx \frac{1}{m} \int_0^{\infty} \mathrm{d}p\, p\, h(p) \bar{d}(E) + \frac{1}{\hbar} \sum_\gamma \sum_{k=1}^{\infty} \frac{l_\gamma \chi_\gamma^k g(kl_\gamma/\hbar)}{\sqrt{|2 - \mathrm{Tr} M_\gamma^k|}} a_{\gamma,k} \; , \; E = p^2 \; , \tag{84}$$

where $\bar{d}(E) = mA(2\pi\hbar^2)^{-1}$ is the mean level density of the billiard system. On conditions a), b) and c) all series and the integral in eq. (84) converge absolutely.

Eq. (84) was published previously in [57] for the case that $a_{\gamma,k} = 1$. By using a Gaussian smoothing one obtains a series, which is absolutely convergent, independently of the width of the peaks. This technique was applied successfully in [36,59,60,61] for the Selberg trace formula, in [58] for the hyperbola billiard and in [62] for the diamond billiard.

III The Classical Trajectories of the Hyperbola Billiard

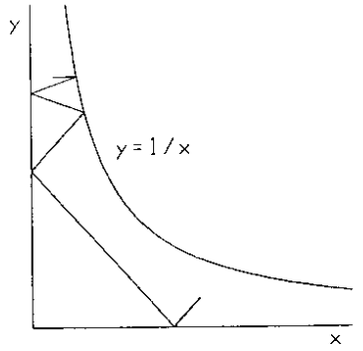

Figure 1: A classical trajectory in the hyperbola billiard

The system which is studied in this paper is a two-dimensional plane billiard system, the so-called hyperbola billiard. Its domain is given by

$$D := \{(x,y) | x \geq 0 \wedge y \geq 0 \wedge y \leq \frac{1}{x}\}\,, \tag{85}$$

i.e. it is bounded by the x-axis, the y-axis and the hyperbola $y = 1/x$. This system is unbounded and has an infinite area. However, no classical trajectory can escape to infinity, if trajectories along the axes are excluded. Every trajectory that runs into one of the two horns of the billiard region comes back after a finite time. Thus despite of the infinite billiard area the system is no scattering system, which on the quantum mechanical side is reflected by the fact, that the energy spectrum is purely discrete as was shown by Simon [63]. Previous studies of the hyperbola billiard have been published in [58,64]. Several reasons qualify the hyperbola billiard as a system, which is well suited for a systematic test of Gutzwiller's periodic-orbit theory.

Two-dimensional billiards are the simplest conservative systems that can show chaos. The classical motion in a billiard system consists of the motion along straight lines within the billiard area and elastic reflections on the boundary. For that reason the computational effort to follow a trajectory is low, since the equations of motion need not be integrated numerically. Neighbouring trajectories in a billiard system are focussed or defocussed depending on the curvature of the boundary and the lengths of the trajectories between consecutive hits on the boundary. The choice of the boundary determines, whether the system shows regular, chaotic or mixed behaviour (for examples see [65]). In case of the hyperbola billiard all orbits are isolated and unstable (see appendix B), and the system thus is chaotic.

For an efficient application of Gutzwiller's trace formula it is necessary to have a classification of the periodic orbits. This means that every orbit is characterized by a sequence of letters, which contains information about certain properties of the orbit. Without such

a code the search for periodic orbits is difficult, since one has no clue where to seek for the orbits in phase space. In addition, one has no control if any orbits have been missed. The simple geometrical form of the hyperbola billiard is the origin of a very effective code. All the periodic orbits can be classified by sequences of three different letters.

The most important advantage of the hyperbola billiard, however, is the fact, that there exists a very powerful method for the determination of the periodic orbits with high accuracy. Chaotic systems have the property that initially close neighbouring trajectories diverge exponentially with time. For that reason small numerical errors grow very rapidly and it seems impossible to determine very long orbits with any reasonable accuracy. In case of the hyperbola billiard it is possible to avoid this problem by determining the reflection points on the hyperbola not one by one while following the trajectory, but all of them at the same time. This can be done since there exists an extremum principle for the periodic orbits, which is explained and proved in appendix C. It states that the length of a periodic orbit is minimal within a certain class of neighbouring "trial" trajectories, which do not satisfy the elastic reflection condition on the boundary curve $y = 1/x$.

For theoretical considerations it is sometimes of advantage, to consider the hyperbola billiard as limiting case of a family of chaotic billiard systems, which are bounded and have a finite area. This family of billiard systems is described most conveniently in hyperbolic coordinates

$$\begin{aligned} \eta &= xy \\ \xi &= \frac{1}{2}(x^2 - y^2) \quad . \end{aligned} \tag{86}$$

In these coordinates the domain of the hyperbola billiard is an infinite strip and is given by $0 \leq \eta \leq 1$, $-\infty < \xi < \infty$. Now consider the family of billiard systems with $0 \leq \eta \leq 1$ and $-\xi_0 \leq \xi \leq \xi_0$. For $0 < \xi_0 < \infty$ these systems are bounded, chaotic and have isolated unstable periodic orbits only. In cartesian coordinates their form is that of a hyperbola billiard, whose two infinite horns are cut symmetrically by two hyperbolae. Most of the numerical results in this paper would be identical within the numerical accuracy with results for a billiard system with finite ξ_0, if ξ_0 is chosen large enough.

In this chapter the properties of the classical orbits of the hyperbola billiard are examined. The code for the full hyperbola billiard and its desymmetrized version are given. The determination of a large number of periodic orbits allows a detailed study of properties of the lengths and Lyapunov exponents of the periodic orbits.

III.1 Code for the Classical Trajectories

III.1.1 Code for the Full Hyperbola Billiard

Every trajectory in the hyperbola billiard consists of straight line segments and reflections on the axes or the hyperbola. For geometrical reasons there are only three possibilities for the particle to move between two consecutive hits on the hyperbola. It can be reflected on the x-axis only, on the y-axis only, or once on both axes. From this property an efficient code for the periodic orbits is obtained. A periodic trajectory is traversed once and the number of reflections on the hyperbola is counted. Let this number be N. The N points on the

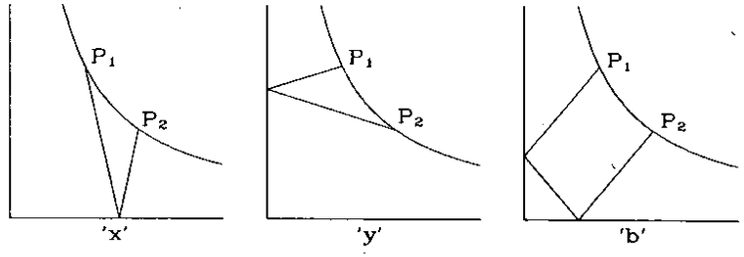

Figure 2: Illustration of the code for a segment of an orbit

hyperbola divide the orbit into N segments. Each segment is denoted by one of the letters "x", "y" or "b" according as the particle is reflected in the segment on the x-axis only, on the y-axis only or on both axes, respectively. In this way a ternary sequence of the form

$$a = (a_1, \ldots, a_N) \ , \ \text{where} \ \ a_i = \text{x, y or b} \ , \tag{87}$$

is associated to every periodic orbit. In order to obtain a code word, a starting point on the hyperbola has to be chosen. If one starts at a different point, one obtains a word which is a cyclic permutation of the original one. Thus all cyclic permutations of a word describe the same periodic orbit. For that reason it is useful to associate not one code word but a class of code words to a periodic orbit. This class is called cyclic class. Two words a and $\bar{a}$ belong to the same cyclic class if

$$a \equiv \bar{a} \Longleftrightarrow a_i = \bar{a}_{i+n} \, \forall \, i = 1, \ldots, N \quad \text{for one } n \in \{1, \ldots, N\} \ , \tag{88}$$

where $a_{j+N} = a_j$.

The code can also be used in order to characterize unperiodic trajectories. In this case the sequence, that is assigned to a trajectory, is infinitely long. The sequence of letters labels a trajectory uniquely in the sense, that there is at most one trajectory for every sequence. This is a consequence of the exponential divergence of neighbouring trajectories and of the fact, that the starting points of trajectories, which have a first finite part of their sequences in common, form a connected set. However, not for every sequence a corresponding trajectory exists. For example, periodic orbits corresponding to the code words (x) and (y) must have the property, that they are reflected on the hyperbola and one of the axes only. Those orbits cannot exist, since the slope of the hyperbola is negative and finite everywhere. For other sequences the question, if a corresponding orbit exists, is examined numerically.

Various properties of a periodic orbit follow directly from the code. It can be seen, for example, if a periodic orbit is primitive or if there exists an underlying shorter periodic orbit, which is traversed several times. In the latter case the code word is a multiple repetition of a shorter word. For example the word

$$a = (\underbrace{\text{x,x,y,b}}, \underbrace{\text{x,x,y,b}}, \underbrace{\text{x,x,y,b}}) \tag{89}$$

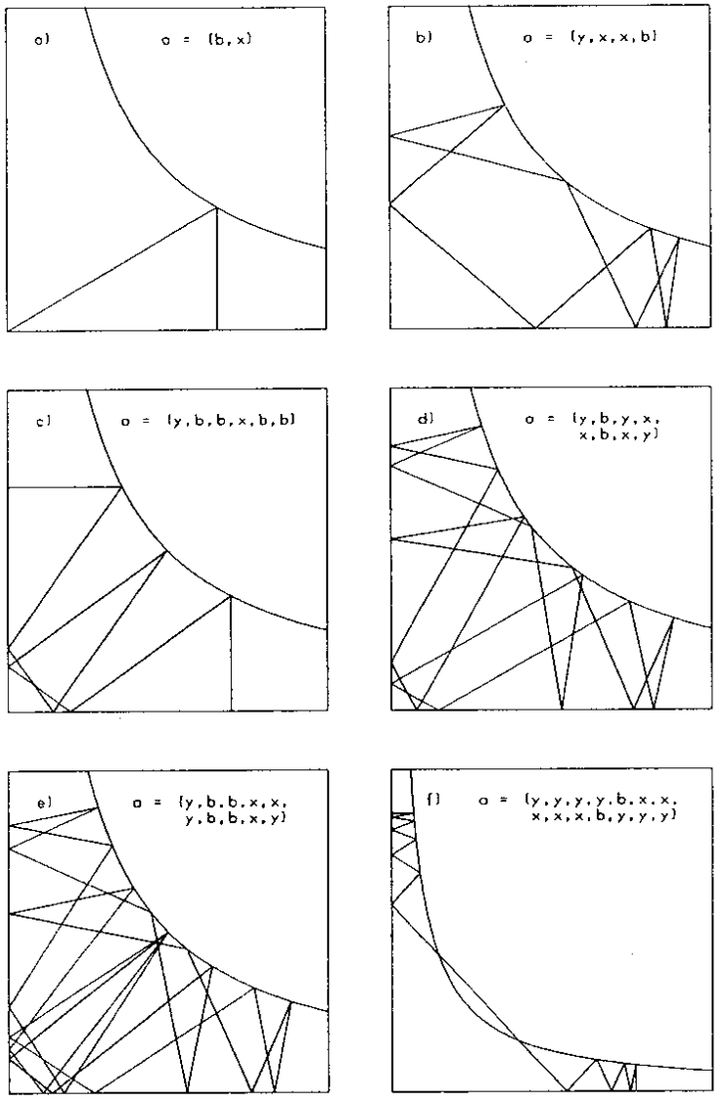

Figure 3: a) to e) Examples of periodic orbits f) Forbidden periodic orbit

describes an orbit, which is a three times repetition of the primitive orbit that is associated to the word (x,x,y,b). The number of cyclic classes of N letters, which correspond to a primitive orbit are given by the recursion relation

$$Z(N) = \frac{1}{N}(3^N - \sum_{\substack{M|N \\ M<N}} M \cdot Z(M)) \,, \tag{90}$$

where the sum runs over all integers M which are divisors of N excluding $M = N$. For $N = 1$ the result is $Z(1) = 3$. As has been mentioned above for two of this three cyclic classes there exists no corresponding periodic orbit.

Possible symmetries of an orbit can be read off from the code. If a periodic orbit is geometrically reflected on the straight line $y = x$, another periodic orbit is obtained, since the system is invariant under the reflection R on this line. The sequence belonging to the reflected orbit, "Ra", is obtained from the sequence of the original orbit "a" by replacing all "x" by "y" and all "y" by "x":

$$\mathrm{R}a := \bar{a} \text{ where } \bar{a}_i = \left\{ \begin{array}{lll} \mathrm{x} & \text{if} & a_i = \mathrm{y} \\ \mathrm{y} & \text{if} & a_i = \mathrm{x} \\ \mathrm{b} & \text{if} & a_i = \mathrm{b} \end{array} \right\} \,, \; i = 1, \ldots, N \,. \tag{91}$$

An orbit is invariant under this reflection, if R$a \equiv a$ holds.

Another possible symmetry of an orbit is time-reversal. If an orbit is traversed in reverse direction, the sequence of the reversed orbit, "Ta", is the reverse sequence of the original orbit:

$$\mathrm{T}a := \bar{a} \text{ where } \bar{a}_i = a_{N+1-i} \,, \; i = 1, \ldots, N \,. \tag{92}$$

An orbit is invariant under time-reversal, if T$a \equiv a$ holds.

In the following a more detailed examination of the properties of code words with a certain symmetry is given, and formulae for their numbers are presented. The form of code words with a certain symmetry are obtained from geometrical properties of orbits with this symmetry.

Code words with R$a \equiv a$:
Primitive code words with this symmetry exist only for even N or $N = 1$. For $N = 1$ there is only one code word, which is $a = (\mathrm{b})$. For even N all cyclic permutations of the code word have the form

$$a = c \oplus \mathrm{R}c \,, \tag{93}$$

where c is an arbitrary word of length $N/2$. The symbol $\oplus$ denotes the composition of the word a by words of smaller length. For example (x,y)$\oplus$(y)=(x,y,y). The number of primitive cyclic classes with this symmetry satisfies $Z_R(1) = 1$ and

$$Z_R(N) = (3^{N/2} - \sum_{\substack{M|N, M\nmid N/2 \\ M<N}} M \cdot Z_R(M) - 1)/N \,, \; N \text{even} \,, \tag{94}$$

where the sum runs over all integers $M \neq N$, which are divisors of N but not of $N/2$. The derivation is given in appendix D.

Code words with $\mathrm{T}a \equiv a$:
N odd: One cyclic permutation of the code word has the form

$$a = c \oplus e \oplus \mathrm{T}c \ , \tag{95}$$

where c and e stand for arbitrary words of lengths $(N-1)/2$ and 1, respectively. The number of primitive cyclic classes with $\mathrm{T}a \equiv a$ then is given by

$$Z_T(N) = 3^{(N+1)/2} - \sum_{\substack{M|N \\ M<N}} Z_T(M) \ . \tag{96}$$

Again for two of the three cyclic classes with $N = 1$ no corresponding periodic orbit exists.
N even: Two cyclic permutations of the code word have the form

$$a = e \oplus c \oplus f \oplus \mathrm{T}c \tag{97}$$

or

$$a = d \oplus \mathrm{T}d \ , \tag{98}$$

where c, d, e and f are arbitrary words of lengths $(N-2)/2$, $N/2$, 1 and 1, respectively. The recursion relation for the number of primitive cyclic classes follows as

$$Z_T(N) = 2 \cdot 3^{N/2} - \sum_{\substack{M|N \\ M<N}} Z_T(M) \ . \tag{99}$$

Code words with $\mathrm{RT}a \equiv a$:
N odd: One cyclic permutation of the code word has the form

$$a = c \oplus (\mathrm{b}) \oplus \mathrm{RT}c \ , \tag{100}$$

where c is an arbitrary word of lengths $(N-1)/2$. The number of primitive cyclic classes with $\mathrm{RT}a \equiv a$ is given by

$$Z_{RT}(N) = 3^{(N-1)/2} - \sum_{\substack{M|N \\ M<N}} Z_{RT}(M) \ . \tag{101}$$

N even: Two cyclic permutations of the code word have the form

$$a = (\mathrm{b}) \oplus c \oplus (\mathrm{b}) \oplus \mathrm{RT}c \tag{102}$$

or

$$a = d \oplus \mathrm{RT}d \ , \tag{103}$$

where c and d are arbitrary words of lengths $(N-2)/2$ and $N/2$, respectively. The recursion relation for the number of primitive cyclic classes then is given by

$$Z_{RT}(N) = 2 \cdot 3^{(N-2)/2} - \sum_{\substack{M|N \\ M<N}} Z_{RT}(M) \ . \tag{104}$$

N	cyclic classes	symm. classes	$\mathrm{T}u \equiv u$	$\mathrm{T}u \equiv \mathrm{R}u$	$\mathrm{R}u \equiv u$	$\mathrm{T}u \equiv u \equiv \mathrm{R}u$
1	3	2	3	1	1	1
2	3	2	3	1	1	1
3	8	4	6	2	0	0
4	18	9	12	4	2	2
5	48	20	24	8	0	0
6	116	44	42	14	4	4
7	312	104	78	26	0	0
8	810	253	144	48	10	8
9	2184	624	234	78	0	0
10	5880	1628	456	152	24	16
11	16104	4268	726	242	0	0
12	44220	11534	1392	464	60	24
13	122640	31388	2184	728	0	0
14	341484	86840	4290	1430	156	52

Table 1: For $N = 1$ to $N = 14$ this table contains the total number of primitive cyclic classes, the number of primitive symmetry classes, the number of primitive cyclic classes with $\mathrm{T}u \equiv u$, $\mathrm{T}u \equiv \mathrm{R}u$, $\mathrm{R}u \equiv u$ and $\mathrm{T}u \equiv u \equiv \mathrm{R}u$.

Code words with $a \equiv \mathrm{R}a \equiv \mathrm{T}a \equiv \mathrm{RT}a$:
These code words exist for $N = 1$ and even N only. For $N = 1$ there is one code word with this symmetry: $a = (\mathrm{b})$. In the case of even N two cases have to be considered separately:
$N/2$ odd: Two cyclic permutations of the code word have the form

$$a = c \oplus (\mathrm{b}) \oplus \mathrm{RT}c \oplus \mathrm{R}c \oplus (\mathrm{b}) \oplus \mathrm{T}c \tag{105}$$

or

$$a = e \oplus d \oplus \mathrm{RT}d \oplus \mathrm{R}e \oplus \mathrm{R}d \oplus \mathrm{T}d \ , \tag{106}$$

where c and d are arbitrary words of length $(N-2)/4$, and e is an arbitrary word of length 1. The recursion relation for the number of primitive cyclic classes is given by

$$Z_{R,T,RT}(N) = 2 \cdot 3^{(N-2)/4} - \sum_{\substack{M|N \\ M<N}} Z_{R,T,RT}(M) \ , \tag{107}$$

where it is implied that $Z_{R,T,RT}(1) = 1$ and $Z_{R,T,RT}(2M+1) = 0$ for $M = 1, 2, \ldots$.
$N/2$ even: Two cyclic permutations of the code word have the form

$$a = c \oplus \mathrm{RT}c \oplus \mathrm{R}c \oplus \mathrm{T}c \tag{108}$$

or

$$a = e \oplus d \oplus (\mathrm{b}) \oplus \mathrm{RT}d \oplus \mathrm{R}e \oplus \mathrm{R}d \oplus (\mathrm{b}) \oplus \mathrm{T}d \ , \tag{109}$$

where c, d and e are arbitrary words of length $N/4$, $(N-4)/4$ and 1, respectively. The recursion relation for the number of primitive cyclic classes is given by

$$Z_{R,T,RT}(N) = 3^{N/4} - \sum_{\substack{M|N, M\nmid(N/2) \\ M<N}} Z_{R,T,RT}(M) - 1 \ . \tag{110}$$

Different orbits which are related by reflection and/or time-reversal give an identical contribution to the periodic-orbit sum in the trace formula. For that reason it is useful to combine different cyclic classes to a bigger class, which we call symmetry class, if their sequences can be transformed into each other by reflection and/or time-reversal. A multiplicity is associated to every symmetry class, which counts the number of different cyclic classes which are contained in it. This number can be 1, 2 or 4. It then suffices to determine one periodic orbit for each symmetry class. In table 1 the number of all cyclic classes, symmetry classes, and the number of cyclic classes with certain symmetries are listed for N=1 to N=14.

III.1.2 Code for the Desymmetrized Hyperbola Billiard

If a system has discrete geometrical symmetries, the periodic-orbit theory can be applied separately to subspaces of the quantum mechanical energy spectrum, which are defined by having fixed eigenvalues of the geometrical symmetry. In order to do this, the periodic orbits of a desymmetrized version of the full system have to be determined.

In case of the hyperbola billiard the desymmetrized system is that billiard system, which is obtained by introducing an additional wall along the axis of symmetry $y = x$, i.e. the billiard system which is bounded by the x-axis the hyperbola $y = 1/x$ and the line $y = x$. There is a direct correspondence between orbits of the full system and orbits of the desymmetrized system. Every orbit of the full system is mapped onto an orbit of the desymmetrized system by reflecting down that part of the orbit, which is above the line $y = x$, into the lower half of the billiard system. In this way an orbit in the full system, which is not invariant under reflection on the line $y = x$, is mapped onto an orbit in the desymmetrized system, which has the same length. Orbits which in the full system are related by reflection on the line $y = x$ are mapped onto the same orbit in the desymmetrized system. An orbit which in the full system is invariant under reflection on the line $y = x$ is mapped onto an orbit which has half the length. (An exception is the orbit along the symmetry line $y = x$.)

A code for the orbits of the desymmetrized system is obtained from the original code according to the following rules:

A code word is read from left to right. Every "b" is replaced by a "0". If one arrives at a letter "x" or "y", two cases have to be considered. If the first letter to the left of the this letter, which is different from "b", is identical to the considered letter, it is replaced by a "+". If this is not the case, it is replaced by a "−". If there are only letters "b" to the left of the considered letter, the comparison has to be made with the utmost right letter in the code word, which is different from "b". For example

$$(\mathrm{x,b,b,x,y,x,b,y}) \longrightarrow (-,0,0,+,-,-,0,-) \ .$$

Original code words a and $\bar{a}$, which are related by $\bar{a} \equiv \mathrm{R}a$, are replaced by identical code words in the new code. Symmetrical code words $a \equiv \mathrm{R}a$, $a \neq (\mathrm{b})$, are replaced by a word, which consists of two identical halves, so that the underlying primitive code word is half as long. The relation between the two codes thus correctly reproduces the relation between the orbits in the full and the halved system.

The number of primitive cyclic classes of words with word length N is identical to that of the full billiard system.

In the desymmetrized system the only symmetry an orbit can have is the invariance under time-reversal. The code word for a time-reversed orbit in the new code is obtained in two steps:

— The letters "b" are kept fixed in the code word, and the remaining letters are cyclically permuted one step to the left.

— Then the sequence of all letters in the word is reversed.

For the above example the two steps result in

$$(-,0,0,+,-,-,0,-) \longrightarrow (+,0,0,-,-,-,0,-) \longrightarrow (-,0,-,-,-,0,0,+) \ .$$

If after the two steps a word is obtained, which is a cyclic permutation of the original word, then this word corresponds to an orbit which is invariant under time-reversal.

An equivalent code is used by Eckhardt and Wintgen for the hydrogen atom in a magnetic field [66]. For this system the equipotential lines are shaped like hyperbolae in an appropriate coordinate system. The difference between their code and the code used here, is that the meaning of "+" and "−" is exchanged.

III.2 Properties of the Classical Trajectories

In the following section properties of the periodic orbits of the desymmetrized billiard system are examined. The reason for the restriction to the desymmetrized hyperbola billiard is the fact, that the application of the periodic-orbit theory to this system yields much better results than the application to the full system. If in both cases all orbits up to a certain length l are included in the periodic-orbit sum, then in the desymmetrized case much more energy levels can be resolved. One reason for this is that the energy density is about half as large as in the full system. A further reason is that the energy spectrum of the desymmetrized billiard shows level repulsion, i.e. it has the tendency to avoid small distances between neighbouring energy levels. In the full system small spacings between neighbouring energy levels occur frequently and make the resolution of single energies difficult.

The total number of orbits that are needed in order to resolve a certain energy difference ΔE is in both systems about the same. In the full system, however, only about one fourth of this number of orbits have to be determined numerically. Most orbits are not invariant under time-reversal or reflection on the line $y = x$, and thus they belong to a group of four orbits, which give an identical contribution to the periodic-orbit sum. It suffices to determine one member of this group and multiply its contribution to the periodic-orbit sum by four. In the desymmetrized system orbits, which give an identical contribution to the periodic-orbit sum, can only be related by time reversal. Thus about twice the number of orbits as in the full system have to be determined.

The method by which the periodic orbits are determined is for both systems the same. As has been mentioned above there is a direct correspondence between orbits of the full system and orbits of the halved system. For that reason the orbits of the halved system can be determined by finding the corresponding orbits of the full system. The method of determination of the orbits consists of the following steps:

— The code word is fixed for the orbit one is looking for. Let the number of letters in this code word be N.

— N arbitrary points are chosen on the hyperbola $y = 1/x$ and are labelled by $P_1, \ldots, P_N$.

— These points are connected by N segments which correspond to the N letters of the code word as is shown in figure 2. For example, if the first letter is an "x", then P_1 and P_2 are connected by a segment, which is reflected on the x-axis once. By this construction a unique closed curve is defined, which in general does not represent a physical orbit for two possible reasons. First although the reflection condition is satisfied on the x-axis and the y-axis, it in general is not satisfied on the hyperbola. Second the segment which connects two consecutive points P_i and P_{i+1} on the hyperbola may run partly outside of the billiard region.

— The obtained curve has a length, which is a function of the points $P_1, \ldots, P_N$. The periodic orbit which belongs to the given code word is found by determining the minimum of this function of N variables.

The minimum of the length function was found by using a NAG-routine. The accuracy of the obtained result was improved by subsequently applying a Newton method with quadruple precision. In this way the periodic orbits are determined very quickly and with a very high accuracy. The mean CPU time on an IBM 3090 for the determination of a periodic orbit with an accuracy of 16 significant digits was 0.03 seconds.

The method was slightly varied when applied to orbits, whose length in the full system is twice the length of the corresponding orbits in the desymmetrized system. The code words of these orbits in the full system have an even number $2N$ of letters, and the orbits are invariant under reflection on the line $y = x$. It suffices to search for these orbits within the class of orbits, which are invariant under this reflection, too. This reduces a $2N$-parameter search to a N-parameter search.

III.2.1 The Periodic Orbits with Code Lengths $N \leq 14$

All orbits with code length $N \leq 14$ were determined. The number of orbits that were found for each N are given in table 2. Their number is approximately equal to $3^N/N$. In addition, the number of different lengths, the mean degeneracy of lengths $\bar{g}_l(N)$ and the numbers n_s and n_u of orbits, whose corresponding orbits in the full system are symmetric and unsymmetric, respectively, with respect to reflection on the line $y = x$, are listed. The degeneracy of the length of an orbit is one, if the orbit is invariant under time reversal. It is two, if the orbit is not invariant under time reversal, since then a different time reversed orbit exists, which has the same length. No accidental degeneracy of lengths has been found, i.e. no pair of different orbits has been found, which have the same length, but are not related by time reversal. The mean degeneracy $\bar{g}_l(N)$ approximates two if $N \to \infty$ since the number of orbits, which are invariant under time reversal, increases only proportional to $3^{N/2}$. The numbers n_s and n_u are approximately equal.

The number of orbits that were found is slightly less than the number of primitive code words for N=1 to N=14. The reason for this is that not to every code word a periodic orbit can be found. There are code words for which the orbit which corresponds to the minimum of the length function is unphysical, since it runs partly outside of the billiard region. An example of such an orbit is shown in figure 3 f). The number of forbidden orbits is, however, very small in comparison with the total number of orbits. In table 3 the number of forbidden orbits and its quotient with the total number of orbits are listed. For $N = 1$ there is one code word, for which no corresponding orbit exists, that is the word (+). The results for

N	orbits	length	$\bar{g}_l(N)$	$n_s(N)$	$n_u(N)$
1	2	2	1.000	1	1
2	3	3	1.000	2	1
3	8	8	1.000	4	4
4	18	16	1.125	10	8
5	48	40	1.200	24	24
6	115	81	1.420	59	56
7	310	206	1.505	154	156
8	808	487	1.659	408	400
9	2182	1246	1.751	1090	1092
10	5878	3202	1.836	2950	2928
11	16102	8534	1.887	8050	8052
12	44217	22919	1.929	22138	22079
13	122630	62768	1.954	61316	61314
14	341439	173211	1.971	170793	170646

Table 2: For $N = 1$ to $N = 14$ this table contains the total number of primitive periodic orbits of the desymmetrized system, the number of different lengths, the mean degeneracy of lengths $\bar{g}_l(N)$, and the numbers $n_s(N)$ and $n_u(N)$ of orbits, whose corresponding orbits in the full billiard system are symmetric and unsymmetric, respectively.

N	2 – 5	6	7	8	9	10
$n_f(N)$	0	1	2	2	2	2
$n_f(N)/n_t(N)$	0	$8.70 \cdot 10^{-3}$	$6.45 \cdot 10^{-3}$	$2.47 \cdot 10^{-3}$	$9.17 \cdot 10^{-4}$	$3.40 \cdot 10^{-4}$
N	11	12	13	14	15	16
$n_f(N)$	2	3	10	45	166	518
$n_f(N)/n_t(N)$	$1.24 \cdot 10^{-4}$	$6.78 \cdot 10^{-5}$	$8.15 \cdot 10^{-5}$	$1.32 \cdot 10^{-4}$	$1.74 \cdot 10^{-4}$	$1.93 \cdot 10^{-4}$

Table 3: The number of forbidden orbits $n_f(N)$ and its fraction with the total number of periodic orbits $n_t(N)$ for $N \leq 16$.

N=15 and N=16 are obtained by a systematic search for forbidden orbits with these values of N. From N=12 on, the fraction of the number of forbidden orbits with the total number of orbits is slightly increasing.

The distribution of lengths $p_N(l)$ of all periodic orbits with a fixed value of N was examined for N=1 to N=14. $p_N(l)\,\Delta l$ is the probability that a randomly chosen orbit with N reflections on the hyperbola has a length between l and $l + \Delta l$. The exact distribution of lengths is a sum over δ-functions with peaks at the lengths of the periodic orbits; here by $p_N(l)$ a distribution is denoted, which is obtained by smoothing the exact distribution over some interval in order to obtain a smooth function. It is found that the length distributions can be approximated very well by Gaussian curves, if N is large enough ($N \gtrsim 8$)

$$p_N(l) \approx \frac{1}{\sqrt{2\pi}\sigma_N} \exp\{-\frac{(l - \bar{l}_N)^2}{2\sigma_N^2}\} \; . \qquad (111)$$

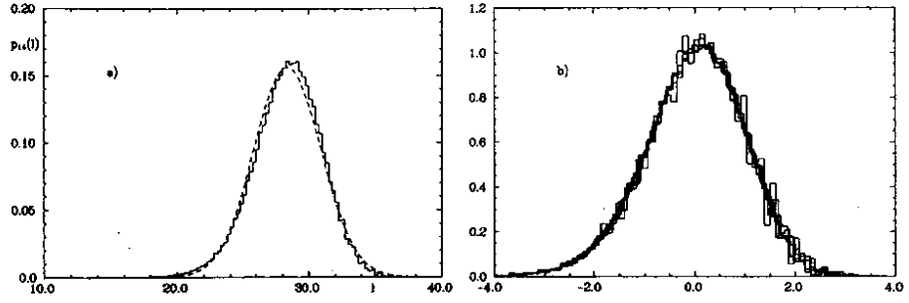

Figure 4: a) The distribution of lengths $p_{14}(l)$ in comparison with a Gaussian. b) Scaled distributions of lengths $p_N(l+\bar{l}N)/p_N(\bar{l}N)$ as a function of $l/(\sigma\sqrt{N})$ for N=10 to N=14.

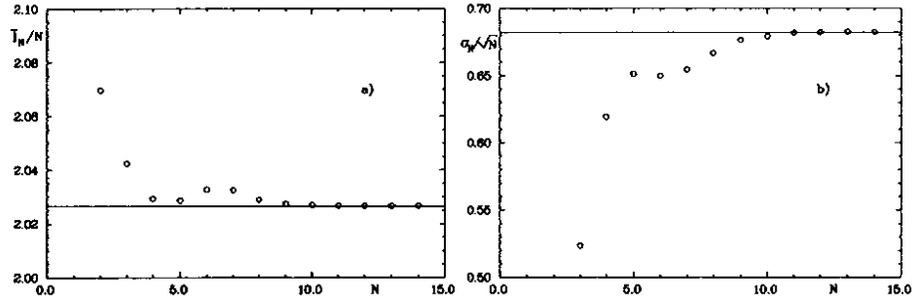

Figure 5: The quantities $\bar{l}_N/N$ and $\sigma_N/\sqrt{N}$. The horizontal lines represent the values of $\bar{l}$ and σ, respectively.

$\bar{l}_N$ and σ_N denote the mean value and the standard deviation of the distribution, respectively. The result for $p_{14}(l)$ and the corresponding Gaussian curve are plotted in figure 4 a). The deviation of the distribution of lengths from the Gaussian curve is slightly asymmetric with respect to the mean value of the distribution.

If N is large enough, the N-dependence of $\bar{l}_N$ and σ_N is to a very good approximation given by

$$\begin{aligned} \bar{l}_N &\approx \bar{l}N \quad , \bar{l} = 2.027 \\ \sigma_N &\approx \sigma\sqrt{N} \quad , \sigma = 0.682 \ . \end{aligned} \tag{112}$$

In order to demonstrate the scaling behaviour of the length distributions, $p_N(l+N\bar{l})/p_N(N\bar{l})$ is plotted as a function of $l/(\sigma\sqrt{N})$ for $N = 10$ to $N = 14$ in figure 4 b). As can be seen there is a good agreement between length distributions that correspond to different values of N.

In figure 5 the N-dependence of $\bar{l}_N$ and σ_N is shown by a plot of $\bar{l}_N/N$ and $\sigma_N/\sqrt{N}$. The horizontal lines represent the values of $\bar{l}$ and σ of eq. (112), respectively.

A characteristic property of chaotic systems is the asymptotic exponential proliferation

of the number of periodic orbits. This is expressed by the asymptotic law eq. (74)

$$\frac{\mathrm{d}}{\mathrm{d}l}\mathcal{N}(l) \sim \epsilon^{\tau l}/l \ , \ l \to \infty \ , \tag{113}$$

where $\mathcal{N}(l)$ is defined as the number of primitive periodic orbits γ with length $l_\gamma \leq l$

$$\mathcal{N}(l) := \#\{\text{primitive periodic orbits } \gamma \text{ with length } l_\gamma \leq l\} \ . \tag{114}$$

τ is equal to $1/v$ times the topological entropy of the billiard system at energy $E = mv^2/2$. In the dimensionless units that are used for the numerical calculations in this paper ($\hbar = 1 = 2m$), τ is equal to the topological entropy at energy $E = 1/4$.

The explicit dependence of the approximated distributions of lengths $p_N(l)$ on N in equations (111) and (112) allows an analytical examination of the asymptotic behaviour of the staircase function $\mathcal{N}(l)$:

$$\begin{aligned} \frac{\mathrm{d}}{\mathrm{d}l}\mathcal{N}(l) &= \sum_{N=1}^{\infty} p_N(l) \cdot Z(N) \\ &\approx \sum_{N=1}^{\infty} \frac{1}{\sqrt{2\pi N}\sigma} \exp\{-\frac{(l-\bar{l}N)^2}{2\sigma^2 N}\} \frac{3^N}{N} \ , \end{aligned} \tag{115}$$

$Z(N)$ is the number of primitive periodic orbits with N reflections on the hyperbola. For large values of l the sum can be approximated by a stationary phase approximation, which yields the following result

$$\frac{\mathrm{d}}{\mathrm{d}l}\mathcal{N}(l) \approx \frac{1}{l} \exp\{\frac{l}{\sigma^2}[\bar{l} - \sqrt{\bar{l}^2 - 2\sigma^2 \log 3}]\} \ , l \gg 1 \ . \tag{116}$$

A comparison with the expected asymptotic behaviour in equation (113) gives an explicit expression for τ of the form

$$\tau = \frac{1}{\sigma^2}\{\bar{l} - \sqrt{\bar{l}^2 - 2\sigma^2 \log 3}\} \ . \tag{117}$$

From this equation a numerical value of $\tau \approx 0.58$ is obtained.

A measure of the stability properties of a periodic orbit γ is given by the stability exponent u_γ. For an unstable orbit it is defined as the absolute value of the logarithm of the absolute value of an eigenvalue of the monodromy matrix. These stability exponents are determined by the method of appendix B. The stability exponents u_γ are related to the Lyapunov exponents λ_γ by the equation $\lambda_\gamma = u_\gamma/T_\gamma(E)$, where $T_\gamma(E)$ is the period of the orbit γ at energy E. Because of the scaling property of billiard systems, that periodic orbits in coordinate space do not depend on the energy, it is convenient to consider the energy independent quantity $\lambda_\gamma := u_\gamma/l_\gamma$, which in dimensionless units is equal to the Lyapunov exponent at energy $E = 1/4$.

The distribution $\tilde{p}_N(\lambda)$ of the so-defined Lyapunov exponents for fixed values of N was examined for N=1 to N=14. Again it was found that this distribution is approximated well by a Gaussian curve, if N is large enough. The values of N for which this approximation is good are, however, higher than in case of the distributions of lengths $p_N(l)$. The distribution $\tilde{p}_{14}(\lambda)$ and the corresponding Gaussian curve are shown in figure 6 a). The deviation of the

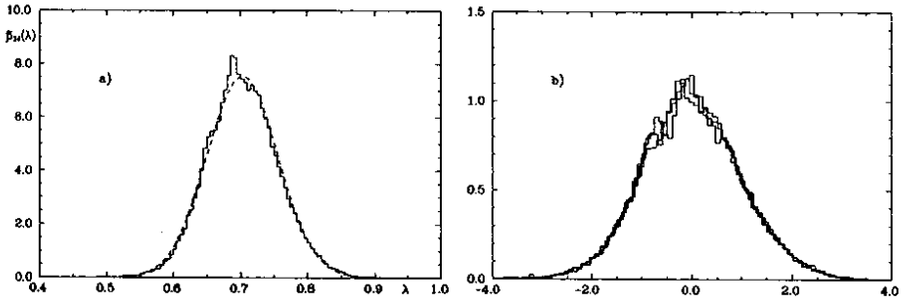

Figure 6: a) The distribution of Lyapunov exponents $\tilde{p}_{14}(\lambda)$ in comparison with a Gaussian. b) Scaled distributions of Lyapunov exponents $\tilde{p}_N(\lambda+\bar{\lambda})/\tilde{p}_N(\bar{\lambda})$ as a function of $\lambda\sqrt{N}/\tilde{\sigma}$ for N=12 to N=14.

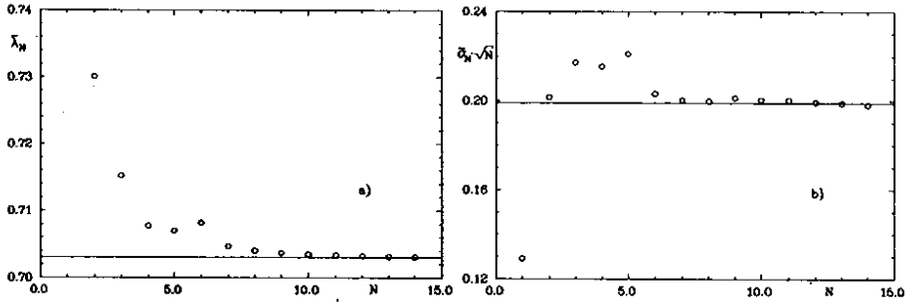

Figure 7: The quantities $\bar{\lambda}_N$ and $\tilde{\sigma}_N\sqrt{N}$. The horizontal lines represent the values of $\bar{\lambda}$ and $\tilde{\sigma}$, respectively.

distributions of Lyapunov exponents from the Gaussian curves is more symmetric than in case of the length distributions.

The mean values $\bar{\lambda}_N$ and the standard deviations $\tilde{\sigma}_N$ of the distributions $\tilde{p}_N(\lambda)$ again have a simple N-dependence, if N is large enough:

$$\begin{aligned} \bar{\lambda}_N &\approx \bar{\lambda} \quad , \bar{\lambda} = 0.703 \\ \tilde{\sigma}_N &\approx \tilde{\sigma}/\sqrt{N} \quad , \tilde{\sigma} = 0.199 \ . \end{aligned} \tag{118}$$

Figure 6 b) shows the scaling property of the distributions $\tilde{p}_N(\lambda)$ by a plot of the scaled distributions $\tilde{p}_N(\lambda+\bar{\lambda})/\tilde{p}_N(\bar{\lambda})$ as a function of $\lambda\sqrt{N}/\tilde{\sigma}$ for N=12 to N=14. The N-dependence of $\bar{\lambda}_N$ and $\tilde{\sigma}_N$ is shown in figure 7 by a plot of $\bar{\lambda}_N$ and $\tilde{\sigma}_N\sqrt{N}$. The horizontal lines represent the values of $\bar{\lambda}$ and $\tilde{\sigma}$, respectively.

The fact that the mean Lyapunov exponents are to a good approximation constant for different values of N is remarkable in view of the fact, that the Lyapunov exponent of a finite segment of a non-periodic trajectory approximates zero, if the length of the segment goes to infinity, as will be discussed below. An explanation for this fact is, that for every value

of N the number of orbits, which are situated in the central region of the billiard area, is much larger than the number of orbits, which run into the horn, because the number of code words which contain a sequence of consecutive "+" are small in comparison with the total number of code words. In addition, forbidden code words are mainly among code words, which contain a sequence of several consecutive "+".

III.2.2 The Periodic Orbits with Lengths $l_\gamma \leq 20$

l	2	3	4	5	6	7	8
orbits	1	1	1	3	4	6	11
lengths	1	1	1	3	4	6	9
$\bar{g}$	1.000	1.000	1.000	1.000	1.000	1.000	1.222
$\bar{\lambda}$	0.881	0.623	0.925	0.731	0.739	0.724	0.720
l	9	10	11	12	13	14	15
orbits	16	24	43	79	124	221	390
lengths	14	19	32	58	88	140	246
$\bar{g}$	1.143	1.263	1.344	1.362	1.409	1.579	1.585
$\bar{\lambda}$	0.736	0.717	0.708	0.705	0.705	0.705	0.703
l	16	17	18	19	20		
orbits	648	1084	1839	3201	5402		
lengths	391	622	1035	1756	2913		
$\bar{g}$	1.657	1.743	1.777	1.823	1.854		
$\bar{\lambda}$	0.707	0.703	0.705	0.704	0.706		

Table 4: For $l = 2$ to $l = 20$ this table contains the total number of primitive periodic orbits with length l_γ in the interval $l-1 < l_\gamma \leq l$. Further it contains the number of different lengths, the mean degeneracy of lengths $\bar{g}$ and the mean Lyapunov exponent $\bar{\lambda}$ of orbits in this interval.

A detailed analysis of the statistical properties of the length spectrum can only be given, if the orbits are completely known up to a certain length. Also for an examination of the accuracy of the periodic-orbit theory it is necessary to have a complete length spectrum up to a certain length. The problem of obtaining such a complete length spectrum is, that one cannot read off the length of an orbit from its corresponding code word. Although there is the general tendency that with increasing word length also the lengths of the orbits increase, there are also orbits, which have a long code word but a relatively small length. For example, for N=14 most lengths are distributed around $\bar{l}_{14} \approx 28.37$ with a standard deviation of $\sigma_{14} \approx 2.55$, but the shortest orbit has the length $l_\gamma \approx 12.99$. However, orbits which have the smallest lengths for a given value of N all have the property that they spend some time in the horn of the billiard system, where the lengths of the sections of the orbit between consecutive hits on the hyperbola are small. In the code word this behaviour is reflected by the occurrence of a group of consecutive "+". This property allows a systematic search for all periodic orbits with a length below a certain given length. In this way all orbits of the hyperbola billiard with length $l_\gamma \leq 20$ were determined. The highest code length that was

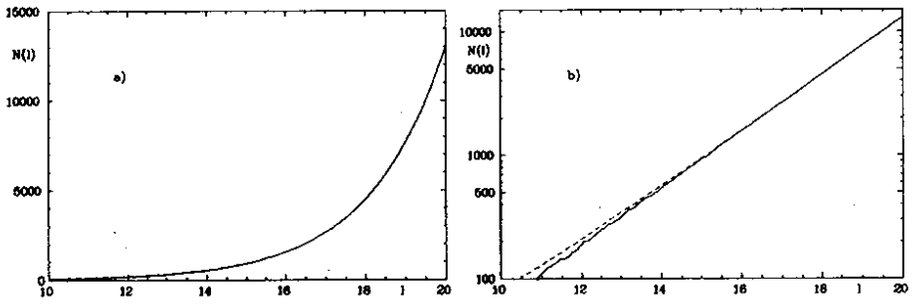

Figure 8: The staircase function $\mathcal{N}(l)$ in comparison with the asymptotic curve $\mathrm{Ei}(\tau l)$ for τ=0.5925 (dashed line), a) linear scale, b) logarithmic scale.

obtained for such an orbit is $N = 32$. Altogether 13098 orbits with 7339 different lengths were determined.

Properties of the periodic orbits within different lengths intervals are listed in table 4. The mean multiplicity of lengths is approximating two as is expected. The mean Lyapunov exponent again lies constantly between 0.70 and 0.71 for $l > 10$.

The obtained length spectrum allows a numerical determination of the topological entropy τ. Figure 8 shows $\mathcal{N}(l)$ for $l \leq 20$ in linear and logarithmic scale. In the range $15 < l < 20$ a fit is made with the asymptotic curve

$$\mathcal{N}(l) \sim \mathrm{Ei}(\tau l) \ , \ l \to \infty \ , \tag{119}$$

which is obtained by integrating eq. (113). A value of $\tau = 0.593$ was obtained for the topological entropy, and the corresponding asymptotic curve is also shown in figure 8. Both curves agree very well for $15 < l < 20$, which is an indication for the quality of the asymptotic approximation, since only a one parameter fit is made.

III.2.3 Statistical Properties of the Length Spectrum

The examination of the statistical properties of quantum mechanical energy spectra is one of the most common tools for the distinction of systems, which are classically chaotic or integrable, respectively. This motivates the examination of statistical properties of the lengths of periodic orbits, which are related to the quantum mechanical energies by means of the periodic-orbit theory. A further reason for the examination of the length statistics is the fact, that in applications of the periodic-orbit theory it often is assumed that the lengths of chaotic systems are Poisson distributed, but there are almost no systems for which a sufficient number of orbits is available so that this assumption can be tested.

Asymptotically the degeneracy of lengths of the periodic orbits of the hyperbola billiard is equal to two. Then all the relevant statistical information is contained in the distribution of different lengths. For that reason this is the distribution which is examined.

The statistics are determined for a scaled spectrum of lengths, which has the property that the mean distance between neighbouring lengths is equal to one. The scaled spectrum is

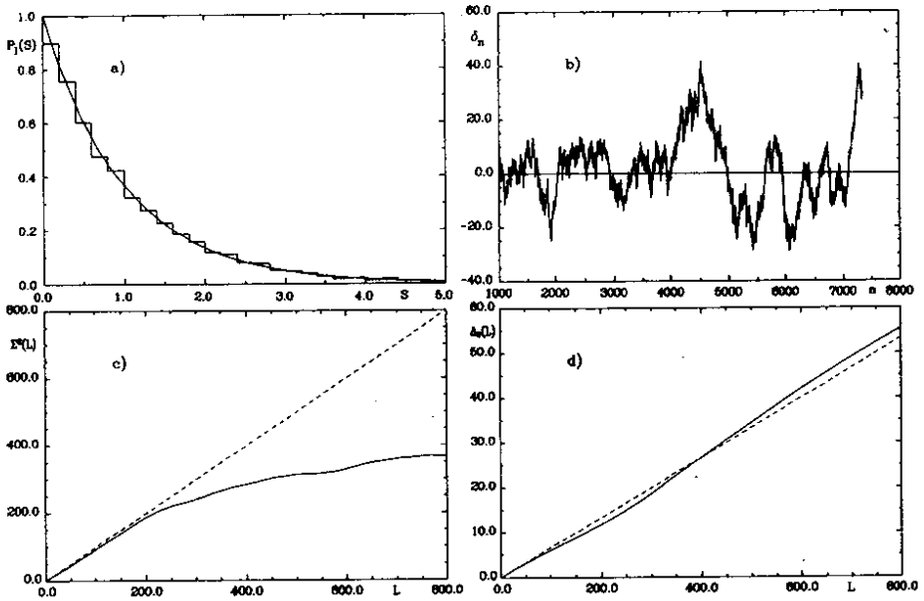

Figure 9: a) The distribution of spacings between neighbouring lengths $P_l(S)$, b) the deviations δ_n of the scaled lengths l'_n from the mean values $n - 1/2$, c) the number variance $\Sigma^2(L)$ and d) the rigidity $\Delta_3(L)$.

obtained with the use of the asymptotic law for the total number of orbits $\mathcal{N}(l)$ of eq. (119) and a smooth approximation for the mean degeneracy $\bar{g}(l)$ of all orbits with length $l_n \leq l$:

$$\bar{g}(l) = \sum_{l_n \leq l} g_n \cdot (\sum_{l_n \leq l} 1)^{-1} \ . \tag{120}$$

In this notation n labels all different lengths l_n, which are ordered in an ascending sequence. g_n denotes the multiplicity of the length l_n. In the range $16 < l < 20$ the function $\bar{g}(l)$ varies slowly and it is approximated by a polynomial of degree three. This approximation is denoted by $<\bar{g}(l)>$. The normalized length spectrum is obtained by the equation

$$l'_n = \frac{\bar{\mathcal{N}}(l_n)}{<\bar{g}(l_n)>} \ , \tag{121}$$

and it is evaluated between $1014 \leq l'_n \leq 7339$, which corresponds to the range $16 \leq l_n \leq 20$ in the original spectrum.

First the distribution of spacings between neighbouring lengths $P_l(S)$ was determined. This distribution contains information about short-range correlations. The result for $P_l(S)$ is shown in figure 9 a). It agrees very well with a Poisson distribution.

In figure 9 b) the deviations of the scaled lengths l'_n from mean values $n - 1/2$ are plotted

$$\delta_n := n - \frac{1}{2} - l'_n \quad . \tag{122}$$

The deviations δ_n that are found are relatively high, and they increase with increasing n. This is in agreement with the expectation for a Poisson distributed spectrum.

The long-range correlations are examined by the number variance $\Sigma^2(L)$ and the rigidity $\Delta_3(L)$. $\Sigma^2(L)$ is defined as the local variance of the number $n(l', L)$ of scaled lengths l'_n in the interval from $l' - L/2$ to $l' + L/2$:

$$\Sigma^2(L) = \left\langle [n(l', L) - L]^2 \right\rangle \quad . \tag{123}$$

Let $\mathcal{N}'(l')$ denote the number of scaled lengths l'_n that are less or equal l'. $\Delta_3(L)$ is defined as the local average of the mean square deviation of the staircase $\mathcal{N}'(l')$ from the straight line that fits it best over the range L:

$$\Delta_3(L) = \left\langle \min_{(a,b)} \frac{1}{L} \int_{-L/2}^{L/2} dl \, [\mathcal{N}'(l' + l) - a - bl]^2 \right\rangle \quad . \tag{124}$$

It can be expressed as

$$\Delta_3(L) = \left\langle \frac{1}{L} \int_{-L/2}^{L/2} dl \, \mathcal{N}'^2(l' + l) - \left[\frac{1}{L} \int_{-L/2}^{L/2} dl \, \mathcal{N}'(l' + l) \right]^2 - 12 \left[\frac{1}{L^2} \int_{-L/2}^{L/2} dl \, l \, \mathcal{N}'(l' + l) \right]^2 \right\rangle \quad . \tag{125}$$

Both statistics are closely related, which is expressed by the equation

$$\Delta_3(L) = \frac{2}{L^4} \int_0^L dr \, (L^3 - 2L^2 r + r^3) \Sigma^2(r) \quad . \tag{126}$$

For a Poisson distributed sequence the number variance is equal to $\Sigma^2(L) = L$ and the spectral rigidity obeys $\Delta_3(L) = L/15$. The result of the numerical determination of the number variance $\Sigma^2(L)$ is shown in figure 9 c). Again there is a good agreement with the Poisson expectation if $L < 200$. But above $L = 200$ the curve $\Sigma^2(L)$ clearly lies under the curve for the Poisson distribution. This means that very long-range correlations are not described by a Poisson distribution. Concerning the energy level statistics the number variance is expected to saturate, i.e. it approaches a finite value if $L \to \infty$. This is a consequence of the fact, that there is a shortest length in the periodic-orbit sum. The results for the Σ^2-statistics of the lengths are an indication that the number variance of the distribution of lengths also saturates. The rigidity $\Delta_3(L)$ is plotted in figure 9 d). Here the agreement with the Poisson expectation is good over the total range of the parameter L. On the other hand a saturation of the number variance $\Sigma^2(L)$ implies also a saturation of the rigidity $\Delta_3(L)$ by eq. (126). But the saturation of $\Delta_3(L)$ in general occurs at higher values of L as the saturation of $\Sigma^2(L)$. This point is discussed in more detail in context with the statistics of energy eigenvalues.

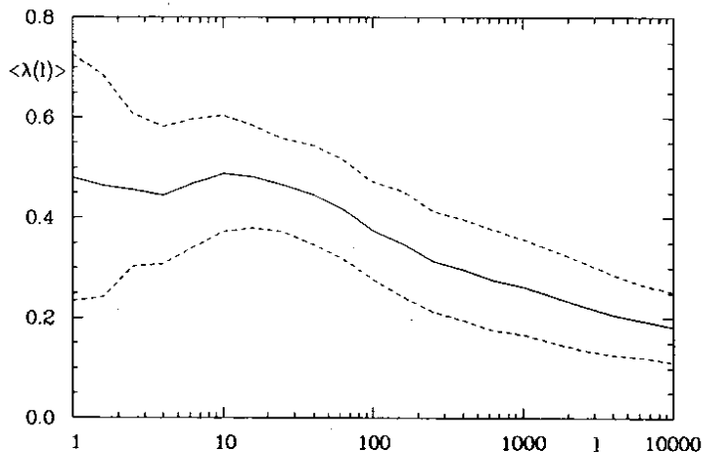

Figure 10: The mean Lyapunov exponent of 100 trajectories as a function of the trajectory length l. The dashed lines mark the distance of the standard deviation below and above the mean value.

III.2.4 The Lyapunov Exponent for Non-Periodic Trajectories

This section contains an examination of the stability properties of non-periodic trajectories, which are followed over a long distance. The stability exponent $u(l)$ of a finite part of length l of a non-periodic trajectory is determined by the method of appendix B. The Lyapunov exponent of this part of the trajectory is defined by $\lambda(l) = u(l)/l$. In figure 10 the mean value of the Lyapunov exponents of 100 trajectories is shown for $l < 10000$. The initial conditions of the trajectories are chosen randomly in the central billiard region. If only one trajectory is considered, the Lyapunov exponent shows an irregular behaviour. Periods in which the trajectory runs into the horn, where the Lyapunov exponent decreases, alternate with periods in which the trajectory is in the central region of the billiard domain, where the Lyapunov exponent increases again. The mean value of the Lyapunov exponents of several trajectories is taken in order to see the average behaviour of $\lambda(l)$ as a function of the trajectory length l. Figure 10 shows that $< \lambda(l) >$ continuously decreases for long l as a function of l. In addition, the standard deviation slowly decreases. This suggests that for a non-periodic trajectory $\lambda(l)$ goes to zero, if $l \to \infty$. An explanation of this behaviour is that periods in which the trajectory runs a very long distance into the horn occur seldom, but they lead to a strong decrease of $\lambda(l)$. Let the maximum x-value that is reached within such a period be x_{max}. As $l \to \infty$ arbitrary large values of x_{max} occur, which possibly have the effect that $\lambda(l) \to 0$ as $l \to \infty$. In this case one has a strongly chaotic system with the property that the Lyapunov exponent of infinitely long non-periodic trajectories is equal to zero. This seemingly contradictionary behaviour is a consequence of the unboundedness of the billiard system.

IV The Energy Spectrum of the Hyperbola Billiard

All information about a conservative quantum mechanical system is contained in the energy eigenvalues and eigenfunctions of the Hamiltonian operator of the system. It is therefore natural to ask what distinguishes the energy spectrum and eigenfunctions of a quantum system which is classically chaotic from one which is not. There are further arguments which suggest the studies of these quantities in the context of the quantum mechanics of classically chaotic systems [10,11]. Chaos is typically connected with the infinite time limit. Chaotic properties like ergodicity, mixing or the emergence of complexity on infinitely fine scales during the time-evolution of initially smooth curves in classical phase space all occur or are defined in the limit $t \to \infty$. The non-existence of chaos in the quantum mechanical time evolution is directly connected with the fact that the two limits $\hbar \to 0$ and $t \to \infty$ in general do not commute. For that reason the properties of a classical system at infinite times are significantly different from the infinite time quantum mechanical behaviour. The energy eigenvalues and eigenfunctions are stationary objects, that is objects, which do not change as t goes to infinity. The studies of these quantities in the semiclassical limit therefore automatically represent also studies of quantum mechanical behaviour at infinite times in the limit $\hbar \to 0$.

Most of the numerical investigations were carried out on the energy spectrum. It was found that a very effective tool for the distinction between quantum systems, which are classically chaotic, and those, which are classically integrable, is the statistics of the energy eigenvalues. More precisely, the characteristic information lies in the deviation of the level density from the mean level density. For that reason one usually considers a scaled energy spectrum, which has a mean level distance of one. For most systems the statistics of the scaled energy levels then depend only upon whether the considered system is classically chaotic or integrable, and also on the presence of certain symmetries. A prerequisite for this is, that the statistics have to be evaluated in the semiclassical regime, and that one has to restrict to statistics, which do not describe very long-range correlations. The property that on these assumptions most systems show the same fluctuation statistics of the level density is called universality.

Berry and Tabor first showed that generic integrable systems have a spectrum, whose short-range statistics is that of Poisson distributed numbers [67]. They also presumed that the spectra of classically chaotic quantum systems show level repulsion. This was based on the analogy with the statistical theory of spectra [68], which was developed in order to explain the spectra of complicated nuclei and atoms. This theory models the level statistics of complex systems by the eigenvalue statistics of certain ensembles of random matrices [69]. Level repulsion in the spectra of classically chaotic systems was also supposed by Zaslavsky [70]. Bohigas, Giannoni and Schmit then demonstrated that the results of random matrix theory can also be applied in order to describe the short-range statistical properties of the spectra of low-dimensional chaotic systems [71,72]. This means that the energy statistics of classically chaotic systems is the same as the eigenvalue statistics of certain ensembles of infinite dimensional matrices, whose elements are Gaussian distributed random elements. The kind of matrices which form a certain ensemble depends on the symmetry properties of the considered system. One distinguishes three cases:

— The Gaussian Unitary Ensemble (GUE), which consists of complex hermitian matrices. It describes the energy statistics of systems without any symmetry.

— The Gaussian Orthogonal Ensemble (GOE), which consists of real symmetric matrices. It describes the energy statistics of systems with time-reversal symmetry, but no geometrical symmetry, which have an integer spin.

— The Gaussian Symplectic Ensemble (GSE), which consists of "quaternion real" matrices. It describes the energy statistics of systems with time-reversal symmetry, but no geometrical symmetry, which have a half-integer spin.

The above classification considers only the most common cases. There is a more general classification, which for example takes into consideration also the existence of arbitrary anti-unitary symmetries, for which the time-reversal symmetry is one example. If discrete geometrical symmetries are present, then one has to consider the subspaces of the spectrum, which are defined by having fixed eigenvalues of the geometrical symmetry, separately. The results of the random matrix theory then have to be applied to every subspace of the spectrum.

The universal properties of the energy statistics have been verified on a variety of systems. The above classification has to be slightly restricted in that it is a property of generic systems, but must not hold for every classically chaotic quantum system. There can be particular quantum systems, which do not have the expected energy statistics, as well as there are integrable systems like the harmonic oscillator, which do not have a Poisson distributed spectrum.

A theoretical explanation for the observed spectral universality was given by Berry for statistics, that are bilinear in the level density, like the spectral rigidity $\Delta_3(L)$ and the number variance $\Sigma^2(L)$ [15,10]. This theory is based on semiclassical formulae, which express these statistical quantities by sums over classical periodic orbits by means of Gutzwiller's trace formula for the spectral density. Universal behaviour in the quantum mechanical energy spectrum then can be explained as a consequence of universal properties of very long classical orbits, which were discovered by Hannay and Ozorio de Almeida [73]. Berry's theory also predicts departure from universality, if long-range statistics are considered, since their properties are determined by short orbits, which are non-universal.

Up to this point only the two extreme cases of completely integrable or completely chaotic systems have been considered. Most systems, however, are partly chaotic and partly integrable. The energy statistics of those mixed systems has properties, which lie in between the properties of the energy spectra of integrable systems on the one hand and chaotic systems on the other hand. Families of systems, which show a transition from integrability to chaos by changing one parameter, in general have an energy statistics, which changes from a Poisson statistics to one, which is described by random matrix theory [74,75,76].

This chapter describes the method by which the energy eigenvalues of the hyperbola billiard were determined and examines the statistical properties of the numerically obtained energy spectrum.

IV.1 Determination of the Energy Eigenvalues

For billiard systems there exists a variety of numerical methods for the determination of the energies. An overview over different methods is given by Kuttler and Sigillito [77]. However, most of these methods yield unsatisfactory results, if one tries to determine higher eigenvalues. First results for the hyperbola billiard were obtained by using the method of Rayleigh and Ritz. This method is numerically stable and gave results, which were sufficient for a first

testing of the periodic-orbit theory [58]. But the accuracy of the results was not very high. A method which yields a higher accuracy for the first eigenvalues is the collocation method, which was used by Heller for the determination of the eigenvalues of the stadium billiard [78]. Even very high-lying stadium energies could be obtained by this method. In case of the hyperbola billiard, however, this method becomes numerically unstable, if one tries to determine more than about the first twenty eigenvalues, although the accuracy for the first eigenvalues is quite high. A variant of this method was used by Schmit in order to obtain the first 1500 eigenvalues of a desymmetrized part of the octagon, a smooth compact Riemannian surface with constant negative curvature [38]. For the hyperbola billiard this method turned out to be numerically too expensive for the determination of a greater part of the spectrum. The method which gave by far the best results is a boundary element method, which is explained in the following.

The quantum mechanics of the hyperbola billiard is described by the stationary Schrödinger equation, which in dimensionless units is equal to the Helmholtz equation

$$-\left(\frac{\partial^2}{\partial x^2}+\frac{\partial^2}{\partial y^2}\right)\psi_n(x,y)=E_n\,\psi_n(x,y)\;,\quad (x,y)\in D\;, \tag{127}$$

with Dirichlet boundary conditions

$$\psi_n(x,y)=0 \text{ if } (x,y)\in \partial D\;. \tag{128}$$

The units are chosen such that $\hbar=2m=1$. D denotes the domain of the billiard system

$$D:=\{(x,y)|\, x\geq 0\wedge y\geq 0\wedge y\leq \frac{1}{x}\}\;, \tag{129}$$

and ∂D is its boundary.

Simon proved that the energy spectrum of this system is purely discrete despite of the infinite billiard area [63]. The invariance of this system under reflection on the straight line $y=x$ allows the choice of a basis of eigenfunctions $\psi_n(x,y)$, which are either even or odd with respect to reflection on the line $y=x$.

The numerical method for the determination of the energies E_n consists in the approximate solution of a one-dimensional integral equation by discretization. Here we give a sketch of the derivation of this equation. The starting point is the free (outgoing) Green function in two dimensions, which is the solution of the inhomogeneous Schrödinger equation

$$\{E+i\varepsilon+\vec\nabla^2\}G(\vec q,\vec q\,',E)\Big|_{\epsilon\to 0}=\delta(\vec q-\vec q\,')\;, \tag{130}$$

and is given by

$$G(\vec q,\vec q\,',E)=-\frac{i}{4}\,H_0^{(1)}(\sqrt{E}|\vec q-\vec q\,'|)\;, \tag{131}$$

where $\vec q=(x,y)$, $\vec q\,'=(x',y')$, $\vec\nabla$ is the gradient vector with respect to $\vec q$, and $H_0^{(1)}$ is a Hankel function. Let $\psi(\vec q)$ be any solution of the Schrödinger equation

$$\{E+\vec\nabla^2\}\psi(\vec q)=0\;. \tag{132}$$

Eq. (131) is multiplied by $\psi(\vec q)$, eq. (132) is multiplied by $G(\vec q,\vec q\,',E)$, both equations are subtracted and integrated over the domain D. After applying Green's theorem one finally

obtains the Helmholtz representation for the wavefunction ψ [79,80,81]

$$\int_{\partial D}\mathrm{d}s'\,\{\psi(\vec q\,')\,\hat n'\cdot\vec\nabla' G(\vec q,\vec q\,',E)-G(\vec q,\vec q\,',E)\,\hat n'\cdot\vec\nabla'\psi(\vec q\,')\}=\begin{cases}\psi(\vec q) & \vec q\in D\setminus\partial D\\ \psi(\vec q)/2 & \vec q\in\partial D\\ 0 & \vec q\notin D\;.\end{cases} \tag{133}$$

Here $\hat n'$ is the outward normal unit vector to the boundary ∂D at point $\vec q\,'$, $\vec\nabla'$ is the gradient vector with respect to $\vec q\,'$, and $\mathrm{d}s'$ denotes the line element along the boundary ∂D.

Eq. (133) is an integral equation for the wavefunction $\psi_n(x,y)$, if the boundary condition eq. (128) is inserted, but the kernel of this equation is singular. This singularity can be removed by taking the normal derivative on both sides of eq. (133), choosing $\vec q$ to lie on the boundary, and inserting the Dirichlet boundary condition. This leads to the equation

$$-\int_{\partial D}\mathrm{d}s'\,\hat n\cdot\vec\nabla G(\vec q,\vec q\,',E)\,\hat n'\cdot\vec\nabla'\psi(\vec q\,')=\frac{1}{2}\hat n\cdot\vec\nabla\psi(\vec q)\;,\quad \vec q\in\partial D\;, \tag{134}$$

which is a Fredholm equation of the second kind for the normal derivative of ψ. Eq. (134) is very efficient for the determination of the energies of billiard systems (see e.g. [82,83,84]). In case of the hyperbola billiard the numerical effort for the computation of the energies can be considerably reduced by making use of the fact, that the x-axis and the y-axis form part of the boundary, and that the system is invariant under reflection on the line $y=x$. This is achieved by choosing instead of the free Green function the Green function for the domain $\{(x,y)|\, x\geq 0\wedge y\geq 0\}$, which vanishes on the x-axis and on the y-axis. This Green function is obtained by the method of images. In addition the eigenvalues of even and odd energy eigenfunctions can be determined separately by requiring the Green function to be even and odd, respectively, with respect to reflection on the line $x=y$:

$$\begin{aligned}G^{\pm}(\vec q,\vec q\,',E):=\;&[G(\vec q,(x',y'),E)-G(\vec q,(-x',y'),E)-G(\vec q,(x',-y'),E)+\\ &G(\vec q,(-x',-y'),E)]\pm[G(\vec q,(y',x'),E)-\\ &G(\vec q,(-y',x'),E)-G(\vec q,(y',-x'),E)+G(\vec q,(-y',-x'),E)]\;.\end{aligned} \tag{135}$$

Here G denotes the free Green function given in eq. (131). Even functions are denoted by plus sign and odd functions by a minus sign. Starting with the Green functions of eq. (13 separate equations for even and odd eigenfunctions can be derived

$$-\int_C\mathrm{d}s'\,\hat n\cdot\vec\nabla G^{\pm}(\vec q,\vec q\,',E)\,\hat n'\cdot\vec\nabla'\psi^{\pm}(\vec q\,')=\frac{1}{2}\,\hat n\cdot\vec\nabla\psi^{\pm}(\vec q)\;,\;\vec q\in C\;, \tag{136}$$

where $C=\{(x,y)|\, y=1/x\,,\, x\geq 1\}$, so that now the line integral is evaluated only along one half of the hyperbola $y=1/x$.

Equations (136) are solved approximately by discretizing the boundary curve C. The infinite boundary is cut off at some finite point $(\bar x,1/\bar x)$, and the remaining boundary is divided into N equal pieces of length ΔL. (The choice of $\bar x$ and ΔL depends on the energy value and the required accuracy.) The function $\hat n\cdot\vec\nabla\psi(\vec q)$ is replaced by a N-dimensional vector v and the integral term by a Riemannian sum. Equations (136) then become systems of N linear equations for the vector v

$$A\,v=0\;,\; A_{ij}=\Delta L\;\hat n_i\cdot\vec\nabla_i G^{\pm}(\vec q_i,\vec q_j,E)+\frac{1}{2}\,\delta_{ij}\;,\; i,j=1,\ldots,N\;. \tag{137}$$

The requirement that these equations have a nontrivial solution v leads to the condition, that the determinant of A has to vanish. Due to the error introduced by the discretization the zeros of the determinant of A as a function of the energy E will in general be complex. But the absolute value of the determinant of A as a function of real energy E shows very pronounced minima at values of E, which are close approximations to the energy eigenvalues, if ΔL is chosen small enough and $\bar{x}$ is large enough ($\Delta L \ll 2\pi/\sqrt{E}$, $\bar{x} \gg \sqrt{E}/2\pi$.)

The results for the energy eigenvalues below $E = 200$ are given in tables 5 and 6. It is estimated that the last given digit is uncertain by ± 1.

11.7358	27.325	36.278	45.79	56.93	62.90	73.62	84.21	87.34
96.55	103.83	111.10	118.29	125.63	135.55	143.36	147.66	154.84
158.17	165.76	174.64	180.73	185.77	194.85			

Table 5: The energy eigenvalues of even wavefunctions below $E = 200$

21.456	36.278	49.43	59.50	67.94	77.04	86.24	97.27	105.12
110.21	120.81	129.20	134.24	138.86	149.54	160.39	163.34	172.02
179.04	185.01	194.91	198.47					

Table 6: The energy eigenvalues of odd wavefunctions below $E = 200$

IV.2 The Spectral Staircase $N(E)$

A test for the calculated energies E_n is carried out by the examination of the spectral staircase function $N(E)$, which is defined by the number of states with energies below E:

$$N(E) := \#\{E_n | E_n \leq E\} \tag{138}$$

The mean increase of this function is described by the smooth function $\bar{N}(E)$. The asymptotic behaviour of $\bar{N}(E)$ for large energies E can be determined analytically, and the comparison of the numerically calculated $N(E)$ with the analytic expression for $\bar{N}(E)$ shows, if the calculated spectrum has the correct mean behaviour. For example, in this way it is noticed, if two adjacent energy levels, which are very close together, are not resolved as two separate energies.

For billiards with finite area A, the first leading terms in the asymptotic formula for $\bar{N}(E)$ are known, and they depend on geometrical properties of the billiard system [85]:

$$\bar{N}(E) = \frac{A}{4\pi}E - \frac{L}{4\pi}\sqrt{E} + \sum_i b(\gamma_i) + \sum_j c(\alpha_j) + \ldots \ , \ E \to \infty \ . \tag{139}$$

This is valid for billiards with Dirichlet boundary conditions, whose boundary consists of a finite number of smooth continuous pieces γ_i and corners with angles α_j. Further it is assumed that no cusps are present. L is the total length of the boundary. If only the first

term on the right hand side is taken into account, this relation is called Weyl's law. The last two terms have the following meaning:

$$b(\gamma_i) = \frac{1}{2\pi}\int_{\gamma_i} K(l)\mathrm{d}l \ , \tag{140}$$

which is an integral over the curvature $K(l)$ along the boundary curve γ_i, and

$$c(\alpha_j) = \frac{1}{24}\left(\frac{\pi}{\alpha_j} - \frac{\alpha_j}{\pi}\right) \ , \ 0 < \alpha_j \leq 2\pi. \tag{141}$$

For many systems formula (139) is a very good approximation to the function $\bar{N}(E)$ down to the lowest energy eigenvalue, so that the asymptotic formula can also be applied in the low-energy regime.

Clearly, formula (139) cannot be applied to the hyperbola billiard, which has an infinite area. But Weyl's law can be used in an intuitive argument for the determination of the leading asymptotic behaviour of $\bar{N}(E)$ [50]. A solution of the Schrödinger equation of the hyperbola billiard with energy E typically has a significant value for the amplitude only in those parts of the billiard region, where the distance of the two opposite boundary curves in the horns is not smaller than the de Broglie wavelength. This leads to the definition of an effective area for this wavefunction, which is given by

$$A_{eff} = 1 + 2\log(1/\lambda_E) = 1 + 2\log(\sqrt{E}/2\pi) \ , \tag{142}$$

where $\lambda_E = 2\pi/\sqrt{E}$ is the de Broglie wavelength in dimensionless units. With eq. (142) the leading asymptotic term for $\bar{N}(E)$ follows as

$$\bar{N}(E) \sim \frac{1}{4\pi}E\log E \ , \ E \to \infty \ . \tag{143}$$

It was shown by Simon [86] that this is indeed the correct asymptotic behaviour. The next leading terms in the asymptotic formula for $\bar{N}(E)$ were derived by Steiner and Trillenberg [87]. Separated into contributions from even and odd wavefunctions the result is

$$\bar{N}^{\pm}(E) = \frac{1}{8\pi}E\log E + \frac{a}{8\pi}E + \frac{1}{8\pi}b^{\pm}\sqrt{E} + O(E^{1/4}\log E) \ , \ E \to \infty \tag{144}$$

$$a = 2(\gamma - \log 2\pi) \ , \ b^{\pm} = 4\frac{\pi^{3/2}}{\Gamma^2(1/4)} \pm 2\sqrt{2} \ .$$

In figure 11 a) the two functions $\bar{N}^+(E)$ and $\bar{N}^-(E)$ are compared to the numerically calculated staircase functions $N^+(E)$ and $N^-(E)$, respectively. The agreement is excellent over the whole energy range, so that for both symmetry subspaces of the energy spectrum the curves for $N(E)$ and $\bar{N}(E)$ cannot be resolved within the given scale. For that reason figure 11 b) shows a section of figure 11 a) for the energy range $1400 < E < 1500$.

The correction terms for eq. (144) are not known analytically, but they can be determined numerically. For that reason the deviation of the spectral staircase $N(E)$ from $\bar{N}(E)$ is examined in both symmetry subspaces. Mean energies $\bar{E}_n$ which are defined by means of the the generalized Weyl's law eq. (144) are given by

$$\bar{N}(\bar{E}_n) = n - 1/2 \ . \tag{145}$$

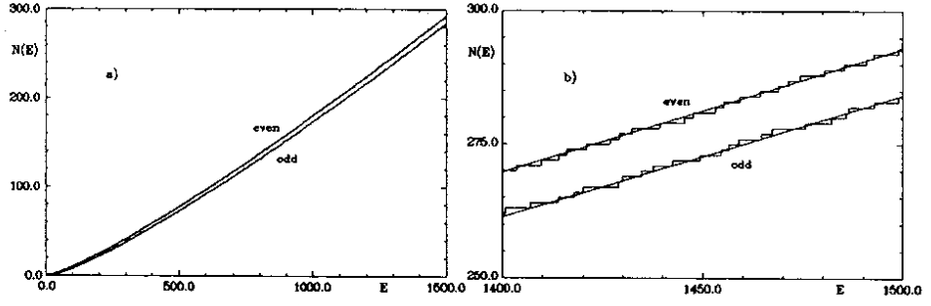

Figure 11: The spectral staircase $N(E)$ in comparison with the generalized Weyl's law eq. (144) for even and odd energy eigenfunctions within the energy ranges a) $0 < E < 1500$ and b) $1400 < E < 1500$.

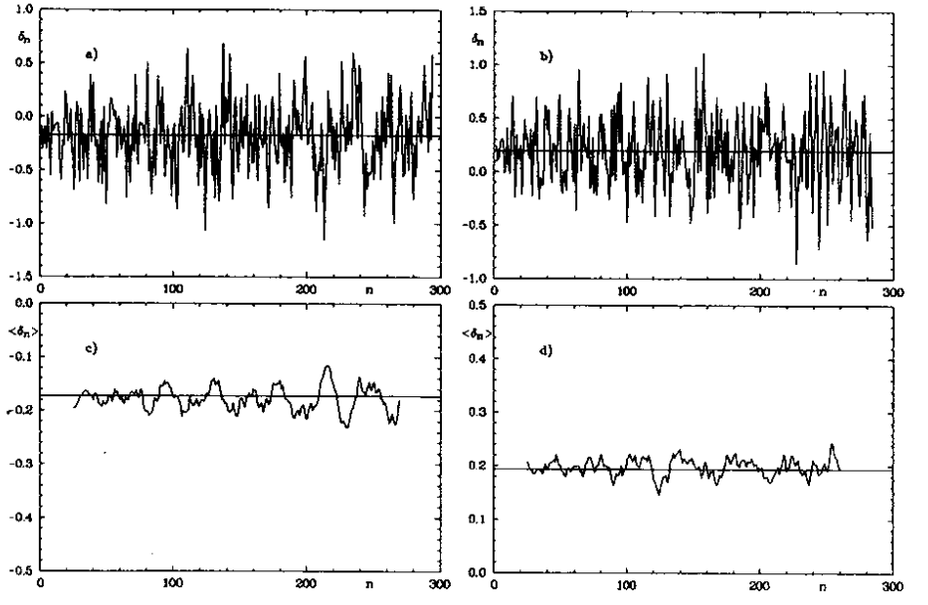

Figure 12: The deviations δ_n from the generalized Weyl's law eq. (144) for the energies of a) even and b) odd wave functions. c) and d) show the results of smoothing the curves in a) and b), respectively, over a range of 50 energies. The horizontal lines represent the mean values of the deviations δ_n.

For that reason the quantities

$$\delta_n = n - 1/2 - \bar{N}(E_n) \tag{146}$$

are a measure of the deviation of the numerically obtained spectrum from $\bar{N}(E)$.

In figure 12 a) and b) the quantities δ_n are shown for even and odd symmetries. The horizontal lines represent the mean values of the δ_n. Figures 12 c) and d) show the same curves smoothed over a range of 50 energies. As can be seen the approximation to the functions $\bar{N}^+(E)$ and $\bar{N}^-(E)$, which is given by eq. (144), is equally good in the lower and higher energy range. Within the numerical accuracy the next correction term to eq. (144) is in both cases a constant with value $c^+ = -0.173$ and $c^- = 0.194$, respectively.

For an interpretation of this result it is assumed in the following that the contributions of the corners and of the curvature of the boundary to $\bar{N}(E)$ is the same as for bounded billiards. For example, the contribution of the part of the boundary along the line $y = x$, which leads to the difference between $\bar{N}^+(E)$ and $\bar{N}^-(E)$, is also the same as for finite billiards. On this assumption the constant contributions to $\bar{N}^+(E)$ and $\bar{N}^-(E)$ are given by

$$c^+ = -c(\frac{\pi}{4}) + b(C) + c_{horn} = -\frac{9}{32} + c_{horn} \tag{147}$$

and

$$c^- = c(\frac{\pi}{2}) + c(\frac{\pi}{4}) + b(C) + c_{horn} = \frac{3}{32} + c_{horn} \ , \tag{148}$$

respectively. $C = \{(x, 1/x) | 1 \leq x < \infty\}$ denotes the curved part of the boundary. The constant contributions to $\bar{N}^+(E)$ for even wavefunctions, which satisfy partly Dirichlet and partly Neumann boundary conditions on the boundary of the desymmetrized billiard system, are obtained by the difference between the constant contributions to $\bar{N}(E)$ for the full system and the constant contributions to $\bar{N}^-(E)$. The curvature term is calculated as

$$b(C) = -\frac{1}{2\pi}\int_1^\infty \frac{2x^3}{(1+x^4)^{3/2}}\frac{\sqrt{x^4+1}}{x^2}\,\mathrm{d}x = -\frac{1}{\pi}\int_1^\infty \frac{x}{1+x^4}\,\mathrm{d}x = -\frac{1}{8} \ . \tag{149}$$

c_{horn} denotes possible contributions to c^+ and c^- from the infinite horn. The difference between both constants is $\Delta c := c^+ - c^- = -0.375$, which is in very good agreement with the numerically obtained value $\Delta c = -0.367$. From this one obtains a value of

$$c_{horn} = 0.10 \tag{150}$$

for the constant c_{horn}.

IV.3 The Level Spacings Distribution

The most frequently used energy statistics is the distribution $P(S)$ of spacings between neighbouring levels. The behaviour of $P(S)$ for small spacings S is significantly different for systems which are classically chaotic and those which are classically integrable. In the integrable case one typically has level clustering, which is expressed by $P(S) \to 1$ as $S \to 0$, while chaotic systems show level repulsion, which implies $P(S) \to 0$ as $S \to 0$.

$P(S)$ is calculated for the scaled energy spectrum, which has a mean level spacing of one. This is obtained with the use of the generalized Weyl's law eq. (144).

$$E_n' = \bar{N}(E_n) \ . \tag{151}$$

Quantities concerning the scaled spectrum are denoted by a prime in the following. For example the spectral staircase for the scaled energies is given by

$$N'(E') = N(E(E')) \ . \tag{152}$$

The functional form of $P(S)$ which is expected for classically integrable systems is that of a Poisson distribution

$$P(S) = e^{-S} \ . \tag{153}$$

The result of random-matrix theory for the level spacings distribution of the GOE-ensemble is approximated well by the Wigner distribution

$$P(S) = \frac{\pi}{2} S \exp\left\{-\frac{\pi}{4} S^2\right\} \ . \tag{154}$$

The corresponding approximation for the distribution $P(S)$ of the GUE-ensemble is given by

$$P(S) = \frac{32}{\pi^2} S^2 \exp\left\{-\frac{4}{\pi} S^2\right\} \ . \tag{155}$$

The hyperbola billiard has a classically chaotic dynamics with time-reversal symmetry. For that reason it is expected that the statistics of level spacings is that of the GOE-ensemble, provided that it is evaluated separately for the energies of even and odd wavefunctions.

In figure 13 level spacings distributions are shown for the energy range $300 < E < 1500$. In figure 13 a) and b) P(S) is plotted for even and odd wavefunctions, respectively. Both distributions agree with the GOE-expectation. In the odd case the agreement with the GOE-curve is slightly better than in the even case. There are less very long and very short spacings than expected, but the deviations are not statistically significant. In figure 13 c) the distribution of all even-even and odd-odd spacings is plotted in order to improve the statistics. Figure 13 d) shows the distribution $P(S)$ of the total spectrum without separating with respect to symmetry classes. It is compared to a superposition of two independent GOE sequences. Again there are slightly less very short and very long spacings than expected.

The most significant feature of the hyperbola billiard are its horns. As the energy is increased, the wavefunctions explore more and more space in the horns, which is expressed by an increase of the effective area defined in eq. (142). On the other hand the local divergence of neighbouring classical trajectories becomes smaller and smaller as one moves into one of the horns. This is also expressed by the fact that the Lyapunov exponents of non-periodic trajectories decrease on an average as their lengths is increased, since they explore more and more space in the horns.

It is of interest to see, if this classical behaviour has any correspondence in the quantum mechanical energy statistics. In figure 14 a) and b) the statistics of spacings is shown for the energy ranges $300 < E < 900$ and $900 < E < 1500$, respectively. Because of the smaller number of spacings in the considered energy ranges, only the distributions of all spacings within both symmetry subspaces are plotted. In figure 14 there is no significant chance observed in the distribution $P(S)$.

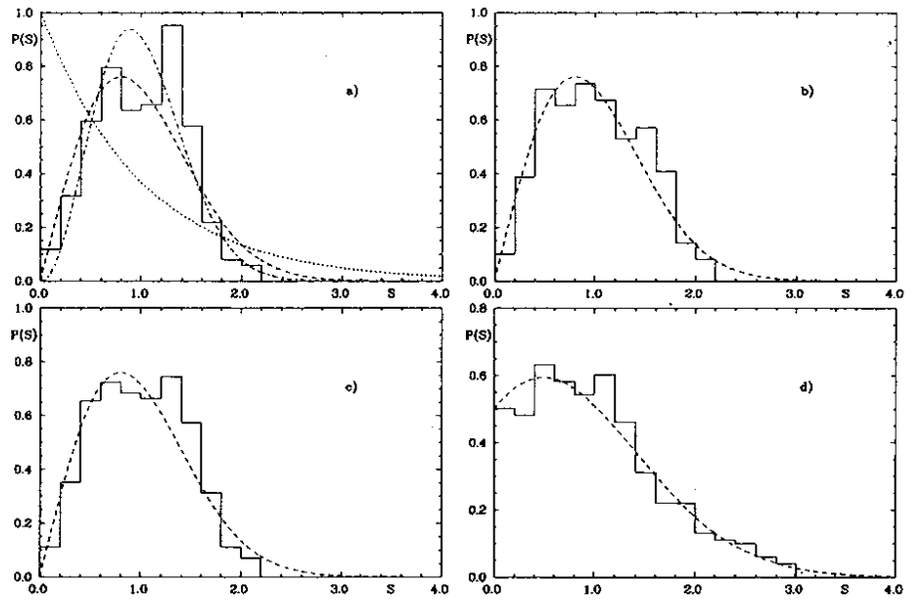

Figure 13: The level spacings distribution for a) even wave functions, b) odd wave functions, c) even and odd wave functions, d) the total energy spectrum. Dotted line: Poisson distribution, dashed-dotted line: GUE expectation, dashed line: in a)-c) GOE expectation, in d) expectation for the superposition of two independent GOE sequences. Energy range: $300 < E < 1500$.

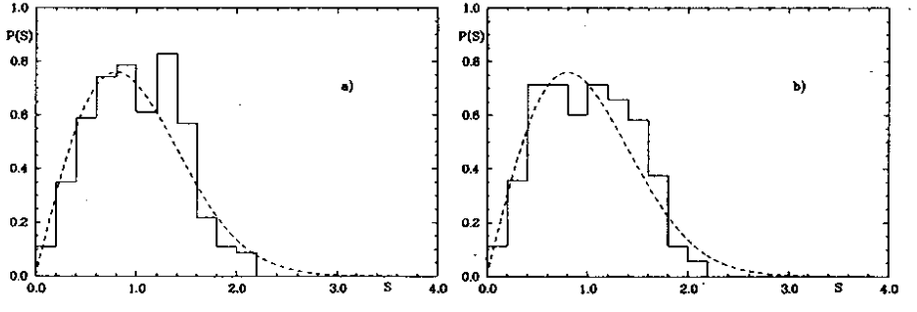

Figure 14: The level spacings distribution for all even-even and odd-odd spacings within the energy ranges a) $300 < E < 900$ and b) $900 < E < 1500$.

IV.4 The Spectral Rigidity and the Number Variance

The spacings distribution $P(S)$ is a short-range statistics. Statistical functions which give information about short-range as well as long-range correlations are the number variance $\Sigma^2(L)$ and the spectral rigidity $\Delta_3(L)$, which are defined in equations (123) and (124), respectively. In terms of the scaled energy spectrum the number variance is defined as the local variance of the number $n(E', L)$ of scaled energy levels in the energy interval from $E' - L/2$ to $E' + L/2$:

$$\Sigma^2(L) = \left\langle \left[n(E', L) - L \right]^2 \right\rangle \quad , \tag{156}$$

and the rigidity $\Delta_3(L)$ is given by

$$\begin{aligned} \Delta_3(L) &= \left\langle \frac{1}{L} \int_{-L/2}^{L/2} \mathrm{d}\varepsilon \, N'^2(E' + \varepsilon) - \left[\frac{1}{L} \int_{-L/2}^{L/2} \mathrm{d}\varepsilon \, N'(E' + \varepsilon) \right]^2 \right. \\ &\quad \left. -12 \left[\frac{1}{L^2} \int_{-L/2}^{L/2} \mathrm{d}\varepsilon \, \varepsilon N'(E' + \varepsilon) \right]^2 \right\rangle \quad . \end{aligned} \tag{157}$$

The relation between both statistics is expressed by eq. (126).

Poisson distributed sequences have the number variance $\Sigma^2(L) = L$ and the rigidity $\Delta_3(L) = L/15$. The results of random matrix theory for the number variance of GOE- and GUE-distributed sequences are given by [88]

$$\begin{aligned} \Sigma^2(L) &= \frac{2}{\pi^2} \left\{ \log(2\pi L) + \gamma + 1 + \frac{1}{2} \mathrm{Si}^2(\pi L) - \frac{\pi}{2} \mathrm{Si}(\pi L) \right. \\ &\quad \left. - \cos(2\pi L) - \mathrm{Ci}(2\pi L) + \pi^2 L \left[1 - \frac{2}{\pi} \mathrm{Si}(2\pi L) \right] \right\} \quad , \end{aligned} \tag{158}$$

and

$$\Sigma^2(L) = \frac{1}{\pi^2} \left\{ \log(2\pi L) + \gamma + 1 - \cos(2\pi L) - \mathrm{Ci}(2\pi L) + \pi^2 L \left[1 - \frac{2}{\pi} \mathrm{Si}(2\pi L) \right] \right\} \quad , \tag{159}$$

respectively. Results for the spectral rigidity follow from eq. (126).

Berry developed a semiclassical theory which predicts, for what values of the parameter L both statistics show universal behaviour, and for what values of L there is a departure from universality. The derivation of this theory is based on Gutzwiller's semiclassical expression for the density of states as a sum over periodic orbits. Here we discuss the theory for the spectral rigidity, but the argumentation is analogous for the number variance.

Berry's theory considers three ranges of the parameter L:

For very small values $L \ll 1$ the rigidity approaches $\Delta_3(L) \to L/15$, which is a consequence of the fact that $N'(E')$ is a staircase. In terms of the periodic-orbit sum the same result can be obtained with the use of a semiclassical sum rule. This sum rule is derived on the assumption that Gutzwiller's periodic-orbit sum is conditionally convergent and results in a series of δ-functions. The fact that the very long orbits are responsible for the δ-peaks, which must be distributed along the real energy axis with the right mean density, leads to constraints for the amplitudes and phases of the periodic orbits in the trace formula. These constraints give rise to the sum rule mentioned above.

The second range of the parameter L is given by $1 \ll L \ll L_{max}$, where L_{max} is the quotient between the largest energy scale $(\Delta E)_{max}$ in the periodic-orbit sum and the mean energy level

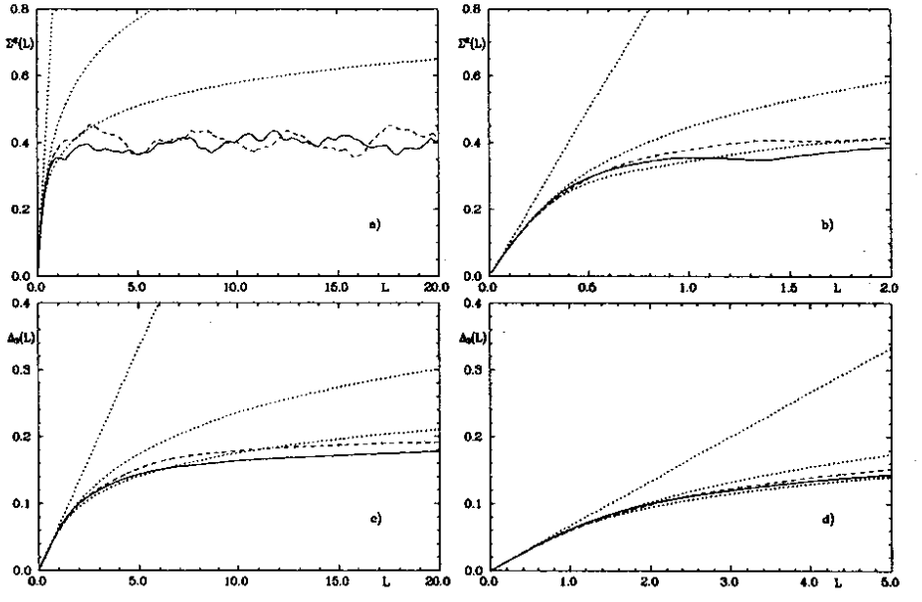

Figure 15: The number variance $\Sigma^2(L)$, a) and b), and the spectral rigidity $\Delta_3(L)$, c) and d). Full lines: results for even energy eigenfunctions, dashed lines: results for odd energy eigenfunctions, dotted lines: in the sequence of increasing functional values: the results for GUE-, GOE- and Poisson distributed sequences.

distance $1/\bar{d}(E)$. $(\Delta E)_{max}$ is the energy range within which the oscillatory contribution of the shortest orbit in the periodic-orbit sum oscillates once: $(\Delta E)_{max} = 2\pi\hbar/T_{min}$. Here T_{min} denotes the period of the shortest periodic orbit. In the considered intermediate range of the parameter L the behaviour of the rigidity is determined mainly by the contributions of orbits to the periodic-orbit sum, whose lengths are in an intermediate range, too. It is assumed that they are large enough in order that the orbits are uniformly distributed in phase space. On the other hand they must be small enough, so that pairs of orbits with an action difference smaller than $\hbar$ occur rarely. On this assumption a classical sum rule is obtained, which is a consequence of the exponential proliferation of long orbits and the uniformity of exploration of phase space by long orbits. Using this sum rule it is shown that the rigidity agrees with the random matrix predictions in the considered range of the parameter L.

Within the third range $L \gg L_{max}$ the properties of the rigidity are determined by the contributions of the very short orbits to the trace formula. These orbits have non-universal properties, which differ from system to system. As a consequence of the fact that there is a shortest orbit the rigidity saturates and approaches a non-universal constant Δ_∞ as $L \to \infty$.

In figure 15 the number variance and the spectral rigidity are shown for the hyperbola billiard. The GOE expectation is met only for very small values of the parameter L. The

number variance $\Sigma^2(L)$ deviates from the GOE curve already at $L \approx 0.4$, and in case of the spectral rigidity $\Delta_3(L)$ the deviation occurs at $L \approx 2.0$. These values of L are much smaller than the values that would be expected from Berry's theory. With the length of the shortest periodic orbit $l_{min} = 2.0$ the value of L_{max} at energy $E = 800$ is given by

$$L_{max} = 4\pi\sqrt{E}\,\bar{d}(E)/l_{min} \approx 37 \tag{160}$$

for both symmetry subspaces. The reason for the disagreement with the predictions of Berry's theory is the fact, that the special properties of the hyperbola billiard prevent Berry's theory from being applicable to this system. One crucial assumption for the derivation of universality is the uniformity of exploration of phase space by long orbits. The hyperbola billiard has a phase space of infinite volume and for that reason it cannot be covered uniformly by a finite number of orbits. Still it would be favourable to understand the properties of the rigidity and the number variance on basis of the periodic orbits of the system. This requires a detailed examination of the validity of the assumptions of Berry's theory in case of the hyperbola billiard and possible replacements of this assumptions.

Both considered statistics show, however, a saturation as is predicted by Berry's theory, and they saturate already for very small values of the parameter L. In most systems the saturation occurs only for large values of the parameter L. The determination of the saturation values of $\Sigma^2(L)$ and $\Delta_3(L)$ then requires the knowledge of a large number of energy eigenvalues, which for most systems are not available. In figure 15 a) $\Sigma^2(L)$ saturates very early and then oscillates around the value $\Sigma_\infty \approx 0.40$ for the eigenvalues of even wavefunctions as well as for the eigenvalues of odd wavefunctions. The rigidity saturates at larger values of L. At $L = 20$ the values of $\Delta_3(L)$ are still slightly increasing. In order to obtain the saturation value Δ_∞ for the two curves, a fit with functions of the form

$$\Delta_3(L) = \Delta_\infty \left(1 + \frac{a}{L} + \frac{b}{L^2}\right) \quad , L \gg 1 \quad , \tag{161}$$

is made. The result is the value $\Delta_\infty \approx 0.20$ for both cases.

Theoretically a relation between Δ_∞ and Σ_∞ follows from eq. (126). $\Delta_3(L)$ is replaced for large values of L by eq. (161) and eq. (126) is differentiated four times with respect to L. This results in a differential equation for $\Sigma^2(L)$ for large values of L [39]. This differential equation implies

$$\Sigma^2(L) = 2\Delta_\infty + O(L^{-3}) \quad , L \to \infty \, , \tag{162}$$

so that $\Sigma_\infty = 2\Delta_\infty$, which is verified by the numerically obtained values. In addition eq. (162) gives an explanation for the fact, that $\Sigma^2(L)$ saturates much faster than $\Delta_3(L)$. Correction terms to the saturation value are of order $O(L^{-3})$ for large values of L, whereas in case of the rigidity correction terms of order $O(L^{-1})$ are obtained.

V Numerical Examination of the Periodic-Orbit Theory

The Gutzwiller trace formula allows the determination of quantum mechanical energies of classically chaotic systems in the limit $\hbar \to 0$ by making use only of classical quantities. It has, however, scarcely been used for the determination of energies. This is due to several theoretical and practical problems, which are connected with the trace formula.

One problem is the sum over an infinite number of periodic orbits and the question of its convergence, as has been discussed in chapter II. Due to the exponential proliferation of the periodic orbits a positive imaginary part must be given to the energy E in order that the periodic-orbit sum converges absolutely. The lower limit for $\mathrm{Im}\,E$ depends on the topological entropy, which is a measure for the exponential increase of the number of orbits, and the asymptotic instability of orbits in the limit that the lengths of the trajectories go to infinity (see eq. (77)). The fact of a finite (positive) lower limit for $\mathrm{Im}\,E$ prevents the determination of the energies by an absolutely convergent periodic-orbit sum. If this sum moreover is not conditionally convergent for real values of the energy E, the trace formula has to be smoothed with suitable test functions as was done in chapter II. As consequence of the smoothing the poles at the energies are replaced by peaks of finite height and width. This does not restrict the accuracy for the determination of the energies, if the width of the peaks can be made arbitrarily small. Whether this can be done depends on the kind of smoothing, which is chosen. If the peaks have the form of Breit-Wigner curves, they must have a minimum width in order that the periodic-orbit sum converges absolutely. In case of a Gaussian smoothing there is no such restriction for the width of the peaks, so that a Gaussian smoothed trace formula allows the determination of the energies with arbitrary accuracy. In the latter case one still has a sum over an infinite number of periodic orbits. Most orbits, however, give a negligible contribution to the periodic-orbit sum, so that the determination of energies with a finite resolution requires the sum over a finite number of orbits only.

A further question is, what the effect of the semiclassical approximations is, that were used in the derivation of the trace formula. There is no estimation for the size of the error of these approximations. The trace formula defines a function, which is an approximation to the trace of the Green function in those parts of the complex E-plane, in which the periodic-orbit sum converges. Let us assume that this function in principle can be defined in parts of the complex E-plane, where the sum diverges, by analytical continuation. Then it is assumed that this semiclassical approximation to the trace $g(E)$ of the Green function has poles at values of E, which are close to the energy eigenvalues of the Hamiltonian operator. But what the actual relationship is between the pole structure of $g(E)$ and its approximation is not known. For this reason it is not clear, for example, if the Gaussian peaks actually converge into a series of delta-functions, if the width of the peaks is made smaller and smaller. There are only few numerical tests of the periodic-orbit theory, and there is no detailed quantitative analysis of the accuracy of the trace formula.

The reason for this is the high numerical effort, that an evaluation of the trace formula requires. In chaotic systems it is very difficult to determine a fairly large number of periodic orbits with sufficient accuracy, as has been discussed at the beginning of chapter III. It is even more difficult to determine a complete spectrum of the shortest orbits, whose actions are smaller than a given value. On the other hand the evaluation of the trace formula requires

the knowledge of a very large number of the shortest orbits, if one wants to determine more than the first few energies. A rough estimate for the order of magnitude of the number of orbits that are needed in order to resolve two adjacent energies, which are separated by an energy difference ΔE, is obtained by observing that every orbit contributes a term to the periodic-orbit sum, which oscillates as a function of E (see eq.(34) or the smoothed trace formulae of this chapter). In order to resolve ΔE one has to include in the periodic-orbit sum at least all the shortest orbits up to those, whose contribution oscillates once as E is changed by ΔE. For small ΔE this leads to the condition $\mathrm{d}S(E)/\mathrm{d}E = T(E) < 2\pi\hbar/\Delta E$, where $T(E)$ is the period of an orbit with energy E. Because of the exponential proliferation of the number of orbits, the resolution of the energy interval $\Delta E/2$ requires the summation over the square of the number of orbits, which are needed for the resolution of ΔE. For this reason soon a limit for the energy resolution is reached in practice.

The fact that for many chaotic systems only a relatively small number of orbits is known is also the reason why in many papers not a smoothed trace formula is used, but the original (divergent) formula, which is truncated. One often finds that the truncated trace formula gives good results for the determination of the first few energies. But this effect is only expected, if not too many orbits are taken into account. If the sum extends over more and more orbits, it is expected that the effect of the divergence of the periodic-orbit sum shows up in the form of wild oscillations, which finally prevent a discrimination of the energies. This does not happen in case of a Gaussian smoothed trace formula, for example. In addition, the smoothing parameter can be chosen small enough, so that the smoothing does not give rise to a decrease of the energy resolution.

It is of strong interest to know what the properties of the periodic-orbit theory as approximative theory actually are. A further point is that almost all the semiclassical theories for chaotic systems use the same kind of approximation methods, that is stationary phase approximations, whether it is the Gutzwiller trace formula or the approximation to the energy eigenfunctions [23] or to the Wigner function [26] or the new quantization method of Bogomolny [16]. For example, in deriving the trace formula a stationary phase approximation is used three times. It is therefore of interest to see, what the effects of these approximations are for one example, for which the trace formula is not exact.

For the reasons already stated the hyperbola billiard gives the possibility to do such examinations. In order to test the trace formula quantitatively it is of importance to use the smoothed trace formula, since in this way one has control over the error that one makes by summing over a finite number of orbits only. In case of the unsmoothed trace formula there is no estimation for this error. By using a Gaussian smoothing, for example, the smoothing parameter can be chosen in such a way, that the sum of the contributions of the infinite number of orbits, which are neglected in the periodic-orbit sum, is small in comparison with the contribution of the shortest orbits, over which the sum is taken. It is even possible to do the periodic-orbit sum exactly. This can be done by choosing the smoothing function $h(p)$ in eq.(84) in such a way that its Fourier cosine transform $g(x)$ is equal to zero, if its argument x is larger than a certain value. In this case the periodic-orbit sum contains a finite number of orbits.

In this chapter the trace formula is evaluated for several examples of the smoothing function $h(p)$. Energies are determined and the accuracy of the trace formula is analyzed. At the end of this chapter the Riemann-Siegel analogue of Berry and Keating is examined and the results are compared to the results for the smoothed trace formulae.

V.1 The Generalized Periodic-Orbit Sum Rules for the Hyperbola Billiard

The basic formula that is used throughout this chapter is given by eq.(84), which is applied to the energy eigenvalues of even and odd wavefunctions of the hyperbola billiard, respectively. This is equivalent to the application of eq.(84) to the desymmetrized hyperbola billiard with Neumann and Dirichlet boundary conditions, respectively, on the line $y = x$, and Dirichlet boundary conditions on the remaining part of the boundary. Again dimensionless units are used with $\hbar = 1 = 2m$, where m is the mass of the particle. Eq.(84) then has the form

$$\sum_n h(p_n) \approx 2\int_0^\infty \mathrm{d}p\, p\, h(p)\bar{d}(E=p^2) + \sum_\gamma \sum_{k=1}^\infty \frac{l_\gamma\, \chi_\gamma^k\, g(kl_\gamma)\, a_{\gamma,k}}{\exp(ku_\gamma/2) - (-1)^{kn_\gamma}\exp(-ku_\gamma/2)} \quad . \tag{163}$$

$\chi_\gamma = (-1)^{\bar{n}_\gamma}$, where $\bar{n}_\gamma$ is the number of reflections on those parts of the boundary, where Dirichlet boundary conditions are required. n_γ is the total number of reflections on the boundary during one traversal of the periodic orbit γ. Every orbit whose code word contains an odd number of "$-$" corresponds to an orbit in the full hyperbola billiard, which has double length and is symmetric under reflection on the line $y = x$. For that reason the number of reflections on the line $y = x$ must be odd. An orbit whose code word contains an even number of "$-$" corresponds to an orbit in the full hyperbola billiard which has the same length, and for that reason the number of its reflections on the line $y = x$ must be even. In addition every "+" and every "$-$" corresponds to an even number and every "0" to an odd number of reflections on the remaining part of the boundary, i.e. the boundary along the hyperbola $y = 1/x$ and the x-axis. It follows that

$$n_\gamma = (n_{0,\gamma} + n_{-,\gamma}) \bmod 2 \quad , \tag{164}$$

where $n_{0,\gamma}$ and $n_{-,\gamma}$ are the numbers of "0" and "$-$", respectively, in the code word of the orbit γ.

Neumann boundary conditions along the line $y = x$:
From the considerations above it follows that

$$\bar{n}_\gamma = n_{0,\gamma} \bmod 2 \quad . \tag{165}$$

The mean energy density is

$$\bar{d}(E) = \frac{\mathrm{d}}{\mathrm{d}E}\bar{N}^+(E) \quad , \tag{166}$$

and $\bar{N}^+(E)$ is given by eq.(144). Further from eq.(55) one obtains

$$a_{\gamma,k} = a^+_{\gamma,k} = \begin{cases} (1 + (-1)^k e^{-ku_\gamma})^{-1} & \text{for the orbit with code word } a = (\mathrm{b}) \\ 1 & \text{otherwise} \quad . \end{cases} \tag{167}$$

Dirichlet boundary conditions along the line $y = x$:

In this case

$$\bar{n}_\gamma = n_\gamma \tag{168}$$

and

$$\bar{d}(E) = \frac{\mathrm{d}}{\mathrm{d}E}\bar{N}^-(E) \quad , \tag{169}$$

where $\bar{N}^-(E)$ is given by eq. (144). Further from eq. (56) one obtains

$$a_{\gamma,k} = a^{-}_{\gamma,k} = \begin{cases} (1+(-1)^k e^{ku_\gamma})^{-1} & \text{for the orbit with code word } a = (\mathrm{b}) \\ 1 & \text{otherwise .} \end{cases} \tag{170}$$

V.2 The Unsmoothed Energy Density

Eq. (77) is a condition for the imaginary part of the momentum $p = \sqrt{E}$, for which the periodic-orbit sum for the trace of the Green function $g(E)$ is absolutely convergent. However, the orbits contribute with different signs to the periodic-orbit sum. As will be seen below the number of orbits, which give a positive contribution to the sum is of the same order of magnitude as the number of orbits, whose contribution is negative. For that reason it can be expected that the region of conditional convergence of the periodic-orbit sum in the complex p-plane approaches much closer the axis of real momentum p than the region of absolute convergence. The question, whether the evaluation of the periodic-orbit sum on the real p-axis gives any sensible results, is examined numerically.

The numerical evaluation is done for the unsmoothed energy density $d(E)$ which is related to the trace of the Green function $g(E)$ by eq. (18). Its periodic-orbit approximation is real for real values of the energy E and it can be obtained formally by choosing the smoothing function $h(p')$ to be a delta-function

$$h(p') = \delta(p^2 - p'^2) \ . \tag{171}$$

Then

$$g(x) = \frac{1}{2\pi|p|}\cos(px) \ . \tag{172}$$

Of course this function $h(p')$ does not obey the conditions, which guarantee absolute convergence of the periodic-orbit sum.

The results of a numerical evaluation of the trace formula for even and odd wavefunctions are shown in figure 16 a) and b), respectively. The periodic-orbit sum is taken over all orbits that have been determined, that is all orbits with code lengths $N \leq 14$ or length $l_\gamma \leq 20$, which are 533 760 orbits altogether. The limit of the k-summation is given by $kl_\gamma \leq 40$. The positions of the energies E_n are marked by triangles. Figure 16 shows distinct peaks at the energies E_n, if neighbouring energies are separated well enough. In the following E_n^+ denotes the n-th eigenvalue of even wavefunctions. The corresponding notation for the eigenvalues of odd wavefunctions is E_n^-.

In figure 16 a) the first 15 energies with exception of the two adjacent energies E_8^+ and E_9^+ can be resolved. E_8^+ and E_9^+ are separated by a momentum difference $\Delta p \approx 0.169$. The resolution of this momentum difference requires at least the summation over orbits with a length below $l = \Delta p/2\pi \approx 37.2$. The mean value of lengths with code length $N = 14$ is $\bar{l}_{14} \approx 28.4$. As a consequence the orbits over which the periodic-orbit sum is taken are not sufficient for the resolution of two different peaks. Only one peak for both energies can be seen in figure 16. The momentum difference between the energies E_{16}^+ and E_{17}^+ is equal to $\Delta p \approx 0.178$, which corresponds to a length of $l \approx 35.3$. But in this case two different peaks can be seen, although the height of the second peak is distinctly smaller than the first peak. The momentum difference between the maxima of the two peaks in the figure is, however, larger than the momentum difference between the corresponding two energy eigenvalues. It

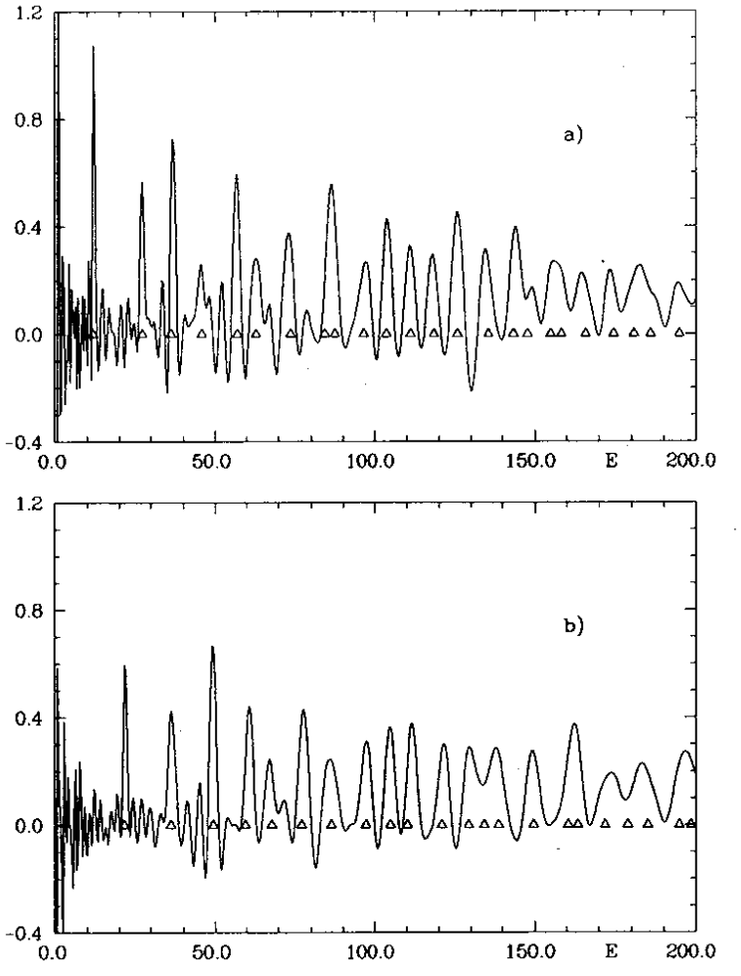

Figure 16: The results of an evaluation of the trace formula for the unsmoothed level density for the energy eigenvalues of a) even and b) odd wave functions. The triangles mark the positions of the energy eigenvalues. The sum is taken over all periodic orbits, which have a length below $l = 20$ or a code length $N \leq 14$.

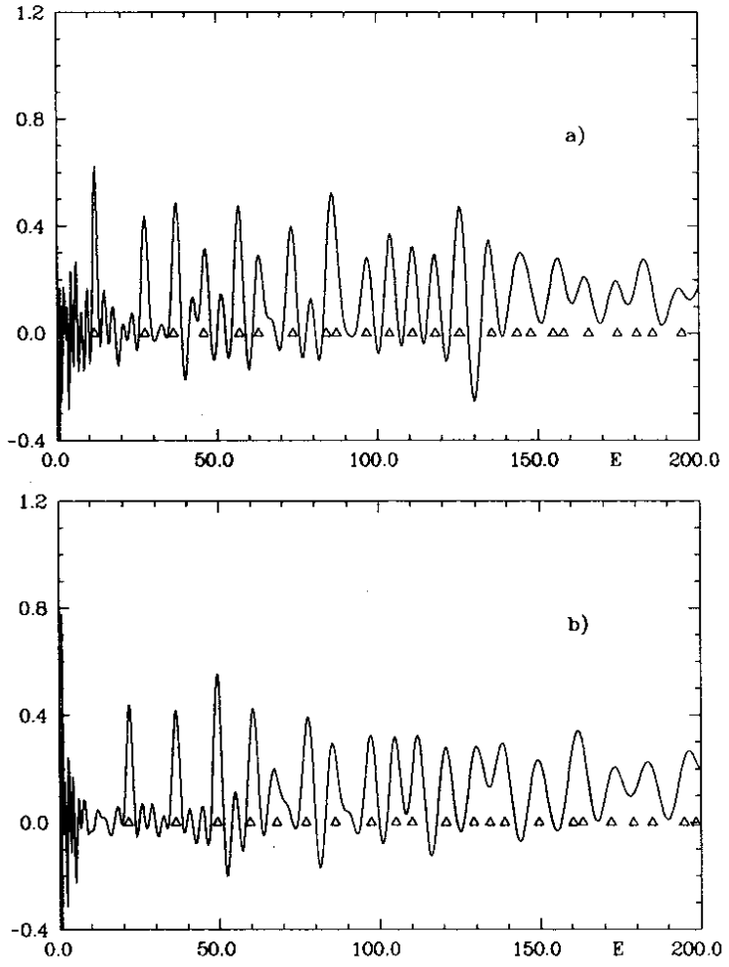

Figure 17: The results of an evaluation of the trace formula for the unsmoothed level density for the energy eigenvalues of a) even and b) odd wave functions. The triangles mark the positions of the energy eigenvalues. The sum is taken over all periodic orbits, which have a length below $l = 20$.

is $\Delta p \approx 0.209$, which corresponds to $l \approx 30.1$. This can be interpreted as the start of the splitting of one peak into two. As more and more lengths are included in the sum it is expected that the second peak increases, and that probably both peaks move closer together.

In case of the eigenvalues of odd wavefunctions the first 11 energies can be resolved. The next energies E_{12}^-, E_{13}^- and E_{14}^- are separated by momentum differences of $\Delta p \approx 0.220$ and $\Delta p \approx 0.198$, respectively. The corresponding lengths, up to which the periodic-orbit sum has to be taken in order to resolve these momentum differences are given by $l \approx 28.6$ and $l \approx 31.8$. respectively. For this reason there are only two peaks for the three energies.

The result of this numerical investigation of the unsmoothed energy density is, that the application of the periodic-orbit theory for this quantity gives good results. There can be different reasons for this. First it is possible that the periodic-orbit sum is conditionally convergent for real values of the momentum p. The trace formula then gives a semiclassical approximation for the level density with peaks at approximations to the energy eigenvalues, although those peaks need not be delta-peaks. Second it is possible that the periodic-orbit sum is divergent. The good results shown in figure 16 are then due to the fact that not too many orbits have been included in the periodic-orbit sum. If more and more orbits are included in the sum, it then is expected that oscillations arise between the peaks at the energies, which gradually increase, so that finally the peaks disappear in the background.

In order to get an impression how the curve for the approximated energy density changes as a different number of orbits is included in the periodic-orbit sum, figures 17 a) and b) show the result of an evaluation of the periodic-orbit sum with all orbits that have a length below $l = 20$. Although the number of orbits is very much less than the number of orbits that have been used for figures 16 a) and b), 13 098 orbits in comparison with 533 760 orbits, the number of peaks that can be resolved is almost the same in both cases. The reason for this is that the momentum differences between an energy, that can be resolved in figure 16, and its neighbouring energies are in most cases so large that the orbits with length up to $l = 20$ are sufficient for the resolution of this energy. One difference between figures 16 a) and 17 a) is that in 17 a) there is no beginning splitting of the peak for the energies E_{16}^+ and E_{17}^+ into two peaks. In figure 17 b) the two energies E_9^- and E_{10}^- can be resolved although their momentum difference is equal to $\Delta p = 0.245$ which corresponds to $l = 25.6$, so that a summation over all orbits with length below $l = 20$ seems not to be enough for the resolution of these peaks. However, for the two corresponding peaks in figure 17 b) one has $\Delta p = 0.344$ and $l = 18.3$. The resolution of two different peaks therefore is probably due to the fact that the semiclassical approximations for the two energies E_9^- and E_{10}^- have a larger separation than the actual energies. If more orbits are included the peaks move slightly together and in figure 16 b) the difference is equal to $\Delta p = 0.313$. Although most of the peaks are improved, if more orbits are included in the periodic-orbit sum, there are peaks, which in the second pair of figures are better than in the first pair of figures. These are the peaks at the energies E_4^+ and E_7^-. However, one has to be cautious with an interpretation of this result as a possible sign of a divergence, since the orbits are only complete up to the length $l = 20$.

A further examination of the change of the curve for the energy density as more orbits are included in the periodic-orbit sum is carried out by a consideration of the contributions of orbits within different ranges of the code length N. Figure 18 shows the results of an evaluation of the trace formula with all orbits with $1 \leq N \leq 7$ and $8 \leq N \leq 14$, respectively, for the eigenvalues of even and odd wavefunctions. The curves are discussed for the even case, but qualitatively the same statements can be made for the odd case. In figure 18 a)

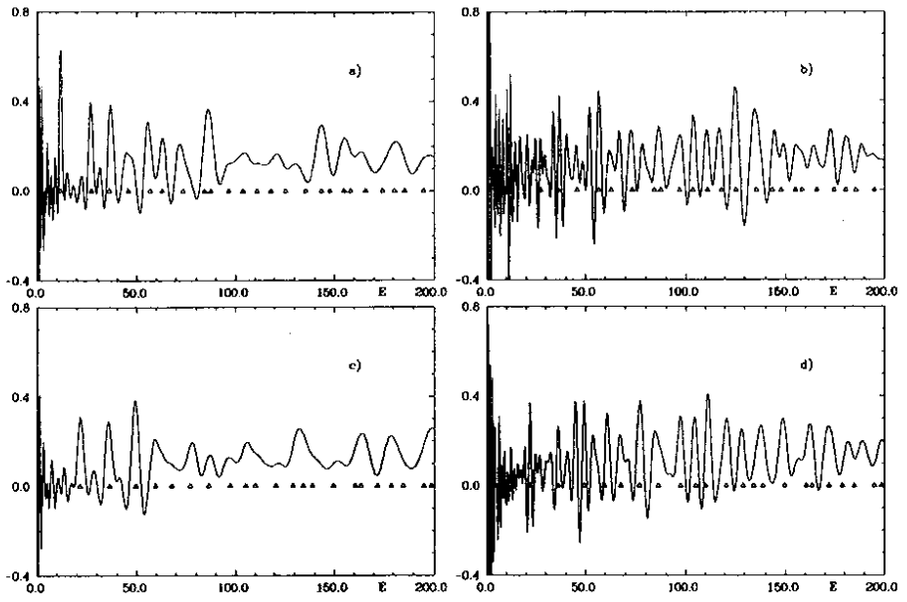

Figure 18: The results of partial sums over periodic orbits in the trace formula for the energy density. a) and b) show the results of a summation over all orbits with code length $1 < N < 7$ and $8 < N < 14$, respectively, for the energy eigenvalues of even wavefunctions. c) and d) show the corresponding results for energy eigenvalues of odd wavefunctions.

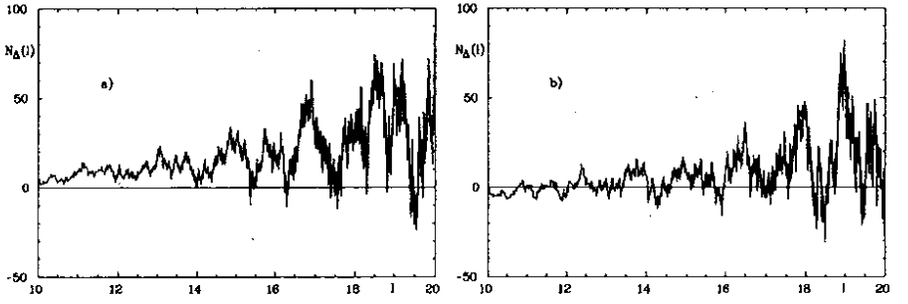

Figure 19: The difference $\mathcal{N}_\Delta(l)$ of the numbers of orbits, which contribute to the periodic-orbit sum with a phase factor $\chi_\gamma^k = +1$ and $\chi_\gamma^k = -1$, respectively, for the a) even and b) odd case.

the first seven peaks can be resolved. For higher energies the curve can be interpreted as a superposition of peaks at the energy eigenvalues, so that the curve can be understood qualitatively over the entire considered energy range. In figure 18 b) there are pronounced peaks also at the higher energies E_{10}^+ - E_{15}^+. In lower energy range there are oscillations, which have maxima at the energies E_1^+ - E_7^+, so that the longer periodic orbits also produce an increase of the peaks at low energies. However, the oscillations between the low energies partly have the same amplitude as the peaks at the energies. In case of the energy E_4^+ the amplitudes on one side are even higher.

In order to get a better estimation of the convergence properties of the periodic-orbit sum the following quantity is defined

$$\begin{aligned} \mathcal{N}_\Delta(l) \;:=\; & \#\{\text{periodic orbits } \gamma \text{ with } l_\gamma \le l \text{ and } \chi_\gamma^k \doteq +1\} - \\ & \#\{\text{periodic orbits } \gamma \text{ with } l_\gamma \le l \text{ and } \chi_\gamma^k = -1\} \ . \end{aligned} \tag{173}$$

Here the total number of periodic orbits is considered, not only the primitive periodic orbits. $\mathcal{N}_\Delta(l)$ is different in the even and the odd case, because of the different phase factors χ_γ. The periodic orbits contribute with different signs to the periodic-orbit sum. The sign depends on the phase factor χ_γ^k and the phase of the cosine-function in eq. (172). If the periodic-orbit sum is evaluated at a fixed value of the momentum p then for large lengths there will be a great number of orbits within one half-period of the cosine-function because of the exponential proliferation of the number of periodic orbits. The mean Lyapunov exponent is for orbits with different values of the phase factor χ_γ^k to a good approximation the same. The change of the function $\mathcal{N}_\Delta(l)$ therefore indicates what the contribution of one half-period of the cosine-function to the periodic-orbit sum is, and thus it allows a better estimation of the convergence properties of the orbit sum. In figure 19 the function $\mathcal{N}_\Delta(l)$ is shown for the even and odd case in the range $0 < l < 20$ where all orbits are known. The function oscillates and its mean increase is very low in comparison with the increase of the total number of orbits which is shown in figure 8. From this one can conclude that the region of conditional convergence reaches up much closer to the real momentum axis than the region of absolute convergence. Possibly the periodic-orbit sum is even convergent for real values of the momentum p.

V.3 The Breit-Wigner Smoothed Energy Density

If the periodic-orbit sum is not convergent, the level density has to be smoothed in order to obtain a convergent sum. A natural kind of smoothing is carried out by giving the momentum p a constant imaginary part $i\alpha/2$ before taking the imaginary part of the periodic-orbit sum for the trace of the Green function $g(E)$. The result is a smoothed energy density, which consists of a superposition of Breit-Wigner curves, that are centered at the quantum mechanical energies. The smoothing function is given by

$$h(p') = \frac{\alpha^2 p^2}{(p^2 - p'^2)^2 + \alpha^2 p^2} \tag{174}$$

It is normalized such that the height at the maximum is equal to one. The Fourier cosine transform of $h(p')$ is equal to

$$g(x) = \frac{\alpha p}{2(p^4+\alpha^2p^2)^{1/4}}\cos\{x\sqrt{\frac{1}{2}(\sqrt{p^4+\alpha^2p^2}+p^2)}-\frac{1}{2}\arctan\frac{\alpha}{p}\}$$
$$\times\exp\{-x\sqrt{\frac{1}{2}(\sqrt{p^4+\alpha^2p^2}-p^2)}\}\ . \qquad (175)$$

The width of the Breit-Wigner curves is energy-dependent, and the condition for the absolute convergence of the periodic-orbit sum is a condition for the parameter α. It is $\alpha > 2\sigma$, where σ is given in eq.(77). Even if the periodic-orbit sum is convergent, it is of use to consider a smoothed energy density. The reason for this is that the numerical evaluation is done with a finite number of orbits. The maximum length l of these orbits sets a lower limit for the momentum difference $\Delta p = 2\pi/l$, which can be resolved. By using a smoothed trace formula with a smoothing parameter α the attainable momentum resolution is limited by the finite width of the peaks at the energies. If one chooses α in such a way that both lower limits for Δp are the same, then the resolution is not diminished by using a smoothed trace formula. But the periodic-orbit sum of the smoothed level density has improved convergence properties because of the exponential damping factor in eq.(175). A relation between Δp and α is obtained by requiring that between two energies the level density falls off to half of its value at the energies levels, if the energies are separated by Δp. This leads to the condition

$$1+\frac{\alpha^2p^2}{(\Delta p)^2(2p+\Delta p)^2+\alpha^2p^2} = 4\frac{\alpha^2p^2}{(\Delta p)^2/4(2p+\Delta p/2)^2+\alpha^2p^2}\ , \qquad (176)$$

which for $\Delta p \ll p$ results in

$$\alpha = \Delta p\left(\frac{5+\sqrt{33}}{4}\right)^{-1/2} \approx \Delta p/1.64\ . \qquad (177)$$

In practical calculations there is some difficulty in the estimation of the minimal Δp, that can be resolved with a finite number of orbits. Normally the periodic orbits, that are used for the evaluation of the trace formula, are not complete up to the maximum length of the orbits. For that reason Δp is not necessarily determined by the maximum length, but by some smaller length. In figure 20 the Breit-Wigner smoothed energy density is shown for the energy eigenvalues of even and odd wavefunctions, respectively. The parameter α is chosen to be $\alpha = 0.15$, which corresponds to $\Delta p \approx 0.25$. The dashed curve is calculated from the quantum mechanical energy spectrum. Both curves agree well in their main features over the whole energy range. In comparison with the approximation for the unsmoothed level density the oscillations between the peaks are suppressed. This allows a better discrimination of the peaks at the energy eigenvalues. For example the peaks at the energies E_4^+, E_6^+ and E_5^- now are more distinct. As a consequence of the smoothing the maxima of the peaks are slightly shifted, as can be seen in tables 8 and 10 at the end of this chapter.

Most of the peaks of the curve, that is obtained from the periodic-orbit sum, have a smaller height than the peaks of the dashed curve. The reason for this are the missing contributions of orbits, which are neglected in the periodic-orbit sum, that is orbits with code length $N > 14$ and length $l_\gamma > 20$. The contributions of these orbits can be diminished by increasing the smoothing parameter α. The requirement that the contributions of orbits,

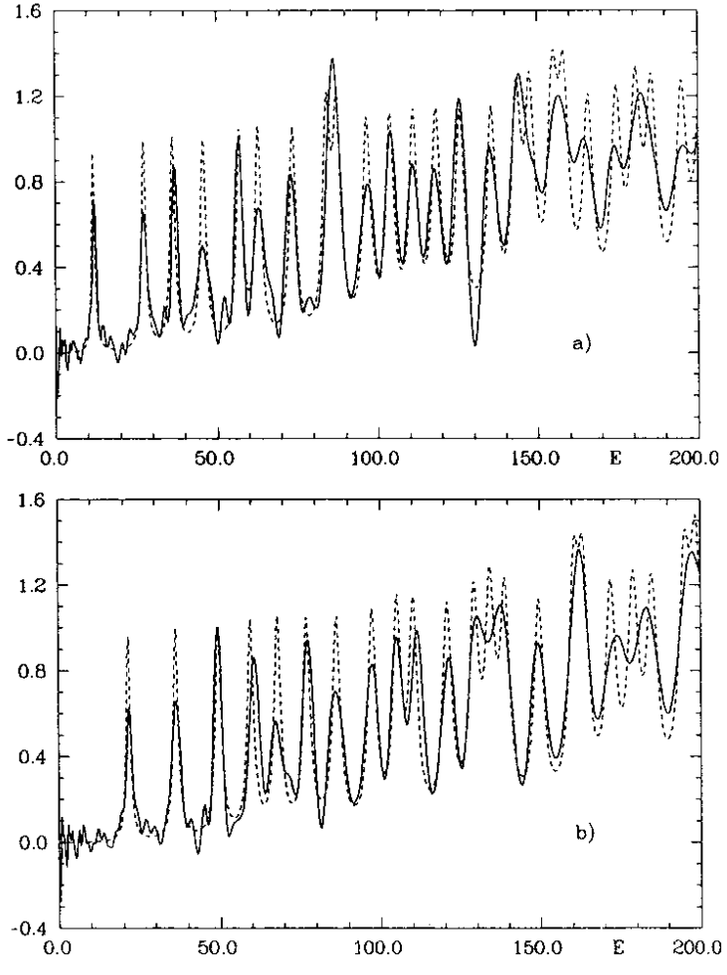

Figure 20: The Breit-Wigner smoothed level density calculated from the periodic-orbit theory (full line) and the quantum mechanical energy spectrum (dashed line) for the energy eigenvalues of a) even and b) odd wavefunctions. The smoothing parameter is equal to $\alpha = 0.15$.

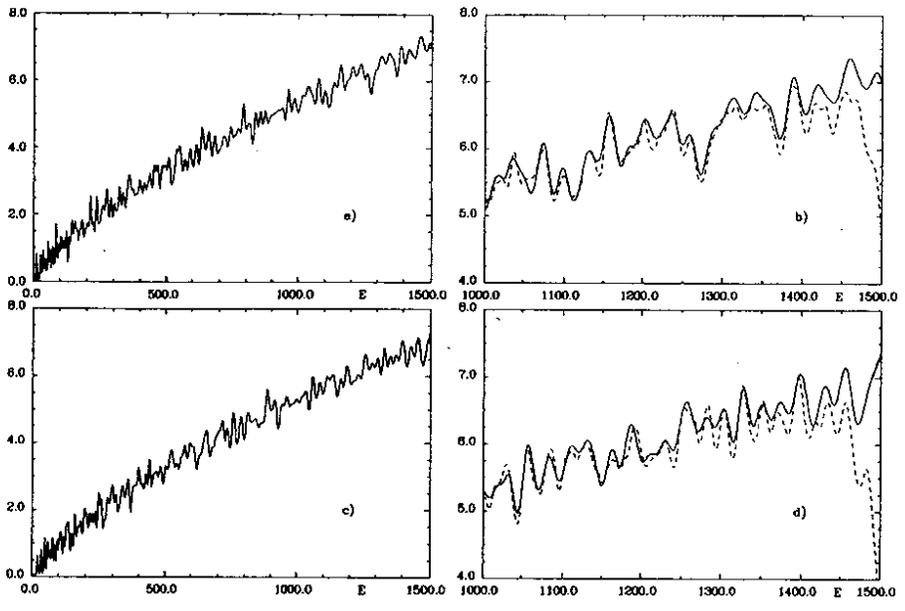

Figure 21: The periodic-orbit approximation for the Breit-Wigner smoothed level density with $\alpha = 0.25$ for the eigenvalues of a) even and c) odd wavefunctions. b) and d) show a section of a) and c), respectively, in comparison with corresponding curves, that are obtained from the quantum mechanical energy spectrum (dashed line).

which are neglected, is not significant gives a condition for α. However, the estimation of the value of α which is determined by this condition is difficult, because the orbits contribute with different phase factors to the sum. In figure 21 an evaluation of the Breit-Wigner smoothed trace formula is shown for $\alpha = 0.25$. Figures 21 a) and c) show the results for the energy range $0 < E < 1500$. In figures 21 b) and d) the curves, that are obtained from the periodic-orbit theory, are compared to curves, which are computed with the numerically determined energy eigenvalues, in the range $1000 < E < 1500$. As can be seen there also is a good agreement between corresponding curves in the range of higher energies. Close to the energy $E = 1500$ the dashed curves fall off because of the missing contributions of the energy eigenvalues above $E = 1500$.

A disadvantage of the Breit-Wigner smoothing is the fact, that in general the smoothing parameter α cannot be chosen arbitrarily. If the trace formula for the level density is divergent, then α has to be above a certain minimal value in order that the Breit-Wigner smoothed periodic-orbit sum converges. This sets a limit for the energy resolution, which can be attained in principle, even if an arbitrary number of periodic orbits is available. A kind of smoothing which is free of such a limitation is the Gaussian smoothing, which is discussed in the following section.

V.4 The Gaussian Smoothed Energy Density

The Gaussian smoothed level density has peaks in form of Gaussian curves at the energy eigenvalues. It is obtained, by choosing the smoothing function to be

$$h(p') = \exp\{-\frac{(p-p')^2}{\epsilon^2}\} + \exp\{-\frac{(p+p')^2}{\epsilon^2}\} \ . \tag{178}$$

Then

$$g(x) = \frac{\epsilon}{\sqrt{\pi}} \cos(px) \exp\{-\frac{\epsilon^2 x^2}{4}\} \ . \tag{179}$$

The periodic-orbit sum is absolutely convergent for every positive value of the smoothing parameter ϵ because of the very strong damping of the contributions of orbits with large lengths due to the exponential factor in eq. (179). This in principle gives the possibility to determine the semiclassical energies with an arbitrary accuracy. For that reason the Gaussian smoothing can be considered as an alternative to an analytical continuation of the periodic-orbit sum for the trace of the Green function $g(E)$, in case this sum is not convergent.

Again a relation between the momentum resolution, which is attainable with a finite number of orbits and the smoothing parameter ϵ is obtained by requiring that the momentum resolution is not decreased by smoothing the trace formula. The requirement that between two peaks that are separated by Δp the smoothed level density falls off to half of the value, that it has at the peaks, leads to the following condition ($p \gg \Delta p$)

$$1 + \exp\{-\frac{(\Delta p)^2}{\epsilon^2}\} = 4 \exp\{-\frac{(\Delta p)^2}{4\epsilon^2}\} \ , \tag{180}$$

which yields approximately

$$\epsilon = \Delta p / 2.35 \ . \tag{181}$$

A comparison with eq. (177) shows that this value of ϵ is about 2/3 of the corresponding value of the smoothing parameter α of the Breit-Wigner smoothing.

In figure 22 the Gaussian smoothed level density is shown for $\epsilon = 0.1$. The full line is the result of the periodic-orbit theory and the dashed curve is obtained from the quantum mechanical energy spectrum. The results are similar to the results of figure 20. Most of the remarks that have been made in connection with the Breit-Wigner smoothing can also be made here. But in details there are some differences. Between two peaks that are separated by a momentum difference, which is larger than the momentum resolution Δp, the Gaussian smoothed level density falls off to a smaller minimum value than the Breit-Wigner smoothed level density. This means that the Gaussian peaks are more distinct than the Breit-Wigner peaks. In addition the background from close neighbouring peaks is in case of the Gaussian smoothing smaller than in case of the Breit-Wigner smoothing because of the stronger falling off of a Gaussian peak. A further difference is that the agreement between the height of the dashed peaks and the full peaks is in the Gaussian case in general better than in case of the Breit-Wigner smoothing, because the contributions of long orbits, that are neglected in the sum over periodic orbits, are more suppressed. For these reasons the Gaussian smoothing is preferable over the Breit-Wigner smoothing.

In figures 23 a) and c) the results of an evaluation of the trace formula are shown for the energy range $0 < E < 1500$. Figures 23 b) and d) show a section of a) and c), respectively, and compare it to the corresponding curves, which are obtained from the energy spectrum. The

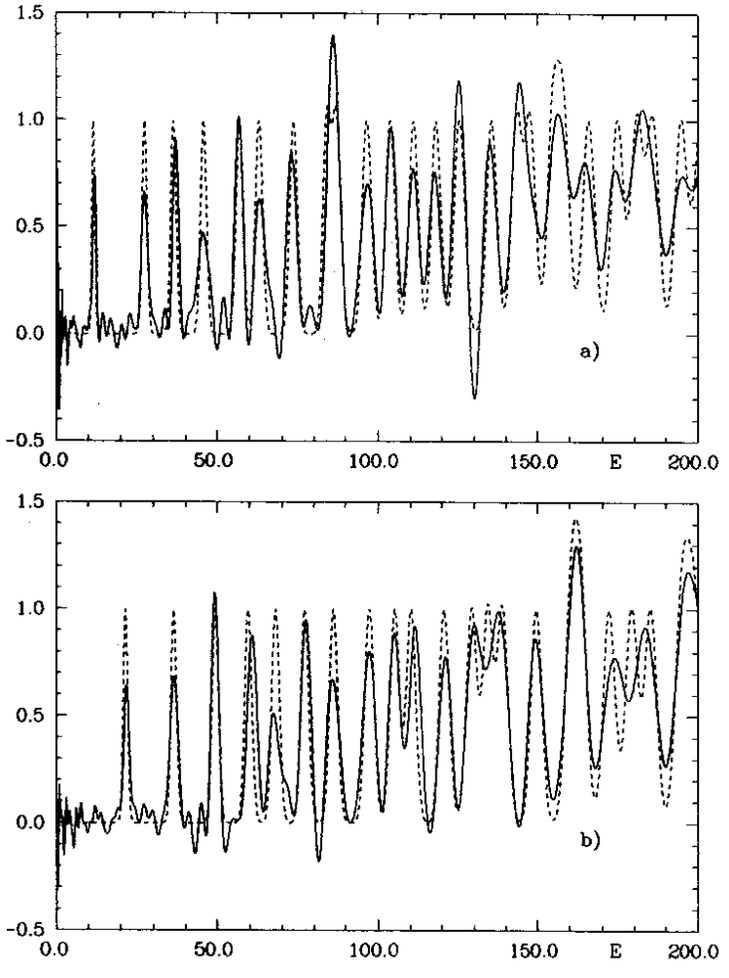

Figure 22: The Gaussian smoothed level density calculated from the periodic-orbit theory (full line) and the quantum mechanical energy spectrum (dashed line) for the energy eigenvalues of a) even and b) odd wavefunctions. The smoothing parameter is equal to $\epsilon = 0.1$.

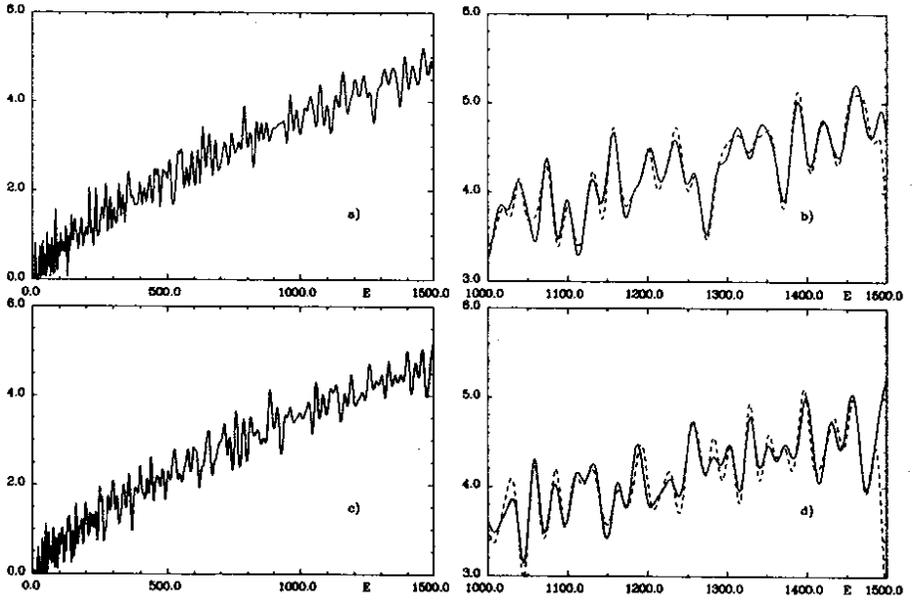

Figure 23: The periodic-orbit approximation for the Gaussian smoothed level density with $\epsilon = 0.15$ for the eigenvalues of a) even and c) odd wavefunctions. b) and d) show a section of a) and c), respectively, in comparison with corresponding curves, that are obtained from the quantum mechanical energy spectrum (dashed line).

smoothing parameter is $\epsilon = 0.15$. Again there is a good agreement between the corresponding curves. In comparison with figures 21 b) and d) the peaks are more marked and the fall off of the dashed curves close to $E = 1500$ occurs later, which is expected because of the stronger falling off of a Gaussian peak.

V.5 The Sine^3-Smoothed Energy Density

It is possible to choose the smoothing function $h(p')$ in such a way that its Fourier cosine transform is zero above a certain value of its argument. As a consequence the periodic-orbit sum is a sum over a finite number of orbits and can be done exactly. This gives the opportunity to examine the accuracy of the periodic-orbit theory as approximative theory. One smoothing function, which has this property, is given by

$$h(p') = \frac{\sin^3[\frac{L}{3}(p-p')]}{[\frac{L}{3}(p-p')]^3} + \frac{\sin^3[\frac{L}{3}(p+p')]}{[\frac{L}{3}(p+p')]^3} \quad , \tag{182}$$

with the Fourier cosine transform

$$g(x) = \frac{27}{8L^3}\cos(px)\begin{cases} 2(L^2/3 - x^2) & , \quad x \le L/3 \\ (L-x)^2 & , \quad L/3 \le x \le L \\ 0 & , \quad L \le x \end{cases} . \tag{183}$$

Figures 24 a) and b) show a plot of the sine^3-smoothed level density for the eigenvalues of even and odd wavefunctions, respectively. The cut-off length is chosen to be $L = 20$, since all orbits with length below $L = 20$ are known. In this figure the effect of the semiclassical approximation can be seen directly. The main features of the dashed curves, which are obtained from the energy spectrum, are reproduced by the full curves, which are the result of the periodic-orbit theory. But in details there are deviations. The main difference between the full curves and the dashed curves is the height of the peaks. Most of the peaks of the full curves are smaller than the corresponding peaks of the dashed curves, some are higher. The positions of the maxima of the peaks are only slightly shifted. This means that the approximations for the quantum mechanical energies do not differ much from the actual energies. The positions of the maxima of the peaks are given in tables 8 and 10. These values agree with the approximations for the energies only in case of isolated peaks. If neighbouring peaks are close together, the superposition of the peaks also shifts their maxima. For that reason only the first few energies can be read off. The accuracy is on an average 3 % of the mean level separation.

The energy resolution in figure 24 is distinctly smaller than in previous figures. This is the disadvantage of the exact evaluation of the periodic orbit- sum. Again a relation between the resolvable momentum difference Δp and the smoothing parameter L is obtained by requiring that between two peaks, which are separated by Δp, the level density falls off to half of the value that it has at the peaks. This yields the following condition ($p \gg \Delta p$)

$$1 + \frac{\sin^3(L\Delta p/3)}{(L\Delta p/3)^3} = 4\frac{\sin^3(L\Delta p/6)}{(L\Delta p/6)^3} , \tag{184}$$

which results in

$$\Delta p \approx 9.522/L . \tag{185}$$

For $L = 20$ this gives $\Delta p \approx 0.476$, which is about twice the value, that was obtained in previous cases.

V.6 The Trace of the Cosine-Modulated Heatkernel

Up to this point it was only considered how the classical periodic orbits determine the quantum mechanical energy spectrum. However, one can also ask the opposite question, what information about the classical orbits is contained in the energy eigenvalues of the Schrödinger equation. This point is examined by choosing an appropriate smoothing function $h(p')$, whose Fourier cosine transform has peaks at the lengths of the periodic orbits:

$$h(p') = \cos(p'L)\exp(-p'^2 t) , \tag{186}$$

$$g(x) = \frac{1}{4\sqrt{\pi t}}[\exp\{-\frac{(x-L)^2}{4t}\} + \exp\{-\frac{(x+L)^2}{4t}\}] . \tag{187}$$

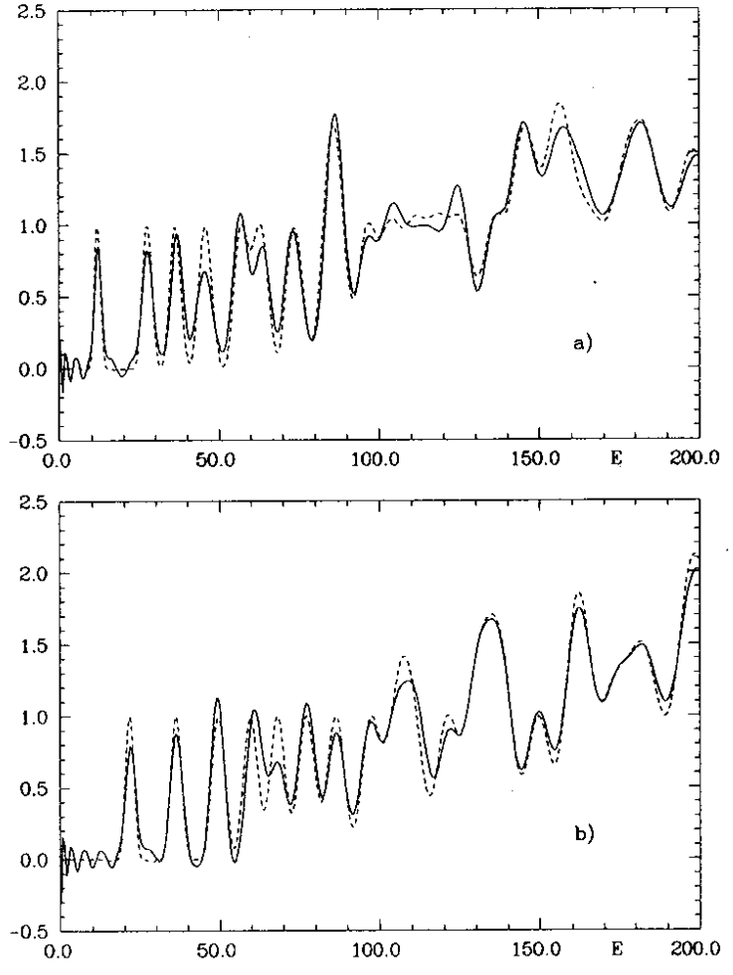

Figure 24: The sine^3-smoothed level density calculated from the periodic-orbit theory (full line) and the quantum mechanical energy spectrum (dashed line) for the energy eigenvalues of a) even and b) odd wavefunctions. The cut-off length is equal to $L = 20$.

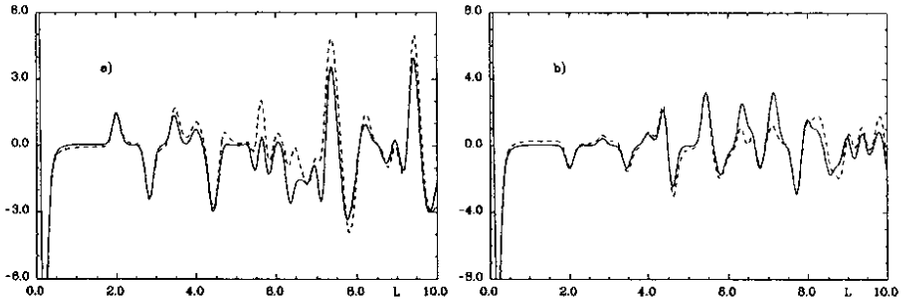

Figure 25: The trace of the cosine-modulated heat kernel with $t = 0.005$ calculated from the periodic-orbit sum (full line) and the quantum mechanical energy spectrum (dashed line) in case of a) even and b) odd symmetry.

The function $\sum_n h(p_n)$ is called the trace of the cosine-modulated heat kernel, since for $L = 0$ the trace of the heat kernel is obtained. The peaks at the lengths are positive or negative depending on the sign factor χ_γ^k in eq. (163). In figure 25 the cosine-modulated heat kernel is plotted with $t = 0.005$ for both symmetries. Only the first few peaks correspond to single lengths. The mean distance between neighbouring lengths is decreasing rapidly with increasing length, and for that reason the peaks above $L \approx 4.5$ in figure 25 are the superposition of several peaks at different lengths. The lengths of the ten shortest primitive periodic orbits are given in table 7. The second shortest orbit is the orbit along the line $y = x$ and in this case in table 7 the sign of its contribution to the periodic-orbit sum is given. There are also peaks at multiple repetitions of primitive orbits. For example the peak of a two times repetition of the shortest orbit can be seen in figures 25 a) and b) at $L = 4$.

	1	2	3	4	5	6	7	8	9	10
l_γ	2.000	2.828	3.464	4.395	4.559	4.596	5.414	5.474	5.547	5.796
a)	+1	+1	+1	−1	−1	+1	+1	−1	+1	−1
b)	−1	−1	−1	+1	−1	−1	+1	+1	−1	−1

Table 7: The lengths l_γ of the first ten periodic orbits of the desymmetrized hyperbola billiard and the sign factors χ_γ for a) even and b) odd symmetry.

V.7 The Dynamical Zeta Function

This section contains an evaluation of the representation of the dynamical zeta function by a sum over pseudo-orbits, which was derived in section II.4. Here we redefine the zeta function in terms of a new variable $s := -ip = -i\sqrt{E}$ by the equation $Z_{new}(s) = Z_{old}(E)$, because for billiard systems the sum over pseudo-orbits takes the form of a general Dirichlet series, if it

is expressed in terms of s. From equations (67) and (68) one then obtains

$$Z(s) = 1 + \sum_{n=1}^{\infty} A_n \exp(-sL_n) \ , \tag{188}$$

where the sum extends over all pseudo-orbits of the system. The lengths L_n of the pseudo-orbits are obtained by all possible linear combinations of the lengths of all primitive periodic orbits

$$L_n = \sum_{i=1}^{k} m_i l_{\gamma_i} \ , \tag{189}$$

where $k \geq 1$, m_i, $i = 1, \ldots, k$ are positive integers, and all γ_i are different. Again $Z^+(s)$ denotes the zeta function of the desymmetrized system with Neumann boundary conditions along the line $y = x$, and $Z^-(s)$ the zeta function of the system with Dirichlet boundary conditions along $y = x$. From equations (69), (65) and (66) one obtains

$$A_n = \prod_{i=1}^{k} \frac{(-1)^{m_i}(-1)^{m_i \bar{n}_{\gamma_i}}(-1)^{n_{\gamma_i} m_i (m_i-1)/2} \exp\{-u_{\gamma_i} m_i (m_i-1)/4\}}{\prod_{j=1}^{m_i} |(\exp(u_{\gamma_i} j/2) - (-1)^{n_{\gamma_i} j} \exp(-u_{\gamma_i} j/2)| c_{\gamma_i,j}^{-1}} \ , \tag{190}$$

where one has for $Z^+(s)$

$$c_{\gamma,j} = \begin{cases} -\exp(u_\gamma)[1 + (-1)^j \exp(j u_\gamma)]^{-1} & \text{for the orbit with code word } a = (\mathrm{b}) \\ 1 & \text{otherwise} \ , \end{cases} \tag{191}$$

and for $Z^-(s)$

$$c_{\gamma,j} = \begin{cases} [1 + (-1)^j \exp(j u_\gamma)]^{-1} & \text{for the orbit with code word } a = (\mathrm{b}) \\ 1 & \text{otherwise} \ . \end{cases} \tag{192}$$

In eq. (188) it is assumed that all pseudo-orbits are ordered in ascending order of their lengths: $L_n \leq L_{n+1}$, for $n \geq 1$. $s = \sigma + it$ is the complex variable of the Dirichlet series. The zeros s_n of $Z(s)$ on the negative imaginary axis or possibly close to this axis give approximations to the quantum mechanical energies: $s_n \approx -i\sqrt{E_n}$. A prerequisite for the determination of these zeros by an evaluation of eq. (188) is the convergence Dirichlet series in the considered region.

The open domain of absolute convergence of the series is some half-plane $\sigma > \sigma_a$, where σ_a is said to be the abscissa of absolute convergence of the Dirichlet series. The half-plane of convergence is given by $\sigma > \sigma_c$, where σ_c is the abscissa of convergence; $\sigma_c \leq \sigma_a$.

If $\sigma_a > 0$ it is determined by

$$\sigma_a = \overline{\lim_{n\to\infty}} \frac{1}{L_n} \log \sum_{\nu=1}^{n} |A_\nu| \ , \tag{193}$$

and if $\sigma_c > 0$ it is determined by

$$\sigma_c = \overline{\lim_{n\to\infty}} \frac{1}{L_n} \log \left| \sum_{\nu=1}^{n} A_\nu \right| \ . \tag{194}$$

These two equations are used for a numerical examination of the convergence properties of the Dirichlet series in eq. (188). All pseudo-orbits with length below $L = 20$ can be determined

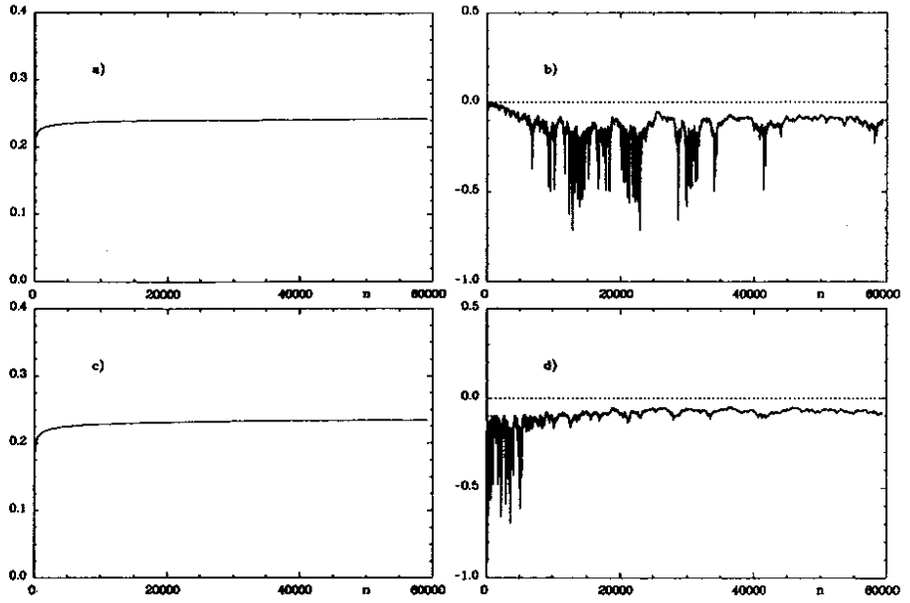

Figure 26: An evaluation of the sequences in equations (193) and (194), whose limit is the abscissa of a) absolute and b) conditional convergence of the Dirichlet series for the zeta function $Z^+(s)$. c) and d) show the corresponding evaluations for $Z^-(s)$.

completely, since all periodic orbits with length $l_\gamma \leq 20$ are known. The combinations of the 13 098 periodic orbits with length below $l = 20$ give 59 370 pseudo-orbits with length below $L = 20$. Out of these pseudo-orbits 40 726 have different lengths.

Figure 26 shows an examination of the domains of absolute and conditional convergence of the Dirichlet series, which approximate the zeta functions $Z^+(s)$ and $Z^-(s)$, respectively. For both zeta functions figure 26 shows an evaluation of the two sequences, whose limiting value is considered in equations (193) and (194), in the range $1 \leq n \leq 59\,370$. In figures 26 a) and c) the absolute convergence is examined. The difference between both curves has its origin in the different contributions of the orbit along the straight line $y = x$ to the periodic-orbit sums, because all other orbits give identical contributions to the considered sequences in figures 26 a) and c). In case of the zeta function $Z^+(s)$, figure 26 a), the sequence approximates the value 0.242. Theoretically a value of 0.2415 is obtained from eq. (77), if the value of the topological entropy $\tau = 0.593$ is inserted, and if $\bar{\lambda}$ is set equal to the mean Lyapunov exponent 0.703. In figure 26 c) the limiting value is slightly smaller. It is equal to 0.234. The reason for this is that the contribution to $Z^-(s)$ of the orbit along $y = x$ is very small. This has a relatively large effect, since this orbit contributes to 11 007 pseudo-orbits. In figure 26 b) and d) the conditional convergence is examined. Both curves clearly are below zero. This suggests that the Dirichlet series for the two zeta functions possibly are convergent on the imaginary s-axis.

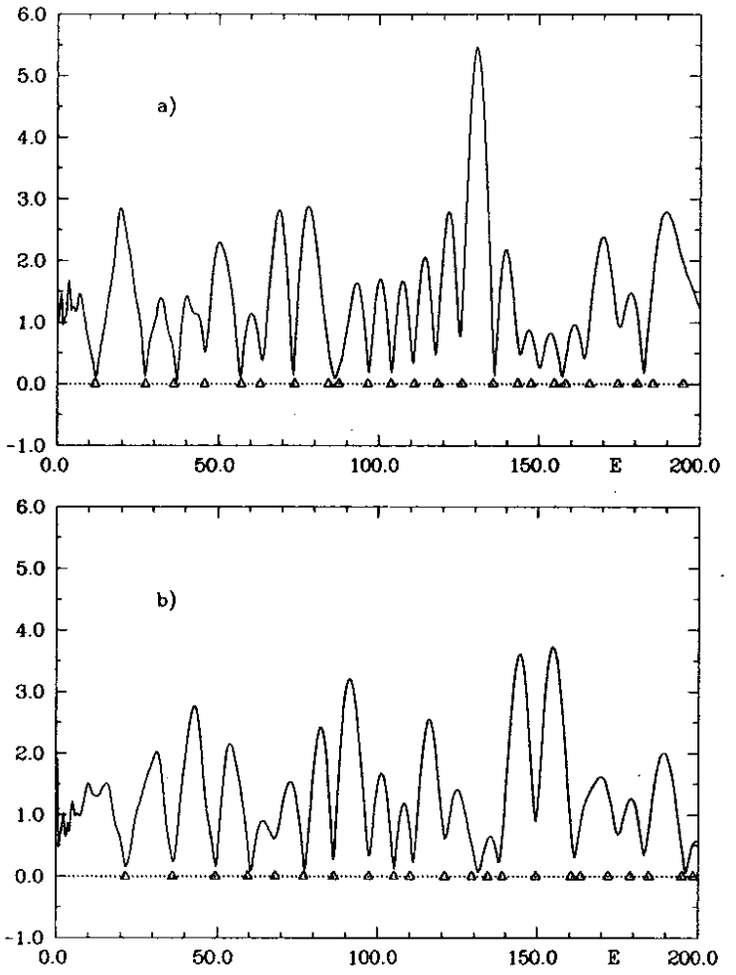

Figure 27: The absolute values of the zeta functions a) $Z^+(s)$ and b) $Z^-(s)$, $s = -i\sqrt{E}$. The triangles mark the positions of the energies.

In this case the zeros of $Z(s)$ can be computed from a convergent series.

Evaluation of the Dirichlet series are shown in figure 27. The sums are taken over all pseudo-orbits with length below $L = 20$. The figure shows a plot of the absolute values of $Z^+(s)$ and $Z^-(s)$, respectively, as functions of $E = -s^2$. The approximations to the zeta functions have no zeros on the imaginary s-axis in the range considered. But they have minima at positions, which are close approximations to the energy eigenvalues. For this reason the representation of the zeta functions by a sum over pseudo-orbits may be used as well as the previous periodic-orbit sums. The values of the energies, that are obtained, are listed in tables 8 and 10. The minimal momentum difference Δp, which can be resolved in figure 27, is estimated in the same way as it is for the unsmoothed level density, since the momentum dependence of a single term in the pseudo-orbit sum shows an analogous oscillatory behaviour. One obtains $\Delta p = 2\pi/20 \approx 0.314$.

V.8 The Riemann-Siegel Analogue

An approximation to the dynamical zeta function by a sum over a finite number of pseudo-orbits, whose number depends on the considered energy, was suggested by Berry and Keating [55]. This formula was proposed in analogy with the Riemann-Siegel formula for the Riemann zeta function $\zeta(z)$:

$$\zeta(z) = \sum_{n=1}^{\infty} \frac{1}{n^z} = \sum_{n=1}^{\infty} \exp(-z \log n) \ . \tag{195}$$

This representation of $\zeta(z)$ by a Dirichlet series is convergent for $\mathrm{Re}\, z > 1$, and in the remaining complex z-plane $\zeta(z)$ is defined by analytic continuation. According to the Riemann hypothesis all the complex zeros of $\zeta(z)$ lie on the critical line $\mathrm{Re}\, z = 1/2$, where the Dirichlet series is divergent. The most effective computation of the zeros of $\zeta(z)$ is done by using the Riemann-Siegel formula, which is an asymptotic representation of $\zeta(z)$, that is valid on the critical line $\mathrm{Re}\, z = 1/2$. The dominant part of this formula is given by

$$\zeta(1/2 + iE) = 2\exp\{-i\pi\bar{N}(E)\} \sum_{n=1}^{\mathrm{Int}[\sqrt{E/(2\pi)}]} \frac{\cos(\pi\bar{N}(E) - E\log n)}{n^{1/2}} \ . \tag{196}$$

Here the value of z on the critical line is denoted by $z = 1/2 + iE$. $\bar{N}(E)$ is the mean approximation to the staircase function $N(E)$, which is defined as the number of zeros z_n of the Riemann zeta function with imaginary part $0 < \mathrm{Im}\, z_n \leq E$. This notation is chosen because of an analogy between the zeros of $\zeta(z)$ and the quantum mechanical energy eigenvalues of a classically chaotic system, which is discussed in [50,15]. $\bar{N}(E)$ is known analytically

$$\bar{N}(E) = \frac{E}{2\pi}(\log\frac{E}{2\pi} - 1) + \frac{7}{8} \ , \tag{197}$$

and the truncation condition for the series in eq. (196) is obtained by requiring, that the argument of the cosine is stationary with respect to the variable E.

Guided by the analogy between the Riemann zeta function and the dynamical zeta function $Z(s)$ of eq. (188), Berry and Keating conjectured a corresponding approximation for $Z(s)$ on the line $\mathrm{Re}\, s = 0$:

$$Z(-ip) \approx 2\exp\{i\pi\bar{N}(E)\} \sum_{n=1}^{n_{max}} A_n \cos(\pi\bar{N}(E) - pL_n) \ , \tag{198}$$

where $E = p^2$, and $\bar{N}(E)$ is the mean approximation to the spectral staircase $N(E)$. The value n_{max} is determined by the condition $L_{n_{max}} \leq L_{max} < L_{n_{max}+1}$, and

$$L_{max} = 2\pi p \frac{\mathrm{d}}{\mathrm{d}E}\bar{N}(E) = 2\pi p\bar{d}(E) \ , \tag{199}$$

where $\bar{d}(E)$ is the mean level density.

Formula eq. (198) has several advantages in comparison with previous applications of the periodic-orbit theory. The sum extends over a finite number of pseudo-orbits only, and the approximation for the combination $Z(-ip)\exp\{-i\pi\bar{N}(E)\}$ is real, so that the zeros of the right hand side of eq. (198) can be found by evaluating real functions only. The main disadvantage of formula (198) is the fact, that its derivation rests on analogy arguments and for that reason a numerical test of eq. (198) is of special importance.

The energy range over which the formula can be applied depends on the maximum length L_{max} in eq. (199) up to which all pseudo-orbits are known. With $L_{max} = 20$ and the generalized Weyl's law eq. (144), one obtains a maximal energy $E_{max} = 330.16$ for the approximation to $Z^+(s)$ and a value $E_{max} = 346.67$ for the approximation to $Z^-(s)$. In figures 28 and 29 an evaluation of the Riemann-Siegel lookalike formula of Berry and Keating is shown for the energy eigenvalues of even and odd wave functions up to the respective maximal energies. The actual energies are marked by triangles. The result of this evaluation is, that the formula gives quite good approximations to the energy eigenvalues. The approximations to the energies, which are determined from figures 28 and 29, are listed in tables 8-11 together with the actual energy values. In the case of the energy eigenvalues of even wavefunctions the mean absolute value of the deviation of the approximate energy values from the actual energy values is $\overline{\Delta E} = 0.46$. In comparison with the mean level spacing $1/\bar{d}(E)$ the deviation is on an average 6.5 %. The quotient of the deviation and the mean level spacing is varying much, but if it is averaged over several neighbouring energies, it is approximately constant. In case of the energy eigenvalues of odd wavefunctions the mean absolute value of the deviation of the approximate energies from the actual energies is $\overline{\Delta E} = 0.55$. The deviation is on an average 7.8 % of the mean level spacing. The quotient of the deviation and the mean level spacing also varies much, but its local average is slightly increasing with increasing energy, although this effect is not very significant.

The formula has some shortcomings. The approximation to $Z(-ip)$ is discontinuous. The maximum length L_{max} of pseudo-orbits which are included in the sum depends on the energy. If the energy is increased, then every time that L_{max} becomes equal to the length of a pseudo-orbit, the finite contribution of this pseudo-orbit is included in the sum, and this results in a discontinuity of the approximation of $Z(-ip)$. This leads especially to difficulties, if by such a discontinuity the functional value $Z(-ip) = 0$ is crossed. In the environment of some zeros of the curves in figures 28 and 29 the functions jump back and forth several times between positive and negative values, so that several zeros are close together. In those cases the values in tables 8-11 were determined by the average behaviour of the functions. More seriously, at some places where energy eigenvalues are, the curves miss to cross the zero-axis and thus give no approximations for these energies. This happens at the energies $E_{30}^+ = 234.24$ and $E_{31}^+ = 236.20$ of even wave functions, and at the energies $E_{37}^- = 296.38$ and $E_{38}^- = 298.05$ of odd wave functions. Although the curves have a maximum and a minimum, respectively, close to these energy values, these extrema do not extend beyond the zero-axis. A possibility to overcome this difficulty is to take the value of the position of the extremum

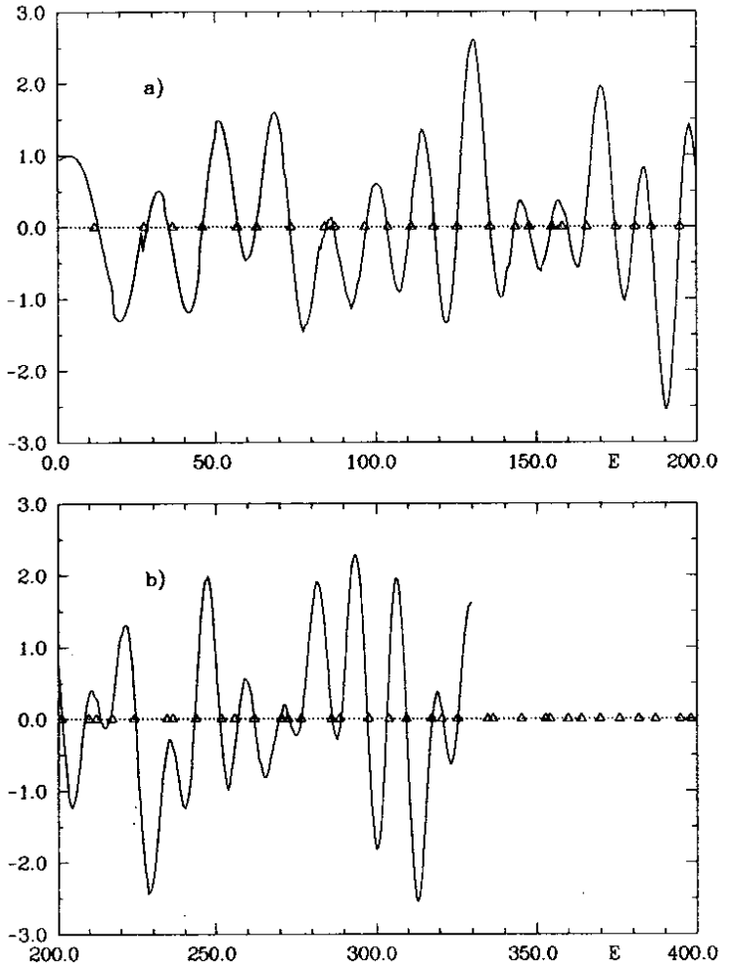

Figure 28: The evaluation of the Riemann-Siegel lookalike formula of Berry and Keating for the function $Z^{+}(s)\exp\{-i\pi\bar{N}^{+}(E)\}/2$, $s=-i\sqrt{E}$.

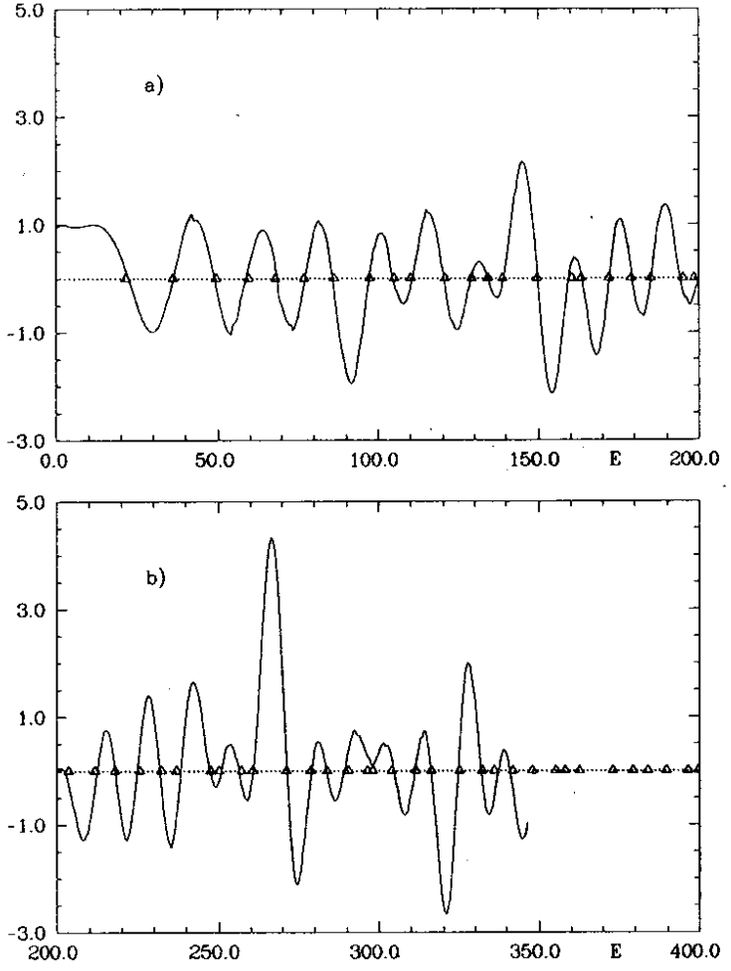

Figure 29: The evaluation of the Riemann-Siegel lookalike formula of Berry and Keating for the function $Z^{-}(s)\exp\{-i\pi\bar{N}^{-}(E)\}/2$, $s=-i\sqrt{E}$.

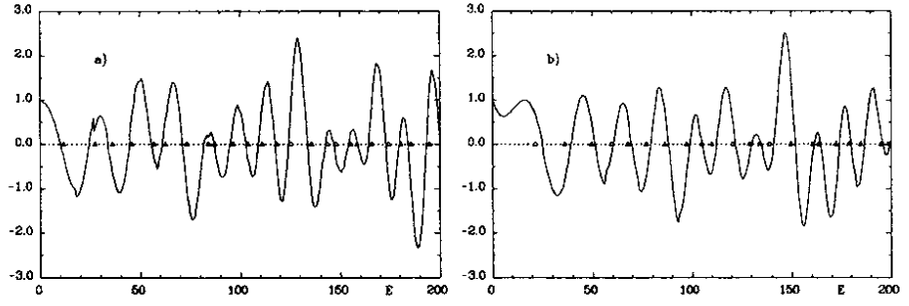

Figure 30: The same as in figures 28 and 29 for a) even and b) odd symmetry, evaluated with asymptotic laws for the mean staircase functions $\bar{N}^+(E)$ and $\bar{N}^-(E)$, which do not contain a constant term.

as approximation for the respective two energy values, but in more complicated cases this method might not be applicable in a unique way.

For the evaluation of formula(198) it is of utmost importance to use a very accurate formula for the mean spectral staircase $\bar{N}(E)$. For the computation of figures 28 and 29 also the constant corrections to $\bar{N}^+(E)$ and $\bar{N}^-(E)$, which were determined numerically from figure 12, were included in the formula for mean spectral staircases. If those constant corrections are neglected, the approximate energies show a clear shift. For a demonstration of this effect the results of the evaluation of eq. (198) with a generalized Weyl's law for $\bar{N}^+(E)$ and $\bar{N}^-(E)$, respectively, without a constant term is shown in figure 30. Here the agreement between approximate energies and actual energies is clearly not as good as in figures 28 and 29. In case of the energies of even wave functions the energy values are shifted on an average by $\Delta E = 1.32$ in direction to lower energies in comparison with the results of figure 28. The maximal shift is $\Delta E = 3.94$. In the case of the energies of odd wave functions the shift is on an average $\Delta E = 1.47$ in direction to higher energies, and the maximal shift is $\Delta E = 2.88$.

One of the main advantages of the formula(198) is the fact that a distinctly larger number of energies can be determined in comparison with previous methods. In case of the unsmoothed level density the resolution of two energies, which are separated by the mean level distance $1/\bar{d}(E)$ at energy E, requires the summation over all orbits with length up to

$$l \approx \frac{2\pi}{\Delta p} \approx \frac{4\pi p}{\Delta E} = 4\pi p \bar{d}(E) \ . \qquad (200)$$

This is exactly twice the value, which is given in eq. (199). Because of the exponential proliferation of the number of periodic orbits this means that the determination of a comparable number of energies requires in case of the Riemann-Siegel lookalike formula roughly the square root of the number of orbits, which are needed for the application of the trace formula for the unsmoothed level density. In this argument it is assumed that the distances between neighbouring energy levels do not deviate much from the mean level distance. On the other hand the good numerical results for the application of formula(198) may also partially be due to the fact, that the spectrum of the desymmetrized hyperbola billiard is very rigid, and that

there are only few pairs of adjacent energy values, which are close together. The problem that at some eigenvalues the curves miss to cross the zero-axis may occur more often in case that short level spacings occur more frequently. Besides this fact formula(198) shares with the original trace formula the problem that in order to achieve the resolution of the mean momentum difference $\overline{\Delta p}/2$ one needs the square of the number of orbits, which are required for the resolution of $\overline{\Delta p}$.

a)	b)	c)	d)	e)	f)	g)	h)
11.74	12.06	11.97	12.08	12.09	11.98	12.05	13.02
27.33	27.16	27.22	27.24	27.24	27.39	27.27	28.26
36.28	36.91	37.12	36.95	36.96	36.91	37.17	34.96
45.79	45.50	46.27	45.54	45.55	45.55	45.97	45.85
56.93	56.68	56.70	56.72	56.72	56.73	56.64	57.29
62.90	62.93	62.94	63.02	63.01	63.49	63.53	62.66
73.62	73.08	73.17	73.01	72.97	73.10	73.09	73.40
84.21	86.23	85.97	86.28	86.27	86.28	86.05	84.71
87.34							86.97
96.55	97.18	96.73	96.91	96.79	96.96	96.81	97.07
103.83	104.05	104.03	104.09	104.07	104.63	103.93	103.42
111.10	110.94	111.08	110.95	110.96	113.97	110.61	110.67
118.29	117.81	118.06	117.82	117.80		117.63	118.54
125.63	125.59	125.68	125.49	125.51	124.42	125.02	125.67
135.55	134.60	134.50	134.97	134.93		135.97	135.54
143.36	143.97	144.39	144.24	144.25	145.22	144.17	142.94
147.66	149.03					150.24	147.50
154.84	155.78	156.11	156.54	156.52	157.48	157.14	154.67
158.17							160.02
165.76	164.45	164.50	164.34	164.51		164.07	165.24
174.64	173.54	174.23	173.97	173.99		175.17	174.48
180.73	182.43	183.19	182.44	182.50	181.86	182.87	180.52
185.77							185.73
194.85	194.44	193.93	195.30	195.28	199.73		194.85

Table 8: The energy eigenvalues of even wavefunctions in comparison with values that are obtained from various applications of periodic-orbit sums. The different rows contain: a) the energy eigenvalues; the positions of the maxima of b) the unsmoothed energy density, c) the unsmoothed energy density using orbits with lengths below $l = 20$ only, d) the Breit-Wigner smoothed energy density with $\alpha = 0.15$, e) the Gaussian smoothed energy density with $\epsilon = 0.1$, f) the sine^3-smoothed energy density with $L = 20$; g) the positions of the minima of the zeta function; h) the positions of the zeros of the Riemann-Siegel analogue.

a)	h)	a)	h)	a)	h)	a)	h)
200.98	201.22	236.20	—	272.40	272.84	309.37	309.41
209.82	208.45	243.51	243.07	276.50	276.74	317.45	317.67
212.22	213.42	251.90	251.37	286.15	286.44	320.78	321.15
217.22	216.83	256.03	257.03	288.73	289.16	325.64	325.72
224.12	224.56	262.00	261.95	297.49	297.13		
234.24	—	270.44	269.70	303.97	303.12		

Table 9: The same as in table 8 for energies above $E = 200$ for the rows a) and h) only.

a)	b)	c)	d)	e)	f)	g)	h)
21.46	21.72	21.82	21.74	21.74	21.75	21.54	22.33
36.28	36.30	36.33	36.38	36.40	36.29	36.54	36.41
49.43	49.26	49.48	49.31	49.32	49.23	49.55	48.87
59.50	60.76	60.47	60.75	60.71	60.75	60.57	58.71
67.94	67.22	67.05	67.30	67.31	67.83	67.67	68.75
77.04	77.51	77.67	77.47	77.47	77.18	77.36	77.38
86.24	85.71	85.39	85.96	85.93	86.33	86.16	85.72
97.27	97.40	97.15	97.32	97.25	97.27	97.40	97.10
105.12	104.98	104.78	105.05	105.00	108.90	105.20	104.76
110.21	111.50	111.94	111.45	111.51		111.24	110.86
120.81	121.42	120.74	121.33	121.24	121.86	120.99	120.43
129.20	129.36	130.06	130.13	130.03	134.66	131.37	129.03
134.24	138.02	138.14	137.51	137.65		137.77	134.46
138.86							139.23
149.54	149.15	149.23	149.30	149.29	149.68	149.49	149.71
160.39	162.24	161.88	162.13	162.06	162.11	161.45	159.33
163.34							163.59
172.02	173.96	173.17	174.00	173.76	181.88	175.22	172.16
179.04	183.13	183.59	183.16	183.25		183.57	179.31
185.01							185.08
194.91	196.74	196.48	197.29	197.11	199.19	196.14	194.00
198.47							200.14

Table 10: The energy eigenvalues of odd wavefunctions in comparison with values that are obtained from various applications of periodic-orbit sums. The different rows contain: a) the energy eigenvalues; the positions of the maxima of b) the unsmoothed energy density, c) the unsmoothed energy density using orbits with lengths below $l = 20$ only, d) the Breit-Wigner smoothed energy density with $\alpha = 0.15$, e) the Gaussian smoothed energy density with $\epsilon = 0.1$, f) the sine^3-smoothed energy density with $L = 20$; g) the positions of the minima of the zeta function; h) the positions of the zeros of the Riemann-Siegel analogue.

a)	h)	a)	h)	a)	h)	a)	h)
203.72	202.34	247.42	247.18	283.85	283.69	316.33	316.23
211.62	212.42	250.03	250.86	290.43	289.23	325.16	324.67
217.87	217.94	257.12	256.31	296.38	—	332.28	331.91
225.55	224.82	260.54	260.59	298.05	—	336.03	337.26
232.43	231.81	271.25	271.46	304.13	304.93	341.91	340.96
237.04	238.42	278.91	279.08	311.47	311.37		

Table 11: The same as in table 10 for energies above $E = 200$ for the rows a) and h) only.

VI Summary

The content of this paper can be divided into two parts. One part contains a detailed numerical examination of classical and quantum mechanical properties of a strongly chaotic system. This system is the so-called hyperbola billiard, a system which has several specific properties, which facilitate such a numerical investigation in comparison with other chaotic systems. There is a very efficient code that allows the classification of all periodic orbits by combinations of three different letters. In addition an extremum principle can be formulated for the periodic orbits, which makes a very fast and very accurate determination of the periodic orbits possible. This method avoids the problem of the exponential divergence of neighbouring trajectories, which is a specific property of chaotic systems. On the quantum mechanical side the first 578 energy levels of the hyperbola billiard were determined by a boundary element method, which for this system turned out to be much more efficient than other methods.

The examination of the classical and quantum mechanics of the hyperbola billiard can be considered as an independent investigation of certain properties of a chaotic system. However, the quantities which have been examined were partly selected in view of an investigation of the periodic-orbit theory of Gutzwiller. A detailed examination of the properties of this theory on the example of a strongly chaotic system is the second main part of this paper. The periodic-orbit theory supplies semiclassical approximations to quantum mechanical energies of classically chaotic systems by a sum over classical periodic orbits. For that reason it can be considered as a substitute for the EBK quantization rules, which can be applied to integrable systems only. The structure of the trace formula of the periodic-orbit theory is, however, much more complicated than the structure of the EBK quantization conditions. Due to this fact only very little is known about general analytical properties of the trace formula, although there have been many publications concerning the periodic-orbit theory in recent years. For a deeper understanding and an effective application of the periodic-orbit theory questions like the following remain to be answered:

— What are the properties and what is the quality of the semiclassical approximations for the quantum mechanical energies?

— What are the convergence properties of the periodic-orbit sums?

— How can the information about the energies be extracted most efficiently from the periodic orbits?

The intention of this work is to examine these questions numerically on the example of one special system, which allows relatively extensive investigations with the use of a reasonable amount of computer time. In detail the content of this work is the following:

After an introduction in chapter I, parts of the derivation of the periodic-orbit theory are discussed in chapter II. Special emphasis is given to the treatment of systems with discrete geometrical symmetries. For these systems the effectiveness of the periodic-orbit theory is increased by applying it to desymmetrized subsystems of the original system. An alternative formulation of the periodic-orbit theory is given in terms of a dynamical zeta function. This zeta function is defined by an infinite product over all periodic orbits, or by a series over all combinations of periodic orbits, which are denoted by pseudo-orbits. The convergence properties of the Gutzwiller trace formula are discussed. In general the periodic-orbit sum is

not convergent for real values of the energy E and thus a direct evaluation of the trace formula on the real energy-axis is not possible. A solution to this problem consists in a smoothing of the original trace formula. It is shown on the example of strongly chaotic billiard systems how smoothed trace formulae can be obtained in a mathematically correct way. These trace formulae contain absolutely convergent series and integrals only and in principle allow the determination of all semiclassical energies.

Properties of the classical periodic orbits of the hyperbola billiard are discussed in chapter III. The code for the orbits of the full hyperbola billiard is introduced. This code not only provides a unique classification of the periodic orbits. Also certain informations about the geometrical form and about symmetries of an orbit are contained in a code word. Vice versa symmetries impose restrictions on the form, code words can have. The general form of code words with a certain symmetry is given and formulae for their numbers are derived. For the desymmetrized hyperbola billiard the code is modified in order to provide a suitable description of the properties of the orbits of the desymmetrized system. All the orbits of the desymmetrized system with code words that consist of at most 14 letters were determined. The distributions of lengths and Lyapunov exponents of all orbits with a fixed code length N were examined, and it was found that these distributions show a significant behaviour, if N is large enough.

The lengths of the periodic orbits with a fixed value of N are to a good approximation Gaussian distributed, and the mean value of this distribution increases proportional to the code length N. The standard deviation increases like $\sqrt{N}$. This very regular behaviour allows an analytical examination of the behaviour of the number $\mathcal{N}(l)$ of orbits with length $l_\gamma \leq l$. On the assumption that the regular dependence on N of the length distributions holds also for $N > 14$ the leading term of the asymptotic behaviour of $\mathrm{d}\mathcal{N}(l)/\mathrm{d}l$ for large values of l is derived. The result is in full agreement with the expected asymptotic form for chaotic systems $\mathrm{d}\mathcal{N}(l)/\mathrm{d}l \sim \exp(\tau l)/l$, $l \to \infty$. A value of $\tau = 0.58$ is obtained for the topological entropy. The special properties of the distributions of lengths can be given a further interpretation. The Gaussian form of the distributions and the N-dependence of their mean values and their standard deviations agrees with the expectation for a one-dimensional random walk process consisting of N steps, where each step is carried out in average with a constant mean-free path and a constant standard deviation. This result already points to a possible random distribution of the lengths of the periodic orbits.

The Lyapunov exponents also are well approximated by Gaussian distributions, if the code length N is large enough. In this case the mean value of the distributions is approximately independent of N and the standard deviation decreases proportional to $1/\sqrt{N}$.

An accurate analysis of the properties of the trace formula requires the knowledge of all periodic orbits, whose length is below a certain value l. A complete determination of these orbits is possible in case of the hyperbola billiard due to certain correlations between orbit lengths and properties of the code words. All orbits with lengths $l_\gamma \leq 20$ were determined, which were 13 098 orbits altogether. With the input of these orbits the topological entropy τ was determined numerically with the result $\tau = 0.593$.

Finally the statistical properties of the total distribution of lengths were examined. This was possible since a sufficient part of the lower length spectrum is known completely. The statistical properties of the length spectrum were studied by means of the nearest neighbour spacings distribution, the scaled deviations of the lengths from their mean values, the number variance and the rigidity. Almost all the results are in agreement with a Poisson distribution.

Only for very long-range correlations the number variance shows a significant deviation from the Poisson distribution. This indicates that the lengths are in some sense randomly distributed with the restriction that very long-range correlations depend on specific properties of the considered system. The analogy with corresponding properties of the energy spectrum suggests a possible generalization of this result to other chaotic systems.

Chapter IV contains an examination of the energy spectrum of the hyperbola billiard, which is divided into partial energy spectra of even and odd eigenfunctions of the Hamiltonian operator, respectively. The boundary element method by which the energy eigenvalues of the Schrödinger equation are determined is discussed. The mean behaviour of the energy spectrum is described by the mean spectral staircase $\bar{N}(E)$. The first three leading terms of the asymptotic expansion of $\bar{N}(E)$ are known analytically. The correction to this approximation is examined numerically for both partial spectra of the hyperbola billiard. It is found that the correction terms are to a very good approximation constant for both spectra. The difference between the constants for the two partial spectra can also be determined analytically, and this value is in good agreement with the numerically obtained value. One of the most common tools for the examination, if quantum systems have a classical chaotic limit, is the consideration of the energy statistics. Short-range correlations in the energy spectrum are examined by considering the nearest neighbour spacings distribution $P(S)$. The results for this statistics are in agreement with the expectations for chaotic systems that are invariant under time reversal, that is with the GOE-statistics. The long-range correlations are investigated by considering the number variance $\Sigma^2(L)$ and spectral rigidity $\Delta_3(L)$. Here the results do not agree in all points with the expectations for generic chaotic systems. According to the semiclassical theory of Berry it is expected that for small values of the parameter L systems show universal behaviour, which in case of the hyperbola billiard corresponds to GOE-statistics. With increasing parameter L there will be a deviation from the universal behaviour, and for $L \to \infty$ both statistics saturate at a final value. Although the two partial spectra of the hyperbola billiard follow this general behaviour, the deviations from the GOE-curve occur at much smaller values of L than would be expected from Berry's theory. This disagreement between theory and numerical result can be explained by the fact that prerequisites of the theory are not satisfied in case of the hyperbola billiard. This is due to the infinite volume of the constant energy surface in phase space.

In chapter V the properties of several versions of periodic-orbit approximations are investigated numerically and the results are compared with each other. First the unsmoothed trace formula for the level density is considered. It is not known, if the periodic-orbit sum is convergent for real values of the energy E. For that reason the evaluation of the periodic-orbit sum is a numerical test, to what extend sensible results can be obtained from the trace formula. The sum was evaluated with all periodic orbits with code length $N \leq 14$ or length $l, \leq 20$, which are 533 760 orbits altogether. As result, all peaks at energy eigenvalues, which were expected to be resolved within the theoretically estimated energy resolution, were obtained from the trace formula. The approximations to the energy values are good down to the lowest energy despite of the semiclassical nature of the approximation. No clear indication of a divergence of the periodic-orbit sum was obtained. Thus the application of the unsmoothed trace formula yields good results in case of the hyperbola billiard. Notwithstanding no definite statement about the convergence of the sum can be obtained from this result. It is possible that although the series is divergent, nevertheless useful results can be obtained from the trace formula, if not too many orbits are included in the sum. Further

investigations of partial contributions to the periodic-orbit sum indicate, that the region of convergence at least reaches up very close to the axis of real momentum $p = \sqrt{E}$.

Two possibilities of smoothing the trace formula were considered next, the Breit-Wigner smoothing and the Gaussian smoothing. It was demonstrated, that even in case that an application of the unsmoothed trace formula gives good results, it is of advantage to smooth the trace formula slightly in order to improve the results. This improvement consists in an enhancement of single peaks and a suppression of background oscillations. Relations between suitable smoothing parameters and the maximal lengths of orbits that are included in the sum are given. The results for the Gaussian smoothing are slightly better than the results for the Breit-Wigner smoothing. The fact that the difference between both results is not bigger is due to the fact that for the considered system the application of the trace formula in its unsmoothed version already gives good results. In general the Gaussian smoothing can be used universally, while the applicability of the Breit-Wigner smoothing depends on the convergence properties of the unsmoothed periodic-orbit sum. The smoothed trace formulae were also evaluated in the range of higher energies, where no resolution of single energies can be achieved with the available number of periodic orbits. In this energy range, too, all the main features of the smoothed spectrum were reproduced by its periodic-orbit approximation.

A smoothing, which has the property, that the corresponding periodic-orbit sum is finite, is the so-called sine^3-smoothing. This smoothing has the advantage that both, the classical and the quantum mechanical side of the trace formula, can be evaluated with high accuracy, and both sides can thus be compared directly. This gives the possibility to see the effect of the semiclassical approximation. The result of the numerical evaluation is, that the classical and the quantum mechanical curves show a good agreement in their main features. Differences exist mainly in the heights of the peaks. The positions of the peaks are only slightly shifted. The disadvantage of evaluating the quantum mechanical side of the trace formula exactly is that one has to accept a lower energy resolution than in case of the unsmoothed trace formula.

An "inverse" application of the periodic-orbit theory, by which peaks at the lengths of periodic orbits are produced by a sum over quantum mechanical energies, is obtained by considering the periodic-orbit approximation for the trace of the cosine-modulated heat kernel. It is shown, that lengths of the periodic orbits can be determined from the energy spectrum.

Next the representation for the dynamical zeta function $Z(E)$ was examined. In case of billiard systems, this zeta function is expressed by a general Dirichlet series over all pseudo-orbits of the system. A numerical examination of convergence criteria for general Dirichlet series points to a convergence of the series for real values of the energy E. The pseudo-orbit representation of $Z(E)$ was evaluated numerically for both desymmetrized systems with all pseudo-orbits, which have a length below $L = 20$, which were 59 370 pseudo-orbits altogether. The absolute values of the obtained functions do not have zeros for real values of the energy E, but they show pronounced minima at positions, which are close to the energy eigenvalues. The energy resolution is about the same as in case of an application of the unsmoothed level density. The zeta function formalism thus can be used alternatively to the usual trace formula.

Finally the Riemann-Siegel lookalike formula of Berry and Keating was examined. This formula was proposed in analogy to the Riemann-Siegel formula for the Riemann zeta function and it approximates the zeta function $Z(E)$ by a finite but energy-dependent number of pseudo-orbits. This formula has the advantage that it can be evaluated exactly, and with

the input of the same number of pseudo-orbits a multiple of the number of energies can be obtained as in case of an evaluation of the semiclassical approximation for the level density. The numerical results were good. Altogether 87 approximations to energy eigenvalues were obtained. The accuracy is on an average about 7 per cent of the mean level spacing. The formula, however, also has some disadvantages. The approximation to $Z(E)$ is discontinuous. Some zeros are not unique in the sense that within a small energy interval the function jumps forth and back between positive and negative values several times, and for some energy values it does not give an approximation, since the curve misses to cross the zero-axis.

Summarizing the results for the periodic-orbit theory, the trace formula gives quite accurate approximations to the energy eigenvalues of the Schrödinger equation of a classically chaotic system. Within the limits of the numerical examinations no deviations from theoretical expectations have been discovered. More precisely, within the theoretically estimated energy resolution all expected peaks at energy eigenvalues or groups of energy eigenvalues were obtained. These results support the statement, that for chaotic systems the periodic-orbit theory can be considered as substitute for the EBK quantization rules. The main disadvantage of the periodic-orbit theory, which sets strong limits to its practical applicability, is the fact, that in going to higher energies the numerical effort for the resolution of single energies increases exponentially. For that reason it is very desirable to have powerful resummation techniques. The formula of Berry and Keating yields first good results. It is however important, to have a deeper understanding of this formula on a theoretical basis, since its derivation rests on analogy arguments. Furthermore, although this formula clearly increases the efficiency of the original trace formula, it shares the same problem of an exponentially increasing numerical effort for the resolution of higher energies.

Acknowledgements

I would like to thank Prof. F. Steiner for the kind supervision of my Ph. D. Thesis, for many fruitful discussions and for a lot of good advice. Furthermore I would like to thank R. Aurich for many valuable suggestions on tackling numerical problems. I also like to thank the Deutsche Forschungsgemeinschaft DFG for financial support.

Appendices

A Contributions of Orbits along the Boundary to the Zeta Function

In this appendix the form of the quantities $b_{\gamma,n}$ in equations (60) and (61), and of the quantities $c_{\gamma,j}$ in equations (65) and (66), is derived for periodic orbits, which run along the line $y = x$ only. More precisely, the contributions of these orbits to the periodic-orbit sum of a desymmetrized system is derived, whose corresponding full system is invariant under reflection on the line $y = x$.

The case of Neumann boundary conditions along the line $y = x$ is considered first. The starting point is the contribution of an orbit along $y = x$ to the oscillatory part of the trace of the Green function $g(E)$, which is given by equations (54) and (55). The transformations of this term are carried out analogously to the transformations in section II.4 for an ordinary orbit.

$$\begin{aligned}
&\frac{1}{i\hbar}\sum_{k=1}^{\infty}\frac{T_\gamma \exp\{ikS_\gamma(E)/\hbar - i\pi k\nu_\gamma/2\}}{\exp(ku_\gamma/2) - \sigma_\gamma^k \exp(-ku_\gamma/2)}\cdot\frac{1}{1+\sigma_\gamma^k\exp(-ku_\gamma)}\\
&= \frac{1}{i\hbar}\sum_{k=1}^{\infty}\frac{T_\gamma \exp\{ikS_\gamma(E)/\hbar - i\pi k\nu_\gamma/2\}}{\exp(ku_\gamma/2) - \exp(-3ku_\gamma/2)}\\
&= \frac{1}{i\hbar}\sum_{k=1}^{\infty}\frac{T_\gamma \exp\{ikS_\gamma(E)/\hbar - i\pi k\nu_\gamma/2 - ku_\gamma/2\}}{1-\exp(-2ku_\gamma)}\\
&= \frac{1}{i\hbar}\sum_{k=1}^{\infty}\sum_{n=0}^{\infty} T_\gamma \exp\{\frac{i}{\hbar}kS_\gamma(E) - \frac{i\pi}{2}k\nu_\gamma - \frac{ku_\gamma}{2} - 2knu_\gamma\}\\
&= \frac{1}{i\hbar}\sum_{n=0}^{\infty} T_\gamma \frac{\exp\{iS_\gamma(E)/\hbar - i\pi\nu_\gamma/2 - u_\gamma/2 - 2nu_\gamma\}}{1-\exp\{iS_\gamma(E)/\hbar - i\pi\nu_\gamma/2 - u_\gamma/2 - 2nu_\gamma\}}\\
&= \sum_{n=0}^{\infty}\frac{\mathrm{d}}{\mathrm{d}E}\log[1-\exp\{\frac{i}{\hbar}S_\gamma(E) - \frac{i\pi}{2}\nu_\gamma - u_\gamma(\frac{1}{2}+2n)\}] \quad . \qquad (201)
\end{aligned}$$

This result is compared with equations (57) and (59). The form of $b_{\gamma,n}$ in eq. (60) then follows directly. Eq. (201) is transformed further with the use of Euler's identity eq. (62):

$$\begin{aligned}
&\prod_{n=0}^{\infty}[1-\exp\{\frac{i}{\hbar}S_\gamma(E) - \frac{i\pi}{2}\nu_\gamma - u_\gamma(\frac{1}{2}+2n)\}]\\
&= \sum_{m=0}^{\infty}\frac{(-1)^m \exp\{imS_\gamma(E)/\hbar - i\pi m\nu_\gamma/2 - mu_\gamma/2 - u_\gamma m(m-1)\}}{\prod_{j=1}^{m}[1-\exp\{-2ju_\gamma\}]}\\
&= \sum_{m=0}^{\infty}\frac{(-1)^m \exp\{imS_\gamma(E)/\hbar - i\pi m\nu_\gamma/2 + u_\gamma\{-m^2/2+m\}\}}{\prod_{j=1}^{m}[\exp(ju_\gamma) - \exp(-ju_\gamma)]}\\
&= \sum_{m=0}^{\infty}\frac{(-1)^m \sigma_\gamma^{m(m-1)/2}\exp\{imS_\gamma(E)/\hbar - i\pi m\nu_\gamma/2 - u_\gamma m(m-1)/4\}}{\prod_{j=1}^{m}[\exp(ju_\gamma/2) - \sigma_\gamma^j\exp(-ju_\gamma/2)]}\\
&\quad\times\prod_{j=1}^{m}\frac{\sigma_\gamma^{(j+1)}\exp(u_\gamma - ju_\gamma/2)}{\exp(ju_\gamma/2)+\sigma_\gamma^j\exp(-ju_\gamma/2)} \quad . \qquad (202)
\end{aligned}$$

The comparison with eq. (64) yields the form of $c_{\gamma,j}$ in eq. (65).

In the case of Dirichlet boundary conditions along the line $y = x$, the contribution of an orbit along $y = x$ to the oscillatory part of the trace of the Green function $g(E)$ is given by equations (54) and (56). The further steps are carried out as before

$$\begin{aligned}
&\frac{1}{i\hbar}\sum_{k=1}^{\infty}\frac{T_\gamma \exp\{ikS_\gamma(E)/\hbar - i\pi k\nu_\gamma/2\}}{\exp(ku_\gamma/2) - \sigma_\gamma^k \exp(-ku_\gamma/2)} \cdot \frac{1}{1+\sigma_\gamma^k \exp(ku_\gamma)} \\
&= \frac{1}{i\hbar}\sum_{k=1}^{\infty}\frac{T_\gamma \exp\{ikS_\gamma(E)/\hbar - i\pi k\nu_\gamma/2\}}{[\exp(3ku_\gamma/2) - \exp(-ku_\gamma/2)]\sigma_\gamma^k} \\
&= \frac{1}{i\hbar}\sum_{k=1}^{\infty}\frac{T_\gamma \sigma_\gamma^k \exp\{ikS_\gamma(E)/\hbar - i\pi k\nu_\gamma/2 - 3ku_\gamma/2\}}{1-\exp(-2ku_\gamma)} \\
&= \frac{1}{i\hbar}\sum_{k=1}^{\infty}\sum_{n=0}^{\infty} T_\gamma \sigma_\gamma^k \exp\{\frac{i}{\hbar}kS_\gamma(E) - \frac{i\pi}{2}k\nu_\gamma - \frac{3}{2}ku_\gamma - 2knu_\gamma) \\
&= \frac{1}{i\hbar}\sum_{n=0}^{\infty} T_\gamma \frac{\sigma_\gamma \exp\{iS_\gamma(E)/\hbar - i\pi\nu_\gamma/2 - 3u_\gamma/2 - 2nu_\gamma\}}{1-\sigma_\gamma \exp\{iS_\gamma(E)/\hbar - i\pi\nu_\gamma/2 - 3u_\gamma/2 - 2nu_\gamma\}} \\
&= \sum_{n=0}^{\infty}\frac{\mathrm{d}}{\mathrm{d}E}\log[1-\sigma_\gamma \exp\{\frac{i}{\hbar}S_\gamma(E) - \frac{i\pi}{2}\nu_\gamma - u_\gamma(\frac{3}{2}+2n)\}] \ . \qquad (203)
\end{aligned}$$

The comparison of this result with equations (57) and (59) gives the form of $b_{\gamma,n}$ in eq. (61). Euler's identity in eq. (62) is used again for the next steps

$$\begin{aligned}
&\prod_{n=0}^{\infty}[1-\sigma_\gamma \exp\{\frac{i}{\hbar}S_\gamma(E) - \frac{i\pi}{2}\nu_\gamma - u_\gamma(\frac{3}{2}+2n)\}] \\
&= \sum_{m=0}^{\infty}\frac{(-1)^m\sigma_\gamma^m \exp\{imS_\gamma(E)/\hbar - i\pi m\nu_\gamma/2 - 3mu_\gamma/2 - u_\gamma m(m-1)\}}{\prod_{j=1}^{m}[1-\exp(-2ju_\gamma)]} \\
&= \sum_{m=0}^{\infty}\frac{(-1)^m\sigma_\gamma^m \exp\{imS_\gamma(E)/\hbar - i\pi m\nu_\gamma/2 - m^2u_\gamma/2\}}{\prod_{j=1}^{m}[\exp(ju_\gamma) - \exp(-ju_\gamma)]} \\
&= \sum_{m=0}^{\infty}\frac{(-1)^m\sigma_\gamma^{m(m-1)/2} \exp\{imS_\gamma(E)/\hbar - i\pi m\nu_\gamma/2 - u_\gamma m(m-1)/4\}}{\prod_{j=1}^{m}[\exp(ju_\gamma/2) - \sigma_\gamma^j \exp(-ju_\gamma/2)]} \\
&\quad \times \prod_{j=1}^{m}\frac{\sigma_\gamma^j \exp(-ju_\gamma/2)}{\exp(ju_\gamma/2) + \sigma_\gamma^j \exp(-ju_\gamma/2)} \ . \qquad (204)
\end{aligned}$$

The comparison with eq. (64) yields the result for $c_{\gamma,j}$ in eq. (66).

B Calculation of the Monodromy Matrix

Consider a certain periodic orbit. In its vicinity a coordinate system can be introduced, whose x-coordinate is parallel to the orbit, and whose y-coordinate is perpendicular to it. A particle that starts at $\vec{q} = (x_0, \mathrm{d}y)$ with momentum $\vec{p} = (p_x, \mathrm{d}p_y)$ infinitesimally close to the periodic trajectory will have after one traversal the coordinates $\vec{q}\,' = (x_0, \mathrm{d}y')$ and momentum $\vec{p}\,' = (p_x, \mathrm{d}p_y')$. The monodromy matrix M of the periodic orbit is then defined by

$$\begin{pmatrix} \mathrm{d}y' \\ \mathrm{d}p_y' \end{pmatrix} = M \begin{pmatrix} \mathrm{d}y \\ \mathrm{d}p_y \end{pmatrix} \ . \qquad (205)$$

It has the property $\det M = 1$. Introducing an angle α between momentum-direction and x-direction one obtains

$$\begin{pmatrix} \mathrm{d}y' \\ \mathrm{d}\alpha' \end{pmatrix} = \tilde{M} \begin{pmatrix} \mathrm{d}y \\ \mathrm{d}\alpha \end{pmatrix} \ , \ \tilde{M} = \begin{pmatrix} M_{11} & M_{12}p \\ M_{21}/p & M_{22} \end{pmatrix} \ , \ p = |\vec{p}| \ . \qquad (206)$$

The matrix $\tilde{M}$ can be decomposed into partial matrices $\tilde{M}_i$

$$\tilde{M} = \tilde{M}_{i_{max}} \cdot \ldots \cdot \tilde{M}_2 \cdot \tilde{M}_1 \ . \qquad (207)$$

This is done by traversing the periodic orbit once and inserting into the product one matrix $\tilde{M}_i$ for every straight line segment and for every reflection on the boundary. It follows from geometrical considerations that for a straight line segment the matrix $\tilde{M}_i$ is of the form

$$\tilde{M}_i = \begin{pmatrix} 1 & l_i \\ 0 & 1 \end{pmatrix} \ , \qquad (208)$$

where l_i is the length of the line segment. For a reflection on the boundary the corresponding matrix $\tilde{M}_i$ has the form

$$\tilde{M}_i = \begin{pmatrix} -1 & 0 \\ 2(R_i \cos\beta_i)^{-1} & -1 \end{pmatrix} \ . \qquad (209)$$

Here β_i is the angle between the incoming trajectory and the normal to the boundary. R_i is the radius of curvature of the boundary at the collision point. R_i is greater than zero if the boundary is convex and it is less than zero, if the boundary is concave. If the reflection takes place on a straight line, $R_i = \infty$.

In case that $|\mathrm{Tr}(M)| > 2$, the periodic orbit is unstable and M has eigenvalues $\Lambda_{1,2} = \exp(\pm u)$ or $\Lambda_{1,2} = -\exp(\pm u)$, where $u > 0$ is the stability exponent. The Lyapunov exponent λ of an unstable periodic orbit is defined as $\lambda = u/T$, where T is the period of the periodic orbit. If $|\mathrm{Tr}(M)| < 2$, the periodic orbit is stable and M has eigenvalues $\Lambda_{1,2} = \exp(\pm iv)$ where v is the angle of stability.

For billiards, whose boundaries consist of concave and straight pieces only, and which have the property that every classical trajectory is reflected from a concave part of the boundary at least once, it is easy to show that the product of matrices $\tilde{M} = \tilde{M}_{i_{max}} \cdot \ldots \cdot \tilde{M}_1$ satisfies the relation $|\mathrm{Tr}(\tilde{M})| > 2$. For that reason all periodic orbits of the hyperbola billiard are unstable and have positive stability exponents.

C Extremum Principle for Periodic Orbits

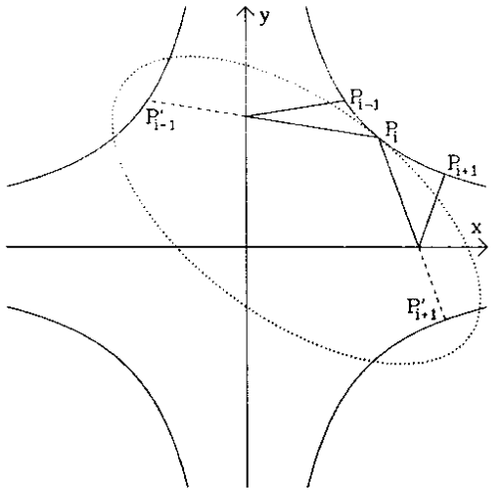

Figure 31: Illustration of the extremum principle

Suppose $P_{i-1}(x_{i-1}|1/x_{i-1})$, $P_i(x_i|1/x_i)$ and $P_{i+1}(x_{i+1}|1/x_{i+1})$ are three successive points of a periodic orbit on the hyperbola. The lengths of the segments of the periodic orbit from P_{i-1} to P_i and from P_i to P_{i+1} are denoted by $l_{i-1,i}$ and $l_{i,i+1}$, respectively. P'_{i-1} and P'_{i+1} are two points that are obtained by extending the two line segments of the orbit that have P_i as common point until they hit one of the hyperbolae $y = 1/x$ or $y = -1/x$ (see figure 31). Now consider an ellipse through P_i with foci P'_{i-1} and P'_{i+1}. Because of the focal property of the ellipse that the lines $P'_{i-1}P_i$ and $P'_{i+1}P_i$ form equal angles with the tangent to the ellipse at point P_i, it follows that the ellipse and the hyperbola have a common tangent at point P_i. It further holds that $l_{i-1,i} + l_{i,i+1} = A$, where A is the major axis of the ellipse. If now the position of the point P_i on the hyperbola is changed, one sees immediately that the major axis of the ellipse through P_i with foci P'_{i-1} and P'_{i+1} is increased and therefore also the sum of the distances $\overline{P'_{i-1}P_i}$ and $\overline{P_iP'_{i+1}}$. Since this argument holds for every point of the periodic orbit on the hyperbola, the following extremum principle for periodic orbits is obtained:

$$\frac{\partial}{\partial x_i} L(x_1, \ldots, x_N) = 0 \; \forall \, i = 1, \ldots, N \tag{210}$$

and

$$\frac{\partial^2}{\partial x_i^2} L(x_1, \ldots, x_N) > 0 \; \forall \, i = 1, \ldots, N \; , \tag{211}$$

where L is the length of a given periodic orbit as a function of its N points on the hyperbola, i.e.

$$L(x_1, \ldots, x_N) = \sum_{i=1}^{N} L_i(x_i, x_{i+1}) \; , \; x_{N+1} := x_1 \; . \tag{212}$$

There are three different possibilities for the functional dependence of the length $L_i(x_i, x_{i+1})$ of the segment of the orbit from $P_i(x_i|1/x_i)$ to $P_{i+1}(x_{i+1}|1/x_{i+1})$:

$$L_i(x_i, x_{i+1}) = \begin{cases} f_x(x_i, x_{i+1}) := [(x_i - x_{i+1})^2 + (1/x_i + 1/x_{i+1})^2]^{1/2} \\ f_y(x_i, x_{i+1}) := [(x_i + x_{i+1})^2 + (1/x_i - 1/x_{i+1})^2]^{1/2} \\ f_b(x_i, x_{i+1}) := [(x_i + x_{i+1})^2 + (1/x_i + 1/x_{i+1})^2]^{1/2} \; . \end{cases} \tag{213}$$

These three cases, respectively, correspond to segments in which there is a reflection on the x-axis only or on the y-axis only or on both axes. Thus if the given periodic orbit is represented by the ternary sequence $a = (a_1, \ldots, a_N)$, its length-function reads

$$L(x_1, \ldots, x_N) = \sum_{i=1}^{N} f_{a_i}(x_i, x_{i+1}) \; . \tag{214}$$

D Form and Number of Code Words with $\mathrm{R}a \equiv a$

In chapter III properties and numbers of code words, which have certain symmetries, are given. Since the derivations of these results are extensive, they are carried out here only for one symmetry, namely for code words with $\mathrm{R}a \equiv a$.

The following notation is used:

An orbit is considered, whose associated code word consists of N letters

$$a = (a_1, \ldots, a_N) \; . \tag{215}$$

This code word fixes the sense of direction, by which the orbit is traversed in coordinate space. The N points of the orbit, which lie on the hyperbola $y = 1/x$, are denoted by $P_1, \ldots, P_N$ in the sequence, in which they are met during one traversal of the orbit. Indices $i > N$ for the points P_i are allowed, with the condition that $P_{i+N} = P_i$.

From now on it is assumed, that the code word satisfies $\mathrm{R}a \equiv a$, and that the corresponding periodic orbit is invariant under reflection on the line $y = x$. Further it is assumed that this orbit is primitive. Consider an arbitrary point P_i of the N points of this orbit on the hyperbola. Then the point, which is obtained by reflecting the point P_i on the straight line $y = x$, also belongs to the set of points $\mathbf{P} = \{P_i | 1 \leq i \leq N\}$. Let this point be P_j. It is possible that several points of the set $\mathbf{P}$ satisfy this condition. Then the index j is determined by requiring, that the point P_{j+1} is obtained by reflecting the point P_{i+1} on the line $y = x$. Since the orbit is primitive, this uniquely fixes the index j. Now the orbit is traversed, starting at point P_i. During this traversal the point P_j is reached. Let $i + n = j \bmod N$, $n \leq N$. This means that the point P_j is reached after n reflections on the hyperbola. After n further reflections on the hyperbola one arrives at the starting point P_i again, because of the invariance of the orbit under reflection on the line $y = x$. Now two cases have to be distinguished. The first case is that $P_i = P_j$ and $i = j$. This is only possible if $N = 1$ and if the orbit runs along the line $y = x$ only. Such an orbit exists, and it corresponds to the code word $a = (\mathrm{b})$. The second case is that $i \neq j$. Then the length of the code word is even and it satisfies $N = 2n$. The code word must be of the form

$$a = c \oplus \mathrm{R}c \; , \tag{216}$$

where c is a word of length $N/2 = n$. This follows from the fact, that the part of the orbit from P_j to P_i is obtained by reflecting the part of the orbit from P_i to P_j along the line $y = x$. Eq. (216) is equal to eq. (93). Since the argument leading to eq. (216) does not depend on the choice of the starting point P_i, it further follows that every cyclic permutation of the word a must be of the general form of eq. (216).

Vice versa every code word, which is of the form of eq. (216), satisfies

$$\mathrm{R}a = \mathrm{R}(c \oplus \mathrm{R}c) = \mathrm{R}c \oplus c \equiv c \oplus \mathrm{R}c = a \ , \tag{217}$$

that is, it belongs to an orbit, which is invariant under reflection on the line $y = x$. But it need not be a primitive periodic orbit. It can be a N-times repetition of the orbit with code word $a =$ (b) for example. If the underlying primitive code word is not equal to (b), then the number of repetitions must be odd, since if it is even and one traverses the periodic orbit, starting at point P_i, then after $n = N/2$ reflections on the hyperbola one arrives at the point $P_{i+n} = P_i$ and not at the point P_j, which is obtained by reflecting P_i on the line $y = x$. Taking this into consideration one obtains the following relation for the $3^{N/2}$ different code words a of the form in eq. (216):

$$3^{N/2} = \sum_{\substack{M|N \\ M\nmid(N/2)}} M \cdot Z_R(M) + Z_R(1) \ , \tag{218}$$

where $Z_R(M)$ is the number of different primitive cyclic classes of code length M with the considered symmetry. $Z_R(M)$ is multiplied by M, since all M cyclic permutations of a primitive code word are different. With $Z_R(1) = 1$ eq. (94) is obtained.

References

[1] H. Poincaré, *Les Méthodes Nouvelles de la Mécanique Céleste*, Gauthier-Villars, Paris (1892).

[2] V. I. Arnold, *Mathematical Methods of Classical Mechanics*, Springer, New York (1978).

[3] J. L. Lebowitz and O. Penrose, Physics Today 26 (February 1973) 23.

[4] Ya. G. Sinai, Russ. Math. Surv. **25** (1970) 137.

[5] L. A. Bunimovich, Funct. Anal. Appl. **8** (1974) 254; Commun. Math. Phys. **65** (1979) 295.

[6] J. Hadamard, J. Math. Pure Appl. **4** (1898) 27.

[7] A. N. Kolmogorov, Dokl. Akad. Nauk. USSR **98** (1954) 527.

[8] V. I. Arnold, Russ. Math. Surv. **18** (1963) 5.

[9] J. Moser, Nachr. Akad. Wiss. Göttingen **1** (1962) 1.

[10] M. V. Berry, Lectures given at the Les Houches school on Chaos and Quantum Physics (August 1989), to be published by North-Holland.

[11] M. V. Berry, Proc. Roy. Soc. London **A 413** (1987) 183.

[12] O. Bohigas and M.-J. Giannoni, in *Mathematical and Computational Methods in Nuclear Physics*, edited by J. S. Dehesa, J. M. G. Gomez and A. Polls, Springer Lecture Notes in Physics No. 209 (1984) 1.

[13] A. Einstein, Verh. Dtsch. Phys. Ges. **19** (1917) 82.

[14] M. C. Gutzwiller, *Chaos in Classical and Quantum Mechanics*, Springer, New York (1990).

[15] M. V. Berry, Proc. Roy. Soc. London **A 400** (1985) 229.

[16] E. B. Bogomolny, Comments At. Mol. Phys. **25** (1990) 67.

[17] M. C. Gutzwiller, J. Math. Phys. **8** (1967) 1979, and **10** (1969) 1004, and **11** (1970) 1791, and **12** (1971) 343.

[18] C. Morette, Phys. Rev. **81** (1951) 848.

[19] G. J. Papadopoulos, Phys. Rev. **D 11** (1975) 2870.

[20] J. H. Van Vleck, Proc. Natl. Ac. Sc. USA **14** (1928) 178.

[21] J. W. Milnor, *Morse Theory*, Princeton University Press (1969).

[22] M. C. Gutzwiller, Lectures given at the Les Houches school on Chaos and Quantum Physics (August 1989), to be published by North-Holland.

[23] E. B. Bogomolny, Physica **D 31** (1988) 169.

[24] E. J. Heller. Phys. Rev. Lett. **53** (1984) 1515; in *Quantum Chaos and Statistical Nuclear Physics*, edited by T. H. Seligman and H. Nishioka. Springer Lecture Notes in Physics No. 263 (1986) 162.

[25] R. Aurich and F. Steiner. Physica **D 48** (1991) 445.

[26] M. V. Berry, Proc. Roy. Soc. London **A 423** (1989) 219.

[27] M. Abramowitz and I. A. Stegun. *Handbook of Mathematical Functions*, National Bureau of Standards, Washington (1964).

[28] E. B. Bogomolny and E. J. Heller, preprint (1989).

[29] R. Balian and C. Bloch, Ann. Phys. (N.Y.) **69** (1972) 76, and **85** (1974) 514.

[30] M. V. Berry and M. Tabor, Proc. Roy. Soc. London **A 349** (1976) 101.

[31] M. V. Berry and M. Tabor, J. Phys. **A 10** (1977) 371.

[32] M. V. Berry, in *Chaotic Behaviour of Deterministic Systems*, Les Houches Lectures XXXVI, edited by G. Iooss, R. H. G. Helleman and R. Stora, North-Holland, Amsterdam (1983).

[33] M. V. Berry and K. E. Mount, Rep. Prog. Phys. **35** (1972) 315.

[34] B. Eckhardt, Phys. Rep. **163** (1988) 205.

[35] N. L. Balazs and A. Voros, Phys. Rep. **143** (1986) 109.

[36] R. Aurich, M. Sieber and F. Steiner, Phys. Rev. Lett. **61** (1988) 483; R. Aurich and F. Steiner, Physica **D 39** (1989) 169.

[37] R. Aurich and F. Steiner, Physica **D 32** (1988) 451; R. Aurich, E. B. Bogomolny and F. Steiner, Physica **D 48** (1991) 91.

[38] Results of the numerical work of C. Schmit are given in [35].

[39] R. Aurich and F. Steiner, Physica **D 43** (1990) 155.

[40] M. C. Gutzwiller, J. Math. Phys. **12** (1971) 343, and **14** (1973) 139, and **18** (1977) 806; Phys. Rev. Lett. **45** (1980) 150; Physica **D 5** (1982) 183; J. Phys. Chem. **92** (1988) 3154; Physica **D 38** (1989) 160.

[41] M. L. Du and J. B. Delos, Phys. Rev. Lett. **58** (1987) 1731.

[42] D. Wintgen and H. Friedrich, Phys. Rev. **A 36** (1987) 131.

[43] D. Wintgen, Phys. Rev. Lett. **58** (1987) 1589, and **61** (1988) 1803.

[44] M. Tabor, Physica **D 6** (1983) 195.

[45] J. P. Keating, Ph. D. Thesis, University of Bristol, U. K. (1989).

[46] M. V. Berry, Ann. Phys. (N.Y.) **131** (1981) 163.

[47] J. P. Keating and M. V. Berry, J. Phys. **A 20** (1987) L 1139.

[48] J. Bolte and F. Steiner, DESY preprint 90-082 (1990), submitted to Commun. Math. Phys..

[49] A. Voros, J. Phys. **A. 21** (1988) 685.

[50] M. V. Berry, in *Quantum Chaos and Statistical Nuclear Physics*, edited by T. H. Seligman and H. Nishioka, Springer Lecture Notes in Physics No. 263 (1986) 1.

[51] P. Cvitanović, Phys. Rev. Lett. **61** (1988) 2729.

[52] P. Cvitanović and B. Eckhardt, Phys. Rev. Lett. **63** (1989) 823.

[53] R. Artuso, E. Aurell and P. Cvitanović, Nonlinearity **3** (1990) 325 and 361.

[54] L. Euler, *Introductio in Analysin Infinitorum* (1748) §§ 306-307.

[55] M. V. Berry and J. P. Keating, J. Phys. **A 23** (1990) 4839.

[56] B. Eckhardt and E. Aurell, Europhys. Lett. **9** (1989) 509.

[57] M. Sieber and F. Steiner, Phys. Lett. **A 144** (1990) 159.

[58] M. Sieber and F. Steiner, Physica **D 44** (1990) 248.

[59] R. Aurich, Ph. D. Thesis, University of Hamburg (1990).

[60] C. Matthies, Diploma Thesis, University of Hamburg (1991).

[61] D. Schleicher, Diploma Thesis, University of Hamburg (1991).

[62] N. Wulff, Diploma Thesis, University of Hamburg (1990).

[63] B. Simon, Ann. Phys. **146** (1983) 209.

[64] M. Sieber and F. Steiner, Phys. Lett. **A 148** (1990) 415.

[65] M. V. Berry, Eur. J. Phys. **2** (1981) 91.

[66] B. Eckhardt and D. Wintgen, J. Phys. **B 23** (1990) 355.

[67] M. V. Berry and M. Tabor, Proc. Roy. Soc. London **A 356** (1977) 375.

[68] C. E. Porter, *Statistical Theories of Spectra: Fluctuations*, Academic Press, New York (1965).

[69] M. L. Mehta, *Random Matrices and the Statistical Theory of Energy Levels*, Academic Press, New York (1967).

[70] G. M. Zaslavskii, Sov. Phys. JETP **46** (1977) 1094.

[71] O. Bohigas, M.-J. Giannoni and C. Schmit, Phys. Rev. Lett. **52** (1984) 1.

[72] O. Bohigas, M.-J. Giannoni and C. Schmit, in *Quantum Chaos and Statistical Nuclear Physics*, edited by T. H. Seligman and H. Nishioka, Springer Lecture Notes in Physics No. 263 (1986) 18.

[73] J. H. Hannay and A. M. Ozorio de Almeida, J. Phys. **A 17** (1984) 3429.

[74] T. H. Seligman, J. J. M. Verbaarschot and M. R. Zirnbauer, Phys. Rev. Lett. **53** (1984) 215; J. Phys. **A 18** (1985) 2751.

[75] M. Robnik, J. Phys. **A 17** (1984) 1049.

[76] H.-D. Meyer, E. Haller, H. Köppel and L. S. Cederbaum, J. Phys. **A 17** (1984) L 831.

[77] J. R. Kuttler and V. G. Sigillito, SIAM Review **26** (1984) 163.

[78] E. J. Heller, Lectures given at the Les Houches school on Chaos and Quantum Physics (August 1989), to be published by North-Holland.

[79] H. v. Helmholtz, J. reine u. angew. Math. **57** (1860) 1.

[80] A. Sommerfeld, Jahresber. Dt. Math.-Ver. **21** (1912) 309.

[81] R. E. Kleinman and G. F. Roach, SIAM Review **16** (1974) 214, and references therein.

[82] A. J. Burton and G. F. Miller, Proc. Roy. Soy. London **A 323** (1971) 201.

[83] R. J. Riddell, J. Comput. Phys. **31** (1979) 21 and 42.

[84] M. V. Berry and M. Wilkinson, Proc. Roy. Soy. London **A 392** (1984) 15.

[85] H. P. Baltes and E. R. Hilf, *Spectra of Finite Systems*, B.I.-Wissenschaftsverlag, Mannheim (1976).

[86] B. Simon, J. Funct. Anal. **53** (1983) 84.

[87] F. Steiner and P. Trillenberg, J. Math. Phys. **31** (1990) 1670.

[88] T. A. Brody, J. Flores, J. B. French, P. A. Mello, A. Pandey and S. S. M. Wong, Rev. Mod. Phys. **53** (1981) 385.